ABSTRACT

MOORE, NANCY JENNINGS. Effects of Leading-Edge Flame Behavior on Flame Stabilization and Blowout. (Under the direction of Dr. Kevin Lyons).

The goal of this work was to identify the mechanisms that effect stabilization of hydrocarbon jet flames. Methane, nitrogen, and co-flowing air were regulated and directed through a burner that created fully-developed fuel flow with concurrent air. The behavior of the reaction zone at the leading-edge was analyzed from digital images obtained from a camera optimally positioned to capture the movements of the entire flame front. Low Reynolds number flows allowed for the investigation of hysteretic behavior. The hysteresis regime refers to the situation where the jet flame has dual positions favorable to flame stabilization: attached and lifted. Results indicate that flame height in hysteresis is significantly impacted by high velocities of co-flow and that past a critical value a local minimum will be created. Fully turbulent, lifted flames were also studied to determine the fluctuations in the height of lifted methane flames in the presence of air co-flow. The partially-premixed flame front of the lifted flame fluctuates in the axial direction, with the fluctuations becoming greater in flames stabilized further downstream. These fluctuations are also observed in flames where blowout is imminent. The height and rate of these fluctuations are studied with respect to average height, flow velocities, and Reynolds number. Additionally, the mechanisms that cause jet-flame blowout, particularly in the presence of air co-flow, are not completely understood. Two types of experiments are described, and the data report that a predictor of blowout is the prior disappearance of the

axially-oriented flame branch which is consistently witnessed despite a turbulent flame's inherent variable behavior. The conclusions are supported by experiments with nitrogen-diluted flames. A blowout parameter is also calculated for methane flames in co-flow and diluted methane flames that can be used to predict at what flow velocities blowout will occur. This work analyzes flames near the burner, in the far field, and approaching blowout. The comprehensive study allows for the realization that the mechanisms of flame stabilization differ throughout the combustible field.

Effects of Leading-Edge Flame Behavior on Flame Stabilization and Blowout

by
Nancy Jennings Moore

A dissertation submitted to the Graduate Faculty of
North Carolina State University
in partial fulfillment of the
requirements for the degree of
Doctor of Philosophy

Mechanical Engineering

Raleigh, North Carolina

2009

APPROVED BY:

_____	_____
Dr. Kevin Lyons Committee Chair	Dr. Tarek Echekki
_____	_____
Dr. Andrey Kuznetsov	Dr. Andre Mazzoleni

DEDICATION

I would like to dedicate this to my parents, Crystal and Bill Moore,
who have always been proud of me.
And to my sister, Virginia,
who long ago set the bar.

BIOGRAPHY

Nancy Moore was born in Concord, NC and grew up in Cary, NC. After graduating from Apex High School, she attended Clemson University and earned a Bachelor's degree in Mechanical Engineering in 2000. She then went to Duke University and received a Master's degree in Mechanical Engineering. After a short break from school, she enrolled in North Carolina State University and began pursuing her doctorate.

ACKNOWLEDGEMENTS

I would like to thank Kevin Lyons for being as helpful and supportive as an advisor can be. His guidance has been invaluable to me during this process.

Thanks also to Dr. Tarek Echekki, Dr. Andrey Kuznetsov, Dr. Andre Mazzoleni, and Dr. Lexin Li for their support and for serving on my committee.

Thank you to Jennifer McCraw and James Kribs for their assistance during experiments out at the lab and to Dr. Stephen Terry for his advice.

TABLE OF CONTENTS

LIST OF TABLES

LIST OF FIGURES

Chapter 1

Introduction

1.1 Scope of Work

To study combustion is to analyze the thermal and transport processes of chemically reacting flows. This knowledge aids in the development and improvement of practical systems to increase efficiency, reduce fuel consumption, and limit the formation of pollutants. Despite advancements in the field, many questions remain about the influences of thermodynamics, chemical kinetics, and fluid mechanics on the mechanisms of flame ignition, stabilization, and extinguishment.

Combustion devices can operate at various fuel velocities while in use. For example, an industrial boiler or furnace undergoes cycles during which the heating load changes. The location and characterization of the flame depends on the fuel velocity and also on the existence of co-flowing air and its velocity. In addition, the multiple burner geometries being used in industry require a comprehensive understanding of flame stability (Junus *et al.*, 1998; and Morcos and Abdel-Rahim, 1999). Flame stability within a combustor or furnace results

from a continuous inflow of reactants that are ignited by hot gases. Insufficient stability can result in unsafe operating conditions (Poinsot and Veynante, 2001).

The circumstances necessary for a flame to remain attached to the fuel jet exit are somewhat predictable. However, the behavior of a lifted flame is not fully understood. In the hysteretic regime, the same fuel and air velocities can result in a stable, lifted flame or an attached flame. For some applications, an attached flame is undesirable due to the consequential corrosion of the burner nozzle. However, a lifted flame can be difficult to control and more easily extinguished. The height of a lifted flame fluctuates, with these fluctuations possibly leading to blowout, the term used to describe the extinguishment of a flame due to the inability to sustain combustion. Unintentional blowout results in the loss of unburned fuel which lowers combustion efficiency as well as causes a potential safety hazard. Improving the efficiency throughout the cycle requires an understanding of the flame's behavior at various flow conditions.

1.2 Characterization of Flames

The type of flame created is dependent on the exit velocity of the fuel. A typical burner can be classified as a buoyant jet in which buoyancy acts in the direction of the jet velocity. At some distance downstream, the buoyant jet becomes a plume, meaning buoyancy forces dominate (Chen and Rodi, 1980). A candle flame is an example of a plume;

the jet velocity is so low that the momentum of the jet is negligible compared to the free convection of the flame (Strehlow, 1984).

1.2.1 Premixed and Diffusion Flames

Traditionally, flames are described as either premixed or diffusion flames. In a premixed flame, the fuel and oxidizer are mixed at the molecular level before a reaction takes place. The velocity of the reactants is equal to the velocity at which the flame front propagates into the unburnt gas upstream (Weinberg, 1963). This velocity, extending in the direction opposite of the fuel flow, is the flame's burning velocity and acts to stabilize a premixed flame (Liñán and Williams, 1993). A flame will flash back to the burner if the burning velocity exceeds the incoming flow velocity (Weinberg, 1963). Almost all hydrocarbons mixed with air have similar burning velocities. Methane has a laminar burning velocity, S_L, of approximately 43 cm/s. Diluting a fuel lowers the burning velocity (Strehlow, 1984).

In a diffusion, or non-premixed, flame the reactants are separated initially, and reaction only occurs where they interact (Turns, 1996). The chemical reactions are limited due to the nature of the mixing; fast mixing can lead to premixed combustion. A diffusion flame has no burning velocity to help stabilize the flame against the flow of fuel. It cannot propagate towards the fuel due to the lack of oxidizer and cannot propagate towards the oxidizer due to the lack of fuel. Diffusion flames are thus more sensitive than premixed flames to turbulence and perturbations in the flow (Poinsot and Veynante, 2001). Data has

shown that a leading-edge structure can form at the edge of the diffusion flame closest to the flow nozzle, extending away from the flow of fuel (Lyons and Watson, 2001). This structure is thought to be a fuel-lean premixed flame that develops due to the air in the surroundings and helps to stabilize the diffusion flame (see Section 1.3.4).

The existence of multi-flame structures has led researchers to create a third category called partially premixed flames (Peters, 2000). In partially premixed combustion, the initially separate fuel and oxidizer are partially mixed by turbulence before combustion takes place. Partially premixed flames have aspects of both premixed and diffusion flames.

1.2.2 Laminar and Turbulent Flames

Flames can also be described as either laminar or turbulent. Examples of laminar combustion are lighters and candles while turbulent combustion is in most combustion systems such as aircraft engines and industrial furnaces (Poinsot and Veynante, 2001). The behavior of laminar flames is dictated by the balance between inertial and gravity forces, known as the Froude number (Strehlow, 1984).

As Hottel and Hawthorne (1949) surmised, the transition of a diffusion flame from laminar to turbulent occurs due to increasing jet exit velocity. At low velocities, the laminar flame (as seen in Figure 1.1) has smooth edges and its length increases as the flow velocity is increased. When a certain velocity is reached, the flame's length begins to decrease with increasing velocity and its appearance changes such that the edges are corrugated along the upper part of the flame. This marks the transition region. As the velocity is further

increased, the flame eventually becomes fully turbulent. In this region, the wrinkled edges of the flame extend almost to the jet exit. Damköhler in 1940 determined that the wrinkling is the main mechanism controlling turbulent flames. A turbulent flame's appearance and length are independent of the Froude and the Reynolds number (Strehlow, 1984).

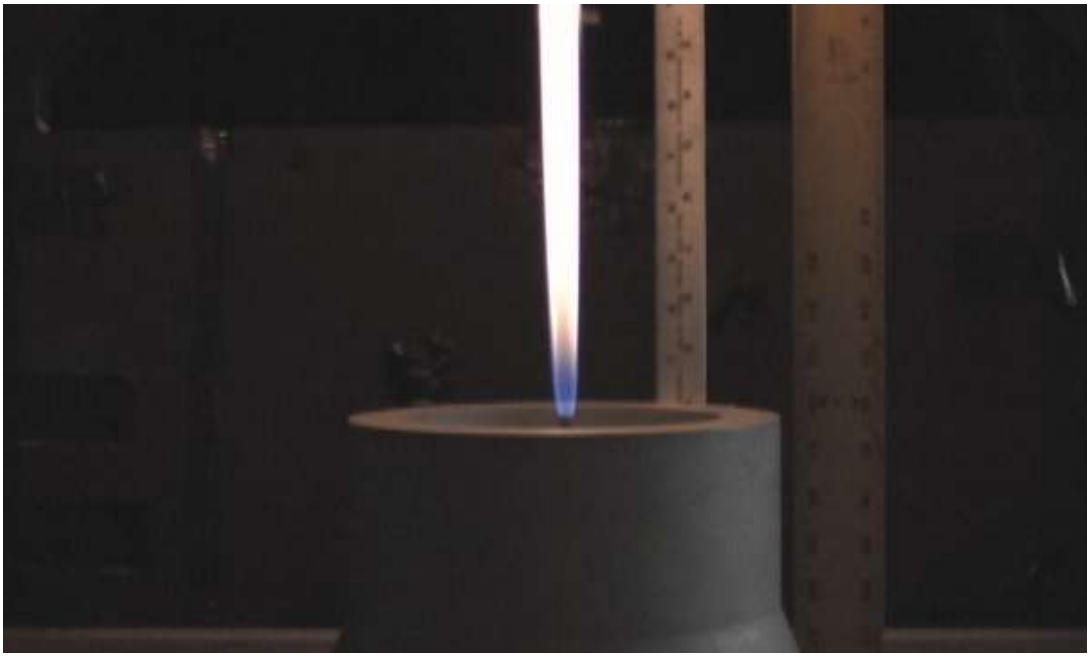

Figure 1.1 Image of a laminar methane flame.

When the flow upstream of a flame front becomes turbulent, the visible luminous zone changes and the flame becomes noisy (Weinberg, 1963). The thickness of a laminar flame goes up to fractions of a millimeter while the thickness of a turbulent flame is a few centimeters (Poinsot and Veynante, 2001). For this reason, a turbulent flame front may be

called a flame brush. Figure 1.2 shows a lifted turbulent flame. The blue luminosity indicates premixed combustion at the flame front.

Figure 1.2 Image of a turbulent methane flame.

Turbulent premixed combustion can be described as the interaction between the flame front and eddies in the flow (Poinsot and Veynante, 2001). Large eddies (of the integral length scale) are created by abstracting energy from the mean flow and result in pockets of gas moving in directions other than those of the overall flow. Continual dissipation reduces the size of the eddies so they eventually exist at the smallest (Kolmogorov) scale (Law, 2006). The largest scales in turbulent flow are controlled by inertia and not viscous

dissipation (Poinsot and Veynante, 2001). Turbulence intensity, calculated as the ratio of the root mean square of the velocity fluctuations to the mean velocity, can be used to establish the strength of turbulence. The amount to which a flame's surface is corrugated depends on the intensity and scale of turbulence. If the intensity is large enough, burning can occur in isolated pockets due to the discontinuity of the flame front (Weinberg, 1963). The burning velocity of a turbulent flame, S_T, is greater than the laminar burning velocity and can be approximated from the empirical relation

$$\frac{S_T}{S_L} \approx 1 + \frac{u'}{S_L} \tag{1.1}$$

where *u'* is the root mean square of the velocity fluctuations (Poinsot and Veynante, 2001). For large *u'*, S_T becomes essentially independent of S_L and from Equation 1.1

$$S_T \approx u' . \tag{1.2}$$

Heat release and temperature changes in a flame create flow accelerations and changes in the kinematic viscosity that affect the turbulence (Poinsot and Veynante, 2001). Due to viscosity, moving particles shift nearby particles causing fluctuating velocity distributions (Weinberg, 1963). Thus, the Reynolds number can vary more in a reacting flow than in a non-reacting flow. It is possible for a turbulent non-reacting jet to become a laminar flame after ignition (Poinsot and Veynante, 2001).

1.3 Theories on Stability of Lifted Flames

Several theories have attempted to explain flame behavior of lifted jet diffusion flames. The models described below differ in their prediction of the amount of premixing that occurs ahead of the flame front. Pitts (1988) presents an overview of the many theories that have been proposed. They can generally be classified as either based on flame propagation or on extinction mechanisms.

1.3.1 Premixedness Model

One of the earliest theories was the premixedness model developed by Vanquickenborne and van Tiggelen (1966). They proposed that the fuel and oxidizer are completely premixed at the base of a turbulent lifted flame. Thus, the flame stabilizes where the stoichiometric mixture is formed. For their experiments with pure and diluted methane, they predicted that the fuel concentration at stability points had a value between 5 and 15%, the flammability limits for methane. The flame propagates at some characteristic premixed turbulent burning velocity. The premixing is due to the equilibrium between the premixed turbulent burning velocity (pointing upstream) and the average axial jet exit velocity at the flame base (pointing downstream). The flame remains attached to the nozzle below a certain critical jet exit velocity because equilibrium with the turbulent burning velocity is not possible.

Vanquickenborne and van Tiggelen's model also investigated the blowout phenomenon. They experimentally determined the fuel velocity at which blowout occurred and found that the flame could exist at greater velocities if the ignition source was maintained, thus proving that blowout did not occur as a result of moving beyond the flammability limits. The flame blows out at high jet velocities when the velocities can no longer balance. The local flame speed is no longer sufficient to stabilize the flame and so it is moved downstream to blowout. Kalghatgi (1981) used the model of Vanquickenborne and van Tiggelen (1966) and dimensional analysis to experimentally investigate blowout. His findings showed that the jet velocity at blowout is linearly dependent on the diameter.

1.3.2 Large Scale Mixing Model

The large scale mixing model (Broadwell *et al*., 1984), challenges the premixedness theory by proposing that lifted flame stabilization depends on turbulent structures of the nearby unignited flow. Fresh ambient air is reentrained into the diffusion flame and comes into contact with a mixture of hot products and fuel. Molecular diffusion occurs at the strained interface until the entire mixture is homogeneous. Broadwell *et al*. (1984) determined a parameter, ε, based on the mixing and chemical times to be an indicator of blowout. The time associated with the mixing of the reentrained air and the hot products, t_m, is divided by the chemical reaction time, t_c,

$$\varepsilon \equiv \frac{t_m}{t_c} \propto \frac{\delta / u}{\kappa / S_L^{\,2}}. \qquad 1.3$$

δ is the width of the flow, u is the centerline velocity, and κ is the thermal diffusivity (see Section 5.4). Dahm and Dibble (1988) determined the critical value for this ratio to be 4.3. If the mixing time is not long enough for the entrained air to be ignited by the hot products, then the gases cool too fast and ignition becomes impossible. Blowout occurs with a ratio of less than 4.3. Also, fluctuations in a flame's lift-off height are assumed to be related to the flame propagating from one large-scale structure upstream to the next (Miake-Lye and Hammer, 1988).

Tieszen *et al.* (1996) explains a link between Broadwell's theory of blowout and the model of Vanquickenborne and van Tiggelen (1966). The role of large scale structures found in jet turbulence is proposed to enhance the turbulent flame speed near blowout. Experiments were performed with ethylene and ethane issuing into a quiescent environment. The scalar field is described using a time-averaged equation for the mass fraction. The mass fraction of fuel, Y, into air at a particular downstream location, z, for a given radial position, r, with no co-flow present is represented as

$$Y = 10 \cdot \left(\frac{\rho_0}{\rho_\infty}\right)^{1/2} \left(\frac{r_0}{z}\right) \exp\left\{-57\left(\frac{r}{z}\right)^2\right\}. \qquad 1.4$$

This equation, making Y a function of the ratio of the densities of the fuel and air and the nozzle diameter, is discussed in more detail in Section 5.2.

1.3.3 Laminar Flamelet Model

The laminar flamelet model suggests that the stability of the lifted flame is governed by the strain rates within laminar diffusion flamelets, as explained by Peters (2000). Flamelets are thin reactive-diffusive layers surrounded by an otherwise nonreacting turbulent flow field. The chemistry is most active within a thin inner layer, the location of which defines the flame surface. The flamelet model assumes that there is a separation between the small scales at which reaction occurs and the larger scales of turbulence. The amount of turbulence determines the size of the Kolmogorov eddies in the flame. If the inner layer is thin, it is embedded in the eddies of the quasi-laminar flow, justifying the assumptions of a laminar flamelet structure. However, if the flow is more turbulent and the eddies are smaller, they can penetrate the inner layer which breaks up the structure and the flame extinguishes. The extinction of laminar flamelets is then the stabilization mechanism. At certain jet exit velocities, the high strain rates from the turbulent eddies cause extinction of the flamelets near the nozzle but not at locations further downstream so the flame stabilizes at a lifted height. At greater velocities, the strain rates are only low enough at locations where the mixture is too lean to support any combustion.

1.3.4 Triple Flame Model

The triple flame model is based on the observed structure of the flame base of a laminar flame. The base consists of a fuel-lean premixed branch, a fuel-rich premixed

branch, and a trailing diffusion flame that all share the same origin. Phillips (1965) first reported this arrangement in the reaction zone after experiments with methane flames in a flame stabilizer that injected methane from the top and air from the bottom creating a two dimensional planar mixing layer for lifted laminar flames. The image he obtained (Figure 1.3) shows an upper area with unburned fuel that results in a fuel-rich branch and a lower area with excess air that results in a fuel-lean branch. The diffusion flame exists due to the diffusion of the fuel and oxidizer towards each other.

Triple, or tribrachial, flames can easily be seen in laminar flames but are rarely witnessed in lifted turbulent flames. Scalar field images from Joedicke *et al*. (2005) indicate a tribrachial point in the fuel rich region. Muñiz and Mungal (1997) used particle image velocimetry (PIV) to study the velocity field of lifted methane flames. Their data indicate that the flow diverges as it approaches the flame front. Consequently, the incoming velocity is less, so the flame has a smaller velocity against which it must propagate. These results provide an explanation for the relatively low burning velocities found for flames in high Reynolds number flows and suggest the presence of a triple flame structure. Several studies have been done to verify the presence of triple flames and determine the role of each branch in flame stabilization (Kim *et al.*, 2006; Echekki and Chen, 1998; Ruetsch *et al.*, 1995; Chung and Lee, 1991; Daou *et al*., 2002; Boulanger *et al*., 2003).

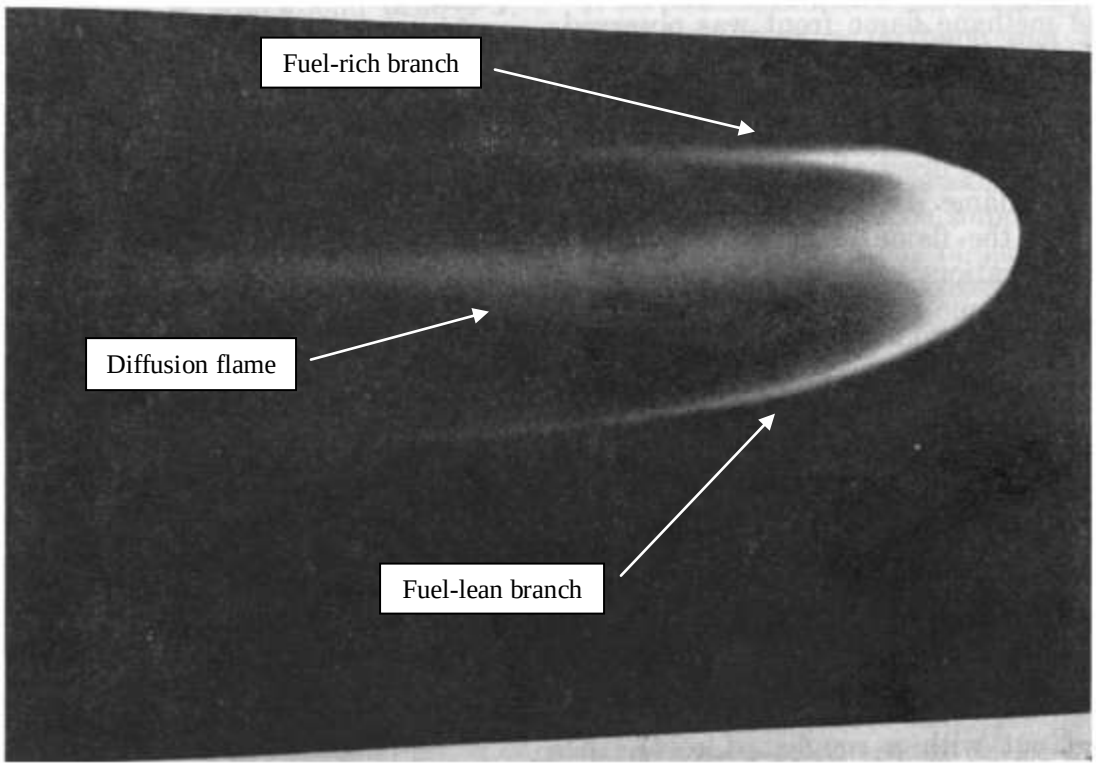

Figure 1.3 Image of a triple flame structure at the base of a lifted, laminar methane flame (Phillips, 1965).

1.4 Experimental Procedure

As will be explained in Section 1.5, this research examined three aspects of flame stability. The procedure for each set of experiments was varied but much of the same equipment was used. Methane fuel was used for all experiments. The ignition source was a butane lighter.

The burner (see Figure 1.4) is designed to provide fuel from a center tube and concurrent air flow. The fuel flow is controlled by a rotameter and then directed through a stainless steel pipe with a length long enough to ensure fully-developed flow. The calibrated rotameter restricts the flow of fuel from the gas cylinder such that the desired volumetric flow rate, determined by the position of the stainless steel ball inside the tube, can be set.

The co-flowing air is delivered by a variable speed centrifugal blower. It enters the burner through a hose connected to the side of the burner and then directed through a flow straightener of honeycomb material. Towards the top of the burner, the cross-sectional area increases to 5.75 inches, diffusing the air flow which then goes through wire mesh screens that help remove flow irregularities. A hot-wire anemometer (TSI Veloci-calc model 8345) measures the co-flow velocity to the nearest 0.01 m/s.

Figure 1.4 Photograph of the burner.

1.5 Objectives

The objective of this work was to identify the mechanisms that effect stabilization of hydrocarbon jet flames by studying the behavior of the reaction zone. The burner used for experiments provides concurrent co-flowing air and multiple pipe diameters for fuel delivery. Thus, a number of experimental cases were possible by modifying the fuel flow rate, the co-flow velocity, and the diameter.

Experiments were performed on flames stabilized at several downstream locations. The locations can be divided into three categories based on the principal characteristics of each. Hysteretic effects dominate in the near-field close to the burner. In the self-similar region further downstream turbulence is fully developed. Flames far from the burner are approaching blowout and thus the limit of stabilization.

Analysis of the data collected has been used to quantify the role of fuel velocity and air co-flow in flame stabilization. Chapter 2 describes experiments on flames in the near-field designed to determine the effect of relatively high co-flow velocities on hysteresis. In Chapter 3, experiments on fully turbulent lifted flames are chronicled and the data establishes how parameters such as co-flow velocity influence stable, lifted flame height fluctuations. The focus of Chapters 4 and 5 are blowout experiments performed to examine the transient behavior of the reaction zone and ascertain causes and precursors of flame extinguishment. The final chapter summarizes the conclusions of the experiments and details the focus of future work in the area of flame stabilization.

Chapter 2

Flame Hysteresis Effects in Methane Jet Flames in Air-Coflow

2.1 Introduction

The turndown of a natural gas industrial burner allows for a boiler to function at low levels when the demand falls below the typical level for which it was designed. At low firing conditions, a flame in the hysteretic region can exist whose behavior varies greatly from lifted flames beyond this region. A better understanding of the mechanisms of flame stability is needed to predict hysteretic behavior of turbulent diffusion flames when burners are operating at low Reynolds numbers and low heat release conditions.

A flame remains attached to the nozzle after ignition at low jet exit velocities. When the lift-off velocity of an attached flame is reached, the flame lifts downstream to a region favorable for stabilization. If the velocity is further increased, the flame recesses downstream to find another stable lifted height and radial position. A distinction is made between the term lifted which refers to a detached flame at any height and the term lift-off

which is used here to signify the height of a flame immediately following detachment from the nozzle due to an increase in the flow velocity.

The case of the laminar flame has been used as a starting point to gain understanding of the more complicated turbulent flame situations. Laminar lifted flames have been studied extensively and the similarity solutions presented by Chung and Lee (1991) predict the velocity and concentration fields for a nonpremixed jet as a function of the Schmidt number of the fuel. Boulanger *et al.* (2003) simulated laminar diffusion flames and found that including the effect of the heat release from the flame front on the flow upstream must be taken into account when predicting the lift-off height. A number of papers have examined the lift-off and reattachment velocities of flames in various co-flows and the flow structure of flames in the near field (Savas and Gollahalli, 1986; Savas and Gollahalli, 1986; Lee and Chung, 1997). A co-flow velocity that is significantly less than the velocity of the exiting fuel can noticeably impact the location and behavior of a flame. Lee *et al.* (2003) used Rayleigh scattering to study propane flames in co-flowing air and validate the approximate solutions. The derivation of the height from the similarity solutions revealed that it is a nonlinear function of the flow velocities in which the co-flow velocity is raised to an exponential power based on the Schmidt number, which helps to explain the dependence of the height of a lifted flame on a relatively small amount of co-flow. Lee and Chung (1997) noted that the difference between the jet velocity when the flame lifts off and when it reattaches for a propane flame increased when co-flow was present.

Experiments on lifted turbulent flames in air co-flow by Brown *et al.* (1999) suggested that premixing is not the governing mechanism stabilizing flames near the nozzle and the propagation speed of such flames reaches a maximum of about three times the laminar burning velocity. Clemens and Paul (1995) used laser imaging techniques to study hydrogen diffusion flames and found that the density ratio in a reacting jet has a stronger influence on the interaction between the shear layer turbulence and the reaction zone than the stoichiometric mixture fraction. Experiments performed by Terry and Lyons (2005) indicated that a minimum local excess jet velocity inversely proportional to the laminar burning velocity squared is needed for lifted flames to remain lifted. Also, the lifted heights and the reattachment velocities varied linearly with the co-flow velocity (Terry and Lyons, 2006).

Since the jet velocity required to lift an attached flame is higher than that needed for reattachment, a stable flame can exist as lifted or attached at velocities between these values. Thus the location of the flame in this hysteretic region depends more on its prior location than solely on the flow velocity. At velocities below the lift-off velocity but greater than the reattachment velocity, an attached flame will remain attached while a lifted flame will stay lifted. Commonly, an attached flame lifts off the nozzle when the lift-off velocity is reached and then, if the jet velocity is decreased, propagates upstream until the reattachment velocity is attained, at which point the flame quickly reattaches to the nozzle.

The current study provides analysis of the flame position in the hysteretic region for turbulent diffusion methane flames with relatively high air co-flow velocities present. For

these experiments, the attached flame is ignited at a low fuel velocity and steady co-flowing air, and images of the flame are taken as the velocity is increased to achieve lift-off and then decreased until the flame reattaches. Analysis of the lift-off height as a function of flow velocity is provided as well as the observed recession of flames in hysteresis and the effect of co-flow on the phenomenon. The focus on high co-flow velocities helps illuminate the significant effect of concurrent air flow on flames in the near field.

2.2 Experimental Setup

The experiments were performed at the Applied Energy Research Laboratory on the campus of North Carolina State University. A jet flame burner with a fuel pipe of 3.5 millimeters (mm) diameter was used to deliver 99% pure methane. The apparatus delivers a fully-developed flow of fuel at the pipe's exit. As shown in Figure 2.1, the fuel pipe is surrounded by an annulus of co-flowing air with a 150 mm diameter. This shrouds the flame from room currents and allows for repeatable and controlled measurements to be performed.

For this investigation, images of methane in the hysteresis region were made with a Panasonic Model PV-GS300 camcorder producing thirty frames per second. Sequences of images were recorded and selected images were analyzed using Adobe Photoshop. A rotameter with $\pm 5\%$ accuracy was used to measure the volume flow rate of the methane entering the fuel pipe, from which the fuel velocity was calculated. The minimum and

maximum co-flow velocities used were 0 m/s and 0.76 m/s, respectively. The velocity was measured using a TSI Veloci-calc model 8345 anemometer.

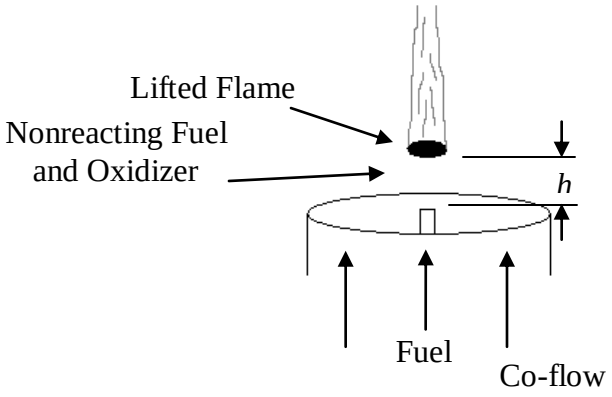

Figure 2.1 Methane is delivered from the pipe that is surrounded by co-flowing air. *h* is the distance from the pipe exit to the lifted flame front.

2.3 Results

The hysteretic behavior was analyzed using images of the stable methane flame obtained during several experiments. In these experiments, the co-flow velocity was measured and held constant while the fuel velocity was changed via variations in the valve of the fuel rotameter. The flame was initially attached to the burner at a low jet velocity. The fuel rate was increased until the flame lifted off of the burner and the rate was recorded. The rotameter was read to the nearest 0.5 scale reading which corresponds to ±0.15 m/s accuracy.

This process was repeated multiple times to determine the lowest velocity at which the flame would lift off, or the lift-off velocity. Then the fuel flow rate was incrementally decreased, allowing the flame to stabilize before the rate was lowered again. The rate was not reduced by more than 1.8 m/s at one time. The procedure ended when the flame reattached to the burner, indicating the reattachment velocity had been reached. The process was repeated for various co-flow velocities.

Multiple images of the flame during hysteresis were used to determine the flame's change in height. The height of the flame front was measured by determining its distance from the burner using the image ruler. The distance was converted to centimeters using static references in the image with ±0.047 cm accuracy. This forms the basis for the observations of the flame hysteretic behavior.

For all cases studied, the height initially decreases with decreasing jet velocity. The results for repeated experiments at varying co-flow velocities are shown in Figure 2.2. The flame lifts off the burner at the maximum fuel velocity for each case (as indicated by the arrow pointing to the right). Then, the exit velocity is decreased while the co-flow velocity is maintained at a constant level. The resulting change in position of each flame should be read on the curve from right to left in the direction of decreasing fuel velocity.

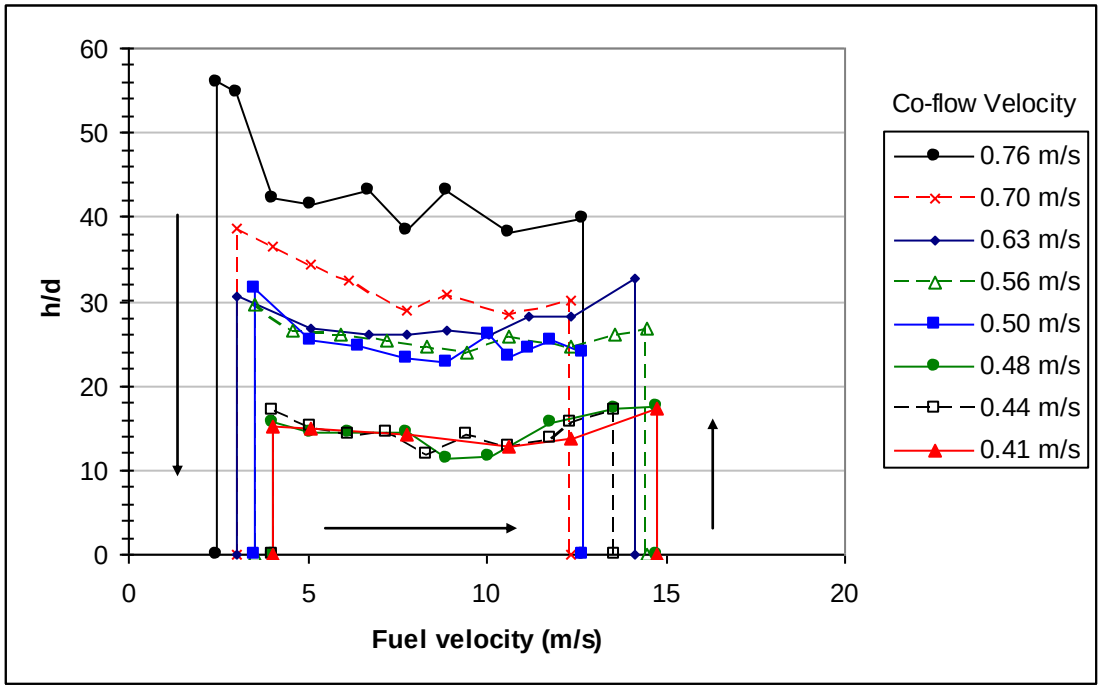

Figure 2.2 Flame position for various co-flow velocities. As indicated by the arrows, the fuel velocity was increased until the flame lifted and then incrementally decreased until reattachment. In each case, a change in the direction of movement of the flame is observed even though the fuel velocity is being decreased.

As the co-flow velocity increased, the corresponding lift-off and reattachment velocities generally decreased. However, while the co-flow velocities tested nearly double from 0.41 to 0.76 m/s, the lift-off velocities decrease about 2.5 m/s and the reattachment velocities about 1.5 m/s. Given that the lift-off velocities are more than three times larger than the reattachment velocities, the change due to co-flow is more significant in the reattachment behavior (Terry and Lyons, 2006).

In each of the cases, the behavior is peculiar in that the flame tends to lift away from the burner as the fuel velocity decreases, creating a local minimum prior to reattachment. Nearly midway between the lift-off and reattachment velocities, the flame begins to move downstream, eventually reaching a height equal to or greater than the initial lift-off height. The change in height between the maximum and minimum observed in this region increases with greater co-flow velocity. Additionally, at higher co-flow velocities, the flame is seen to move farther downstream to a height greater than its lift-off height immediately prior to reattachment. Due to fluctuations in the stable flames at these downstream distances, the heights noted in Figure 2.2 (especially for the two highest co-flows) must be considered approximations. All of the flames lift off at Reynolds numbers greater than 2500 and reach a local minimum between 1500 and 2000. Reattachment occurs below $Re = 800$.

Figure 2.3 shows a sequence of images of the flame in the hysteretic region at a co-flow velocity of 0.5 m/s. Prior to Figure 2.3(a), the flame is fully attached to the burner. The fuel velocity, U_0, is increased to 12.67 m/s causing the flame (a) to lift off and (b) move to a position 8.4 cm downstream. As the fuel rate is subsequently decreased, the flame predictably moves upstream. However, at a fuel rate of 8.89 m/s, the flame stops its upstream stabilization trend and moves to a position farther downstream. Figure 2.3(d) is thus an image of the flame at its local minimum. During this downstream recession, the flame base becomes narrower and generally more defined which indicates a reduction in turbulence, a difference evident when comparing Figure 2.3(f) and Figure 2.3(g) (Weinberg, 1963). This motion continues until the reattachment velocity of 3.52 m/s is reached at which

time the flame (Figure 2.3(h)) reattaches to the burner. For this case, the farthest downstream position of the flame is achieved immediately before reattachment.

A similar sequence of images is shown in Figure 2.4 for a constant co-flow velocity of 0.7 m/s. For this case, the lift-off height is 30.1 cm. The flame moves upstream to a height of 29.0 cm before recessing downstream and reattaching immediately after achieving a maximum height of 38.7 cm. Again, the flame base is seen to change in appearance during this process and the reattachment height is greater than the lift-off height.

Figure 2.3 Sequence of images of a methane flame with co-flow velocity constant at 0.5 m/s. The corresponding fuel velocity, U_0, for each image is given as well as the height of the flame front. The first image was taken just as the flame lifted off of the burner. In the last image, the flame is moving upstream to reattach.

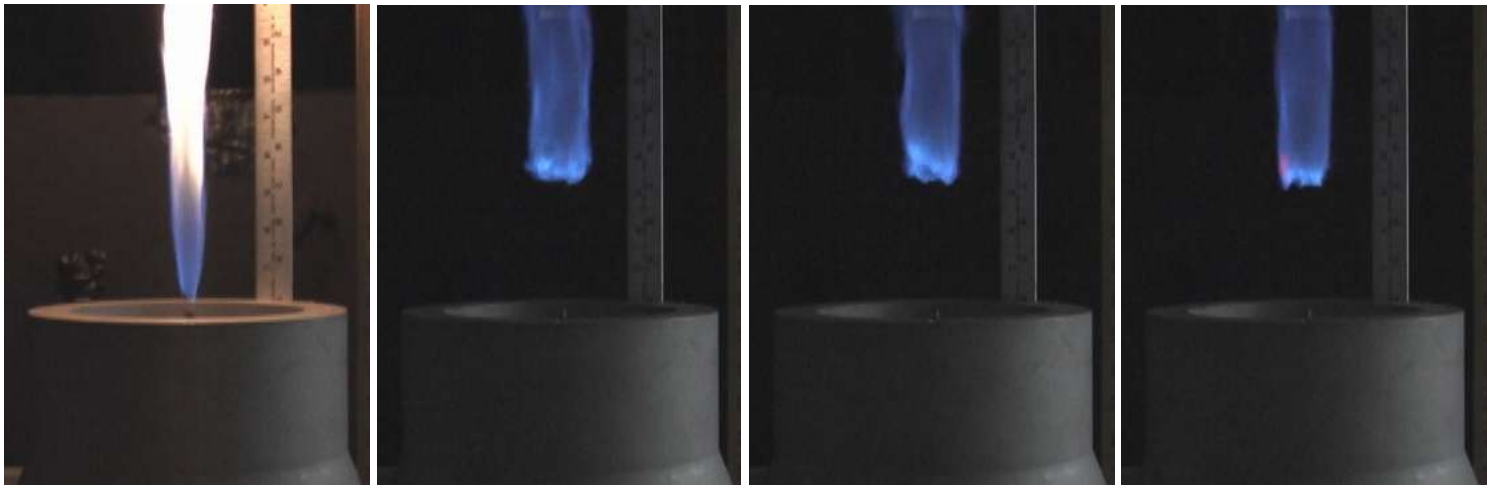

(a) lifting off

(b) U_0 = 12.67 m/s
h = 8.4 cm

(c) U_0 = 10.60 m/s
h = 8.3 cm

(d) U_0 = 8.89 m/s
h = 8.0 cm

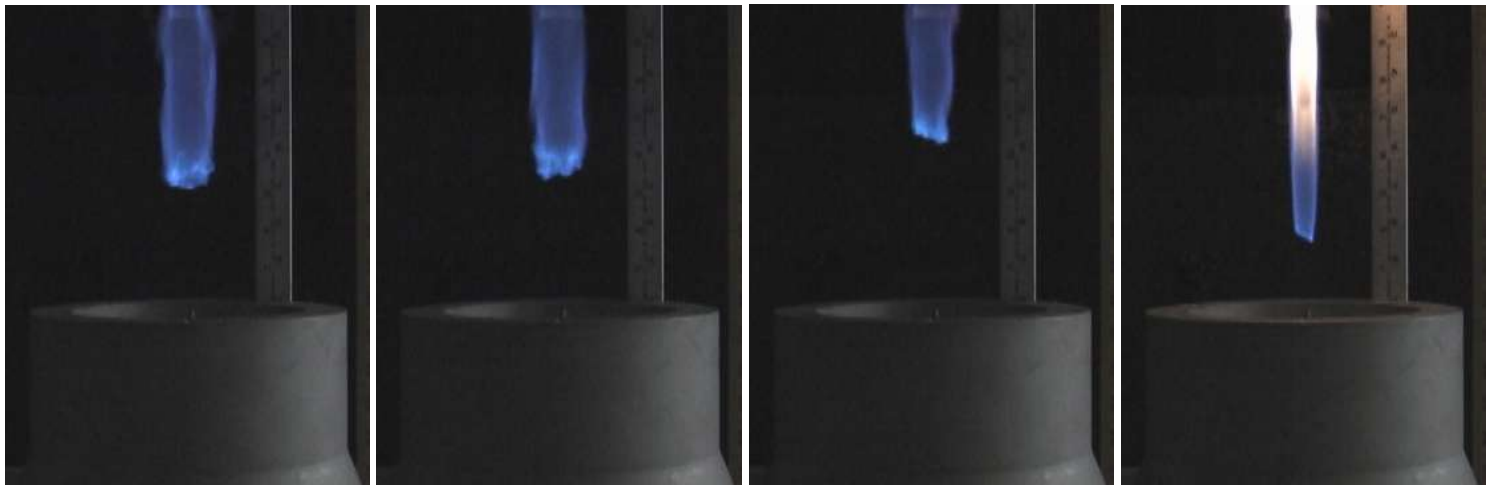

(e) U_0 = 7.76 m/s
h = 8.1 cm

(f) U_0 = 6.43 m/s
h = 8.6 cm

(g) U_0 = 3.52 m/s
h = 11.0 cm

(h) reattaching

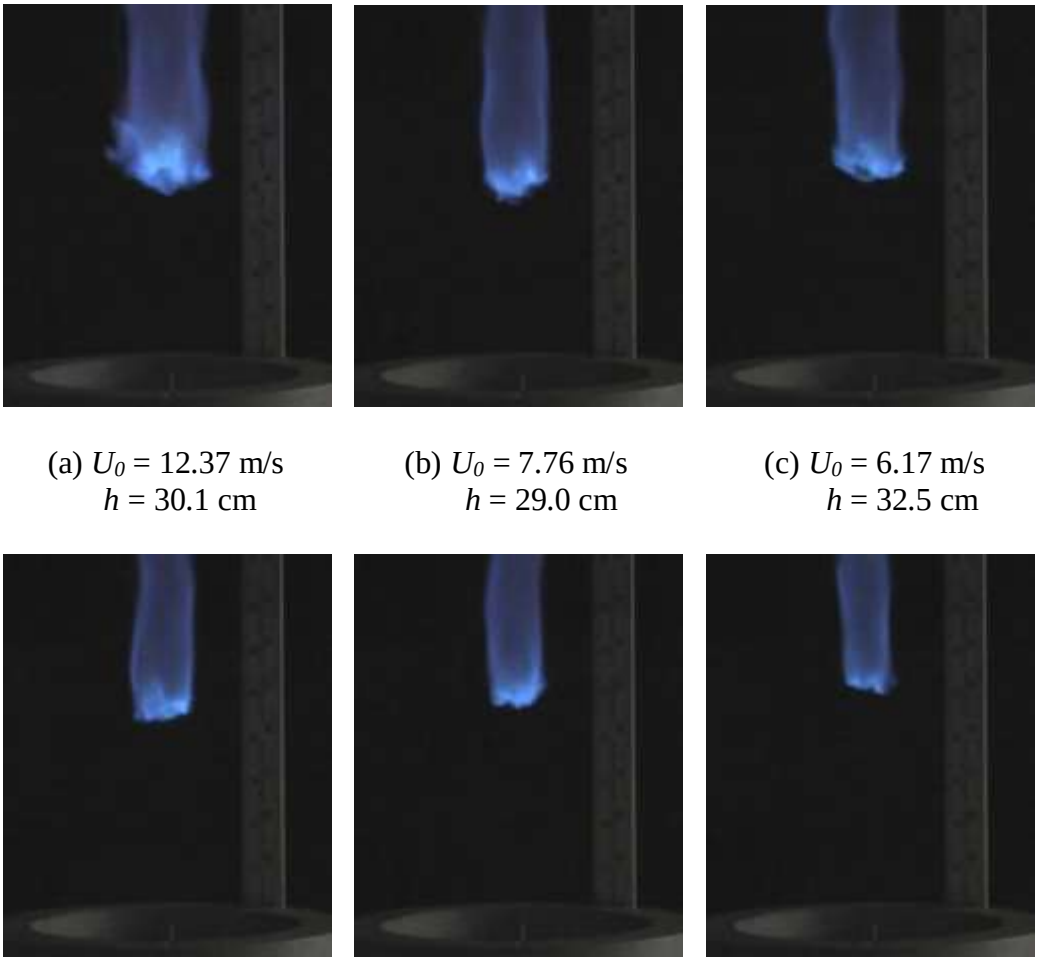

(a) U_0 = 12.37 m/s
h = 30.1 cm

(b) U_0 = 7.76 m/s
h = 29.0 cm

(c) U_0 = 6.17 m/s
h = 32.5 cm

(d) U_0 = 5.09 m/s
h = 34.4 cm

(e) U_0 = 4.05 m/s
h = 36.5 cm

(f) U_0 = 3.00 m/s
h = 38.7 cm

Figure 2.4 Sequence of images of a methane flame with co-flow velocity constant at 0.7 m/s.

2.4 Discussion

To interpret the hysteretic behavior, the stability and characteristics of the flame are further analyzed. While the experiment was designed to allow the flame to stabilize before the height of the flame front was recorded, the stability can be verified using its propagation velocity. In the near field, a flame stabilizes between two and three times the premixed laminar flame speed, S_L (Muñiz and Mungal, 1997). Stabilization at these low velocities is made possible by the deflection of flow caused by the presence of the flame front (Ruetsch *et al.*, 1995). The flow velocity at the stoichiometric contour, U_S, can be approximated as

$$U_S = U_0 Z_S + (1 - Z_S) U_{cf} \tag{2.1}$$

where U_0 and U_{cf} are the fuel and co-flow velocities, respectively, and Z_S is the mixture fraction (Han and Mungal, 2000). Applying this relation to the hysteretic flames gives the average U_S at lift-off as 1.27 m/s ($\approx 3.3 S_L$), at the local minimum as 1.0 m/s ($\approx 2.6 S_L$), and immediately preceding reattachment as 0.72 m/s ($\approx 1.9 S_L$). Though approximations, these calculations affirm that the flame is stable throughout hysteresis and its movement is dictated by the decrease in fuel velocity.

The appearance and width of the flame base are indicators of the turbulence of the flow. A measure of the radius of the flame front, r, in the hysteretic region shows that the radius decreases in each case with the fuel velocity. Figure 2.5 presents the normalized radius values for each co-flow case. As the flame propagates upstream and then recesses

back downstream, its flame front continues to reduce in width. The overall trend seen for each is a proportional relationship with the Reynolds number (Cessou *et al.*, 2004).

Another finding of this work is the shift in lift-off height related to the co-flow velocity. For co-flows of 0.48 m/s and less, the lifted height is never greater than approximately 17 diameters (see Figure 2.2). For co-flows of 0.5 m/s and greater, the heights are not less than about 23 diameters. Further experiments are necessary to develop a clear understanding of this shift, since stable lifted flames can exist in this region. Indeed, the hysteretic behavior of each flame consistently agrees with the lift-off height of each; consequently the lack of data between 17*d* and 23*d* can be assumed to be solely a result of the lift-off mechanism. This behavior could be a consequence of the location of the potential core, even though the lift-off heights exist beyond the potential core region. All height measurements in these experiments were made at the centerline, where the potential core of the co-flowing air would extend the farthest. The potential core, a cone-shaped region extending downstream and bounded by flow instabilities created in the shear layer, is extended in reacting jets due to the density ratio (Clemens and Paul, 1995).

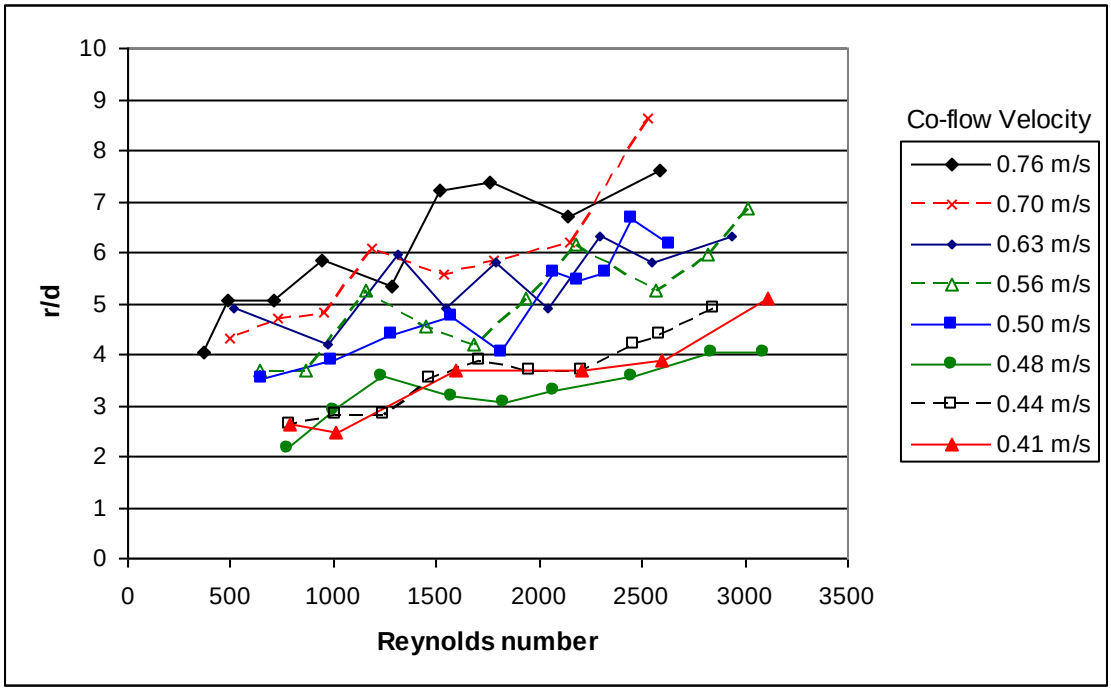

Figure 2.5 The normalized radius, *r/d*, for each case.

Generally, a decrease in the fuel velocity causes an upstream shift in the region that the flame is able to stabilize. Thus, it would seem that the flame would always continue its upstream propagation since the axial velocity is lowered, as is observed for no co-flow and low co-flow velocities (Terry and Lyons, 2006). However, the downstream movement in the hysteretic region with decreasing fuel velocity was observed in all cases of higher co-flow velocities. This observation points to a crossover on the competing effects of the decreased axial velocity field. The stoichiometric mixture required for combustion exists at the fuel/oxidizer boundary whose location is determined by the radial expansion of the jet downstream. Decreasing the fuel rate reduces the spread of the jet downstream resulting in a

flame of smaller radius. At a sufficient velocity, the surrounding co-flow acts to limit radial expansion while simultaneously "pushing" the flammable region downstream.

The directional change between lift-off and reattachment is not observed when the flame burns in quiescent air or in a low co-flow velocity. With a constant co-flow velocity, the relative amount of co-flowing air to fuel increases as the flame moves through hysteresis towards reattachment. Thus, the ratio of co-flow to fuel velocity has been calculated for each of the eight cases to determine a critical point at which conditions allow for the existence of a local minimum during hysteresis. The ratios are evaluated at three locations in the hysteretic behavior: at the moment the flame initially lifts off, at the local minimum, and immediately prior to reattachment. The ratios are plotted versus the co-flow velocity normalized by the fuel pipe diameter in Figure 2.6, along with power curve fits.

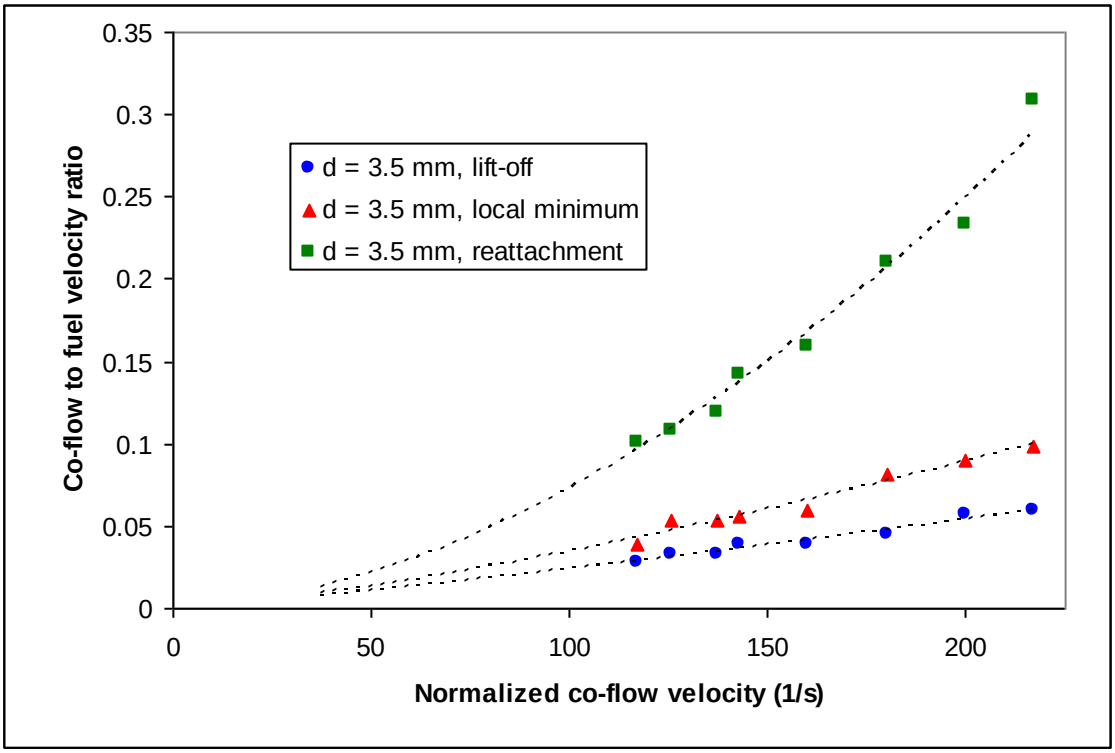

Figure 2.6 The ratio of co-flow velocity to fuel velocity for each case, d = 3.5 mm.

For each case, the co-flow to fuel ratio is highest at reattachment and lowest at lift-off. Since the lift-off and reattachment velocities are not equivalent regardless of the presence of co-flow, the projection of the ratio at reattachment must level off at low co-flow velocities so as not to intercept the projection of the lift-off ratio. From Figure 2.2, it is seen that at lower co-flow velocities, the height of the flame immediately after lift-off and before reattachment is approximately the same. Thus, the same approximate height within the hysteretic region results from two different ratios. The reattachment ratio for these cases is about 3.5 times greater than the lift-off ratio. However, when the co-flow velocity is above

0.50 m/s, the reattachment ratio approaches five times greater than the lift-off ratio at the highest co-flow tested, meaning the reattachment velocity is 0.2 times the lift-off velocity.

The ratio at the local minimum is closer to the lift-off ratio than to the reattachment ratio for all cases in Figure 2.6. Unlike with reattachment, the relationship between the ratios is unaffected by the increase in the co-flow velocity. The jet velocity at the local minimum is approximately 0.625 times the jet velocity at lift-off. No local minimum is observed for low co-flow velocities and so a critical point must exist at which a minimum during hysteresis becomes possible due to the flammable region being moved back downstream. As the projected power curve fits suggest, below a normalized co-flow velocity of 50 s^{-1} the lift-off ratio and the local minimum ratio approach each other and the existence of a local minimum is unlikely.

Figure 2.7 shows results of this analysis being applied to data from Terry (2005) for methane flames in co-flow for pipe diameters of 2.5 mm and 4.0 mm. These data also show a directional change during hysteresis occurred if the normalized co-flow velocity was greater than 50 s^{-1} which supports the conjecture of the current research. In the one case in which the normalized co-flow velocity was 45 s^{-1}, no local minimum occurred. Trends in both sets of data support the idea of a critical point that forecasts a significant change in hysteretic behavior.

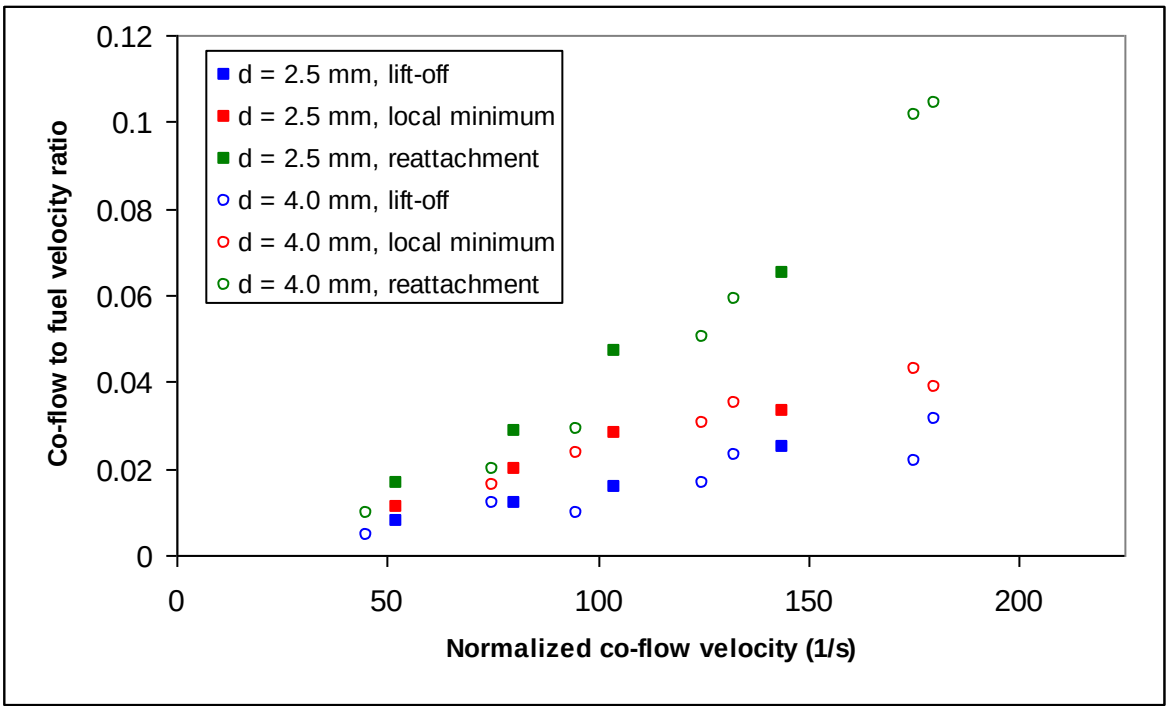

Figure 2.7 The ratio of co-flow velocity to fuel velocity for pipe diameters of 2.5 and 4.0 mm.

2.5 Conclusions

Turbulent methane flames with relatively high co-flow velocities have been studied to determine the effect of co-flow on hysteresis. Within the hysteretic region, a flame can be stable either attached to the burner or lifted for a given jet exit velocity. The results of the current study verify that the presence of co-flow affects the nature of flame stability at low fuel velocities. The new findings reported in the current paper are the following:

1. A flame with co-flow does not steadily decrease in height until the reattachment velocity is reached, but rather is seen to move upstream to a local minimum and then downstream before reattaching. Despite this directional change, the radius of each flame steadily decreases as one would expect, so the reasons for this movement are not fully understood. The formation of the leading-edge flame is theorized to be strongly dependent on the local stoichiometry (Terry and Lyons, 2006). Thus, co-flow velocity would have a strong impact on the height of the flame.
2. A constant of proportionality was calculated to determine the jet velocity at the local minimum from the velocity at lift-off. The magnitude of the co-flow velocity, while important when predicting the existence of a local minimum, does not affect the proportionality constant.
3. Above a critical point defined in terms of the normalized co-flow velocity, enough co-flow is present for entrainment such that the effect of a lower fuel velocity on the flame height is counteracted by a change in the location of the flammable region, resulting in downstream recession before reattachment. Below this critical point, the classic hysteretic behavior is observed in which the flame height decreases with decreasing jet velocity. Data suggest that this change in behavior occurs near a normalized co-flow velocity of 50 s^{-1}.
4. At high co-flow velocities, a stable lifted flame at a low Reynolds number can exist downstream if it is arrived at by hysteresis. The lift-off height of these flames is not indicative of the exact location of the flame front (and maximum heat release) prior to

reattachment. The flame, though appearing laminar, can reach a much greater downstream distance immediately before reattachment than would be possible if not arrived at by hysteresis.

Chapter 3

Leading-Edge Flame Fluctuations in Lifted Turbulent Flames

3.1 Introduction

The mechanisms that govern flame stability can be studied in a system like a lifted turbulent jet flame burning in the presence of co-flowing air. By increasing the fuel or co-flow velocity, an attached flame will lift off the burner and stabilize at a mean lifted height, with a tendency to oscillate axially about that mean position. In numerous industrial applications such as furnaces and burners, the location of the flame base and thus the location of the maximum heat release is an important design element. Flow velocities beyond a critical value result in the flame moving to a region downstream in which the fuel concentration is generally low, and blowout occurs, resulting in the loss of unburned fuel and lower efficiency.

Recent theories on the stability mechanism of lifted flames stem from the premixed model of Vanquickenborne and van Tiggelen (1966), the flamelet extinction model of Peters

(1984, 2000), and the large scale mixing model of Broadwell (1984). Vanquickenborne and van Tiggelen (1966) proposed that the fuel and oxidizer are completely premixed at the lifted flame base and subsequently the flame stabilizes where the stoichiometric mixture is formed. An equilibrium results between the premixed turbulent burning velocity and the flow velocity. The theory of Broadwell (1984) challenges the premixedness model by proposing that lifted flame stabilization depends on the turbulent structures of the nearby unignited flow. Fresh ambient air is reentrained into the diffusion flame and comes into contact with a mixture of hot products and fuel. Molecular diffusion occurs at the strained interface until the entire mixture is homogeneous. The flamelet extinction model of Peters (2000) suggests that the stability of the lifted flame is governed by the strain rates within laminar diffusion flamelets. At certain jet exit velocities, the high strain rates from turbulent eddies cause extinction of the flamelets near the burner resulting in the flame stabilizing at a lifted height downstream.

Numerous studies have investigated the effect of fuel exit conditions on the lift-off height of methane flames both computationally (Müller *et al.*, 1994, Montgomery *et al.*, 1998, Kumar *et al.*, 2007) and experimentally. The increase in liftoff height with increasing jet exit velocity has been observed in many experiments (Muñiz and Mungal, 1997, Brown *et al.*, 1999, Lee *et al.*, 1997, Kalghatgi, 1984). Results of cinema-PIV (particle image velocimetry) experiments on lifted flames performed by Upatnieks *et al.* (2004) suggest that at low Reynolds numbers, edge flame extinction plays the central role in flame stabilization. The turbulence level and the laminar flame propagation speed were not found to be strongly

linked. PIV experiments by Schefer and Goix (1998) at higher Reynolds numbers show that the flow velocities at the stabilization point are below the turbulent flame propagation speed which challenges the theory of Vanquickenborne and van Tiggelen (1966).

Areas downstream, such as at the end of the potential core region and in the far-field, are typically defined as functions of the fuel pipe diameter. The jet development region is considered to be in the range of 4 to 5 pipe diameters downstream, and the fully-developed region is beyond 12 diameters (Cessou *et al.*, 2004). Similarity solutions for the jet velocity are valid beyond 20 diameters downstream (Wygnanski and Fiedler, 2006). Kalghatgi (1984) found that the height of a lifted flame is independent of the pipe diameter in the far-field (approximately 20 diameters). Results from Terry and Lyons (2006) and Cessou *et al.* (2004) show that the heights of turbulent flames (particularly in the near-field) are conditional on the pipe diameter, with a larger diameter resulting in lower positions.

An essential aspect to understanding flame stabilization is the characterization of the magnitude of the axial fluctuations of lifted flame reaction zones (Hammer, 1993). Despite being globally stable, the lifted flame is observed to propagate upstream and recess downstream aperiodically (Hammer and Roshko, 2000). The fluctuations have been observed as increasing with increasing height (Muñiz and Mungal, 1997). Kelman *et al.* (1998) investigated this phenomenon with laser imaging of the temperature and concentrations at the flame base. They conclude from their research that fluctuations result from upstream premixed flame propagation with large-scale fluid structures producing downstream movement. Also, Watson *et al.* (2000) found that CH-PLIF leading-edge

structures facilitated the propagation into the unburned fuel-air mixture. This connection between height fluctuations and large structures in the flow field is consistent with the work of other researchers (Muñiz and Mungal, 1997, Miake-Lye and Hammer, 1988, Chao *et al.*, 2002).

The current paper discusses an experimental study of the fluctuations of a lifted methane-air jet reaction zone with various co-flow velocities. The reaction zone liftoff-height fluctuations are studied to shed light on the stabilization mechanisms that prevent flames from receding downstream and extinguishing. Rather than focus on detailed instantaneous images of reaction zones, the current work has utilized time sequences of the reaction zone to determine temporal oscillatory behavior. Various combinations of fuel and co-flow velocities with Reynolds numbers from approximately 3,000 to 10,000 are used to study lifted flames at a wide range of downstream locations for two different fuel pipe diameters. Details of the flame position and the change in height with time are provided and interpretations of the data are discussed.

3.2 Experimental Setup

The experiments were performed at the Applied Energy Research Laboratory on the campus of North Carolina State University. The jet flame burner consisted of a fuel pipe that is concentric with a pipe of 150 millimeter (mm) diameter through which co-flowing air is released (Figure 3.1). The air co-flow velocity was measured with a TSI Veloci-calc model

8345 anemometer. For this experiment, fuel tubes of 3.5 mm and 5.0 mm inner diameter, with lengths sufficient to create fully-developed turbulent flow, were used to deliver 99% pure methane to the jet. An Advanced Specialty Gas Equipment rotameter (tube FM4336) was employed to measure the volume flow rate, from which the average flow velocity across the pipe exit was ascertained.

Images of the oscillating flame were made with a Panasonic Model PV-GS300 CCD video camera producing thirty frames per second and were post-processed. Figure 3.1 contains two illustrations depicting lifted flames at different moments in time. For each, the instantaneous flame height, h', is herein defined to be the axial distance from the jet exit to the flame base, which is the furthest point upstream at which flame luminosity is detected by the camera. The flame front is in the shape of a ring in the x-y-z plane about which height fluctuations occur. The current research, using two-dimensional images, records the height irrespective of its radial location and is not intended to represent fluctuations in the flame ring that can indicate the passage of large-scale structures in one section of the flow.

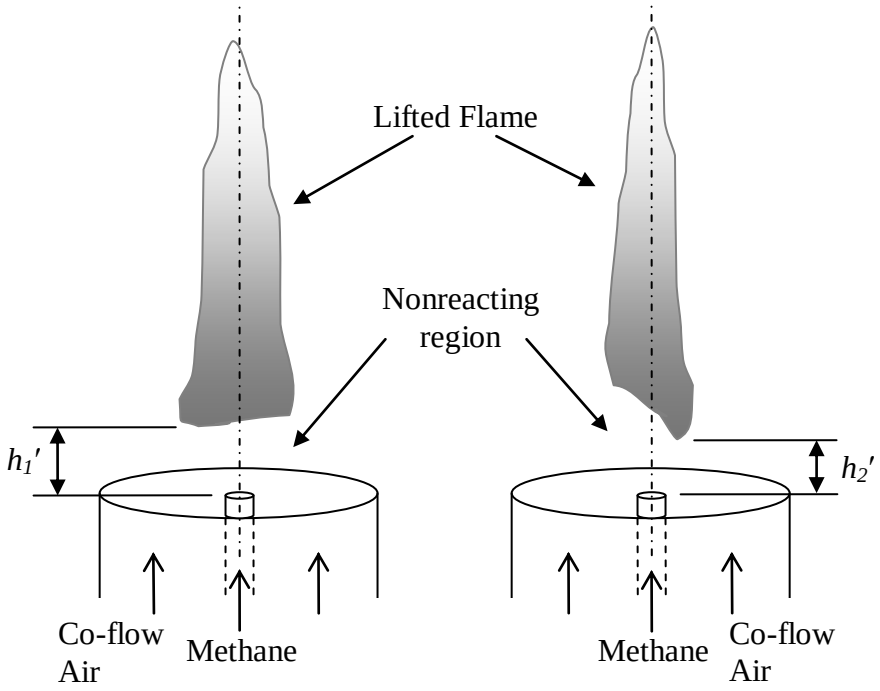

Figure 3.1 Two examples of a lifted methane flame. The fuel is delivered from a pipe that is surrounded by co-flowing air. h' is the instantaneous axial distance from the fuel exit to the lifted flame base.

3.3 Results and Discussion

Numerous cases were studied to determine characteristics of fluctuations with respect to downstream location and flow velocities. Data were obtained from video imaging of the flames subsequent to the flame reaching steady-state behavior. Sequential images of a lifted flame with no co-flow present are shown in Figure 3.2. Figure 3.3 shows the temporal position of the flame for five different fuel exit velocities with no co-flow present and a fuel

pipe diameter, *d*, of 3.5 mm. The instantaneous flame height was measured from the video image once per a time step of approximately 0.167 seconds. This data was used to produce the trace of the flame at each fuel velocity shown in the figure. The fluctuations of the flame in each case are clear from the peaks and valleys in the traces (see also Figure 3.4 and Figure 3.5), but for the time interval studied, no periodic behavior is evident (Hammer and Roshko, 2000). The data was filtered through a fast Fourier transform algorithm and the results showed no peaks at any frequency. The results agree with those of Hammer (1993) whose analysis of the temporal height with a power spectrum also showed no peaks present. Similar data acquired for all of the cases with both pipe diameters confirms the irregularity.

Figure 3.2 Sequenced images (Δt = 1/30 sec) of flame at U_0 = 22.6 m/s, U_{cf} = 0.0 m/s, d = 3.5 mm.

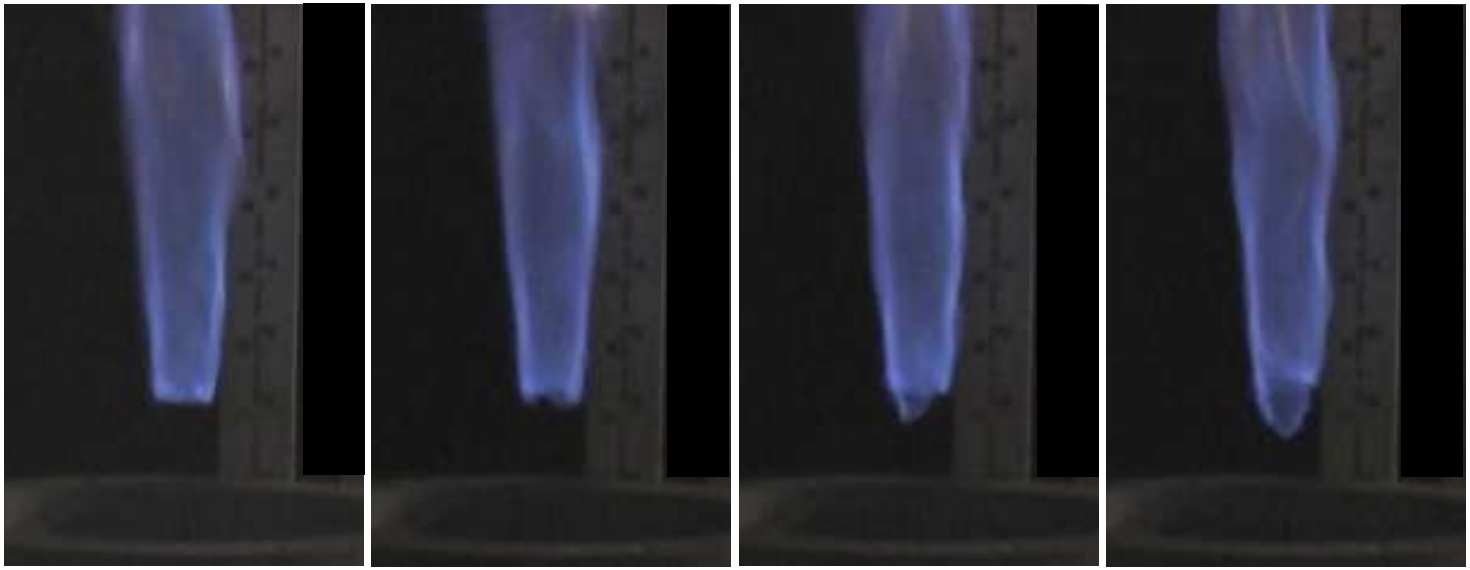

(a) h' = 4.11 cm (b) h' = 3.87 cm (c) h' = 3.27 cm (d) h' = 2.78 cm

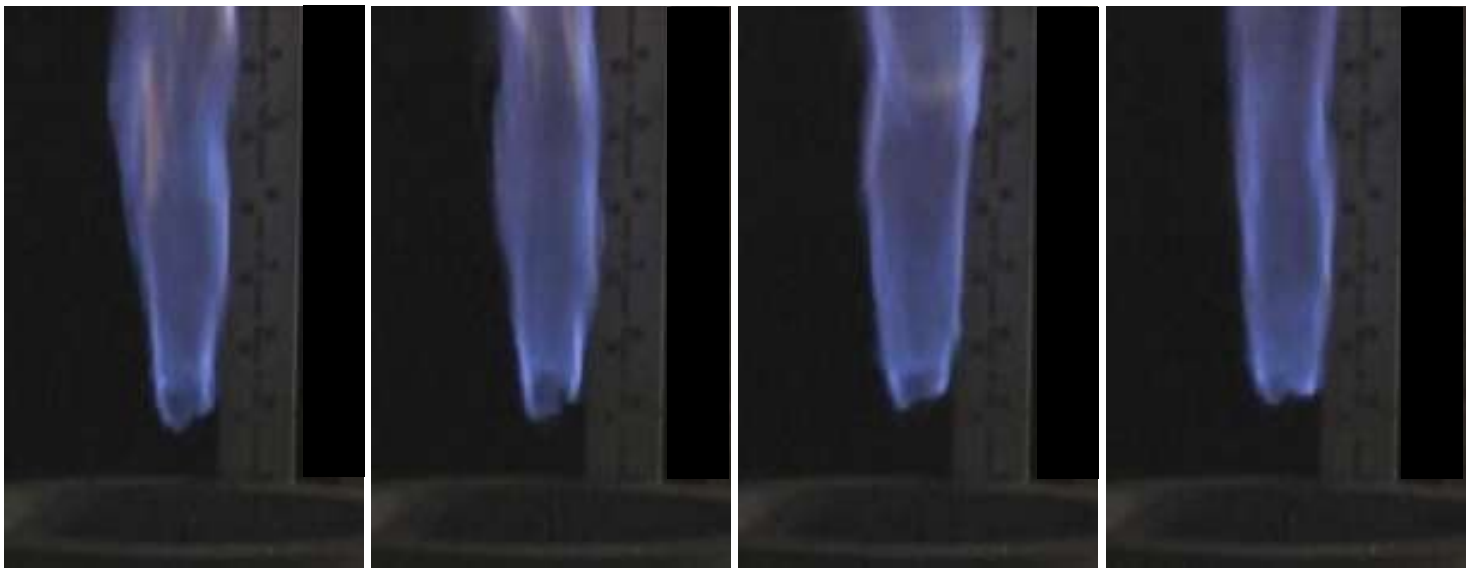

(e) h' = 3.14 cm (f) h' = 3.39 cm (g) h' = 3.87 cm (h) h' = 4.11 cm

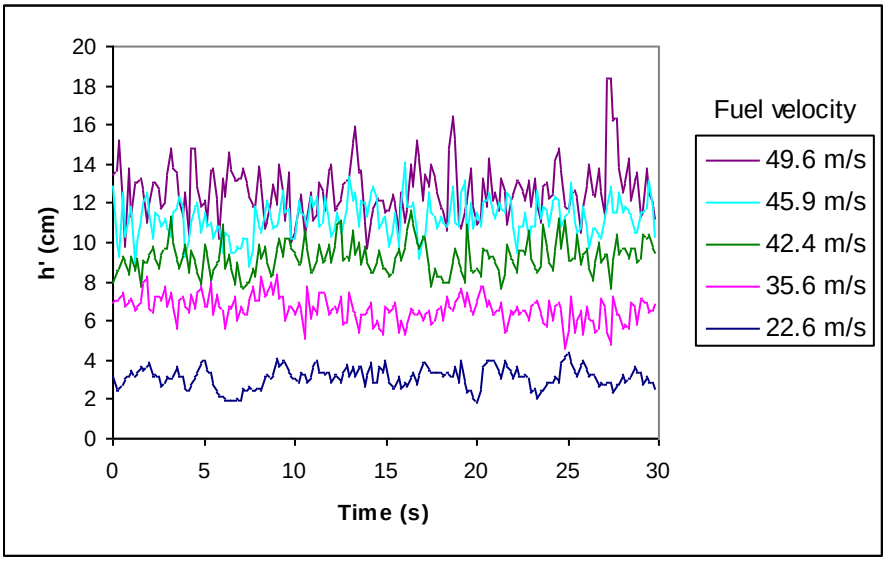

Figure 3.3 Height fluctuations during a 30 second interval for five fuel velocities with no co-flow present, 3.5 mm pipe diameter.

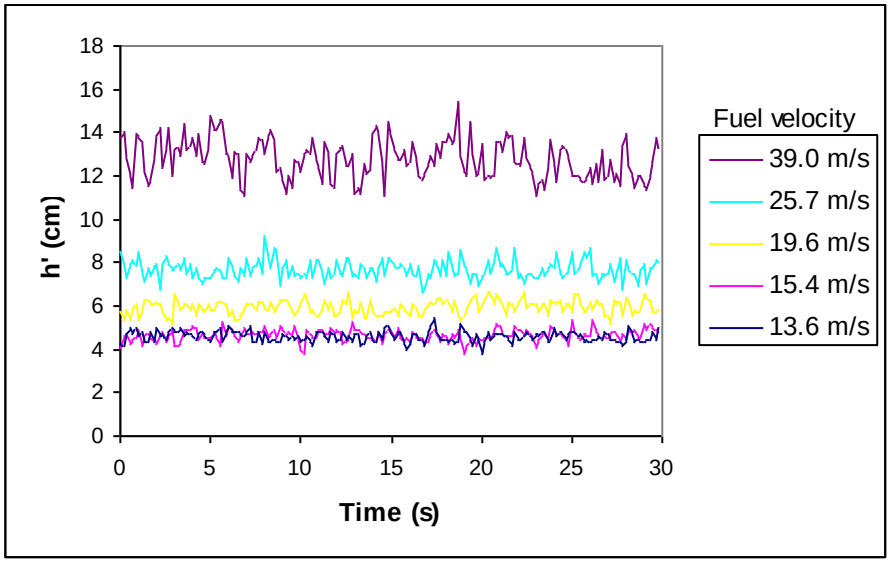

Figure 3.4 Height fluctuations during a 30 second interval for five fuel velocities with 0.35 m/s co-flow, 3.5 mm pipe diameter.

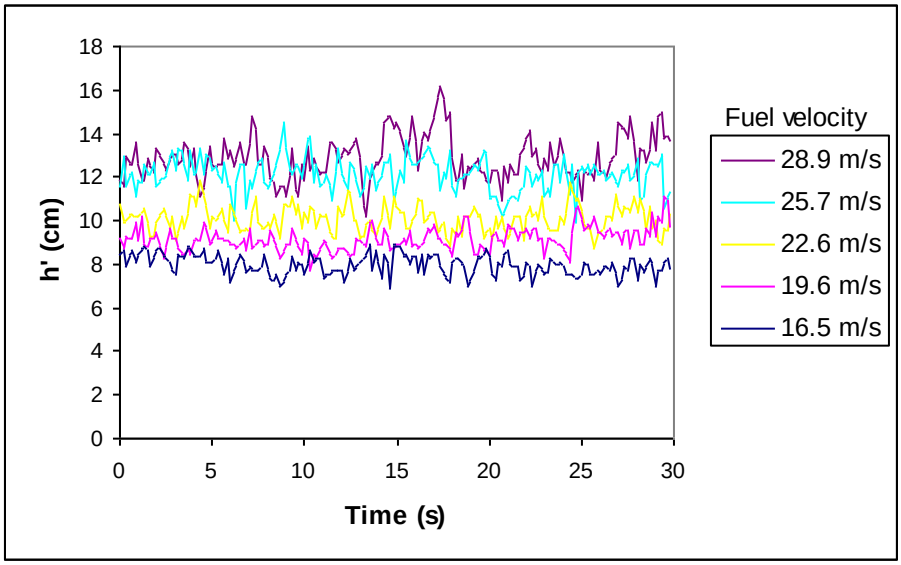

Figure 3.5 Height fluctuations during a 30 second interval for five fuel velocities with 0.52 m/s co-flow, 3.5 mm pipe diameter.

The time interval of thirty seconds was deemed adequate to capture the representative fluctuations and include the trends of the flame movement. The average height was calculated for several time intervals with the same time step. The percent difference between an interval of 15 seconds and one of 30 seconds was nearly 1%. The percent difference decreased to about 0.2% with an interval of 25 seconds. Thus, due to the convergence of the values, an interval of 30 seconds was used for this research. While the smallest possible time step for this experiment is 0.033 seconds, a time step of 0.167 seconds gives a percent difference of less than 0.5%.

For each fuel tube, five different fuel exit velocities were used for each of three predetermined co-flow velocities. The range of co-flow and fuel velocities chosen allowed

for numerous cases to exist as turbulent lifted flames beyond the hysteresis region (Terry and Lyons, 2006). The instantaneous height from each video image was used to determine the average height for each flow velocity combination. Table 3.1 provides the data for each case studied and the calculated average lifted height. The compilation of data shows that for a given co-flow velocity, the height increases as the fuel velocity increases. In addition, the presence of co-flow tends to move the lifted height further downstream. If one compares two flames from the small pipe for 22.6 m/s fuel velocity, the average height with no co-flow present is 3.12 cm, yet with 0.52 m/s co-flow velocity it is 10.09 cm. Similarly, for the large pipe and a 24.3 m/s fuel velocity, the height increases from 4.21 cm to 16.82 cm with the addition of 0.64 m/s co-flow velocity.

Table 3.1 Fuel velocities used for each pipe diameter and co-flow velocity. The average height for each case is also provided.

Pipe diameter, d = 3.5 mm

Co-flow velocity, U_{cf} = 0.0 m/s					
Fuel velocity, U_0 (m/s)	22.6	35.6	42.4	45.9	49.6
Average height, h (cm)	3.12	6.62	9.22	11.23	12.67
Co-flow velocity, U_{cf} = 0.35 m/s					
Fuel velocity, U_0 (m/s)	13.6	15.4	19.6	25.7	39.0
Average height, h (cm)	4.60	4.64	5.93	7.68	12.77
Co-flow velocity, U_{cf} = 0.52 m/s					
Fuel velocity, U_0 (m/s)	16.5	19.6	22.6	25.7	28.9
Average height, h (cm)	7.96	9.15	10.09	12.12	12.89

Pipe diameter, d = 5.0 mm

Co-flow velocity, U_{cf} = 0.0 m/s					
Fuel velocity, U_0 (m/s)	14.2	19.9	24.3	25.4	32.9
Average height, h (cm)	1.05	2.15	4.21	4.71	9.00

Table 3.1 Continued

Co-flow velocity, U_{cf} = 0.41 m/s					
Fuel velocity, U_0 (m/s)	13.2	16.8	23.6	28.8	33.9
Average height, h (cm)	5.58	6.51	9.95	11.71	14.45
Co-flow velocity, U_{cf} = 0.64 m/s					
Fuel velocity, U_0 (m/s)	11.1	15.8	19.1	24.3	28.5
Average height, h (cm)	11.36	13.42	14.99	16.82	16.31

Notable in the above data table is the impact of even a relatively small co-flow velocity on the flame's height. A number of papers have included experiments with co-flowing air and have observed its significant effect on flame behavior (Muñiz and Mungal, 1997, Lee *et al*., 2003, Montgomery *et al*., 1998). For the cases with co-flow, the co-flow velocity is at most 5.8% of the fuel velocity and in most cases less than 3%. Han and Mungal (2000) developed an equation for the stoichiometric contour velocity, U_S, from the governing equations for a Schmidt number of unity and a uniform pressure. This equation,

$$U_S = Z_S U_0 + (1 - Z_S) U_{cf} \qquad 2.1$$

weights the jet exit velocity, U_0, by the stoichiometric mixture fraction, Z_S, which means the co-flow velocity, U_{cf}, is more heavily weighted in the calculation. Thus a small co-flow velocity can greatly impact the axial velocity at the stoichiometric contour of the flame.

The effect of the flow on the lifted height is evident in Figure 3.6(a) and (b) which plot the change in average height due to jet exit velocity for each co-flow velocity and pipe diameter. As the fuel velocity increases, the average height generally increases, for a given co-flow. For the same approximate U_0, the presence of co-flow moves the stable height downstream. The height change with U_0 per co-flow velocity is linear for the majority of

cases, with some exceptions at the upper and lower limits (an observation also noted in Cessou *et al.* (2004)). Also shown in Figure 3.6(a) and (b) are the maximum oscillation amplitudes observed for each case, designated by vertical bars, both upstream and downstream of the average height. Although the amplitude of fluctuations increases with downstream location, the presence of co-flow reduces the amplitude for a given average lifted height. Furthermore, the maximum oscillation amplitude during downstream recession is seen to be equal to or greater than the maximum during upstream propagation with few exceptions.

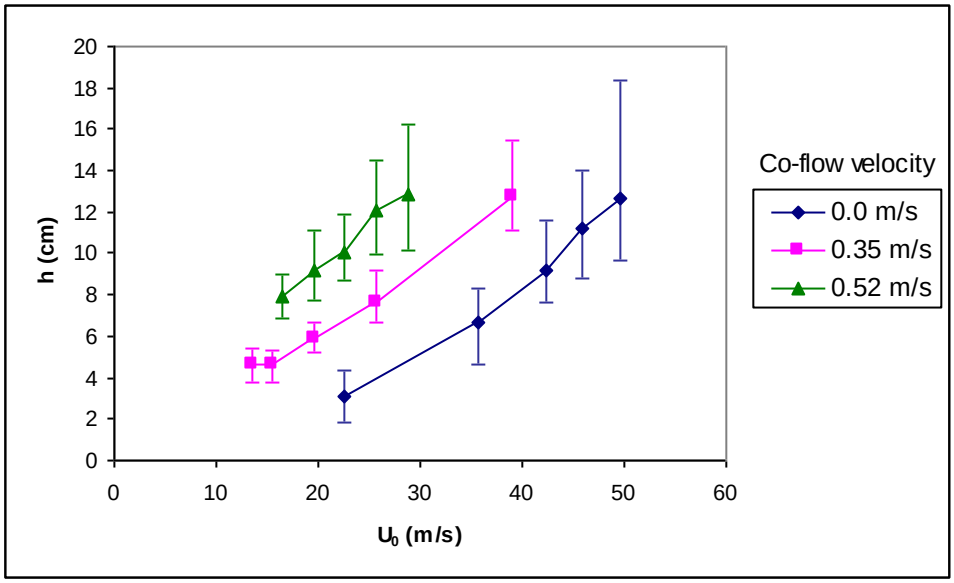

(a) 3.5 mm pipe diameter

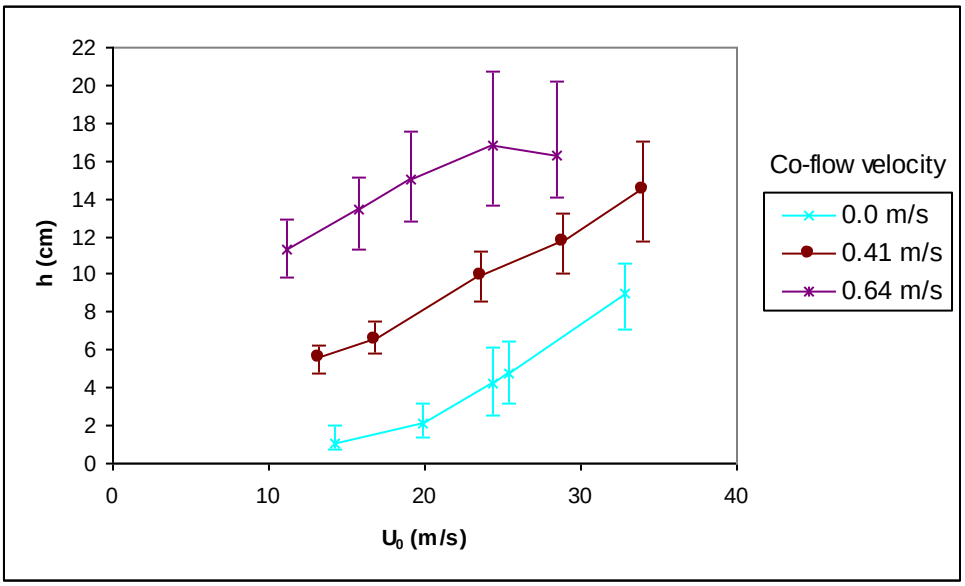

(b) 5.0 mm pipe diameter

Figure 3.6 Average height for each set of flow velocities for the (a) small pipe and (b) large pipe. The vertical bars indicate the greatest oscillation amplitudes observed both upstream and downstream.

Histograms of the normalized height fluctuations for each case per co-flow velocity serve to illuminate the likelihood of the flame at any given instant of time existing near the average height. Figure 3.7 contains data for the small pipe with no co-flow velocity (the same data used in Figure 3.3). The graph shows the probability (in terms of percentage) that the instantaneous height will exist within a particular bin, each 0.2 cm in size. The average height for each case is also provided. Thus for the case with 22.6 m/s fuel velocity, h' was within the bin containing the average height (about 3.12 cm) approximately 20% of the time. As the fuel velocity increases, the oscillation amplitudes increase and the maximum bin percentage decreases; however, the average height is within or close to the most frequented bin. For 49.6 m/s fuel velocity, the maximum percentage is only 10%. Cessou *et al.* (2004) found that pdfs (probability density functions) of the height were symmetric for flames stabilized in medium and high velocity domains. Histograms of the present data exhibit some symmetric behavior but clearly show the tendency of downstream fluctuations to be greater than upstream fluctuations. Figure 3.8 and Figure 3.9 show histograms for the cases with co-flow velocities of 0.35 m/s and 0.52 m/s, respectively. The presence of co-flow reduces the range of fluctuations and therefore increases the likelihood that the instantaneous height will be near the average height.

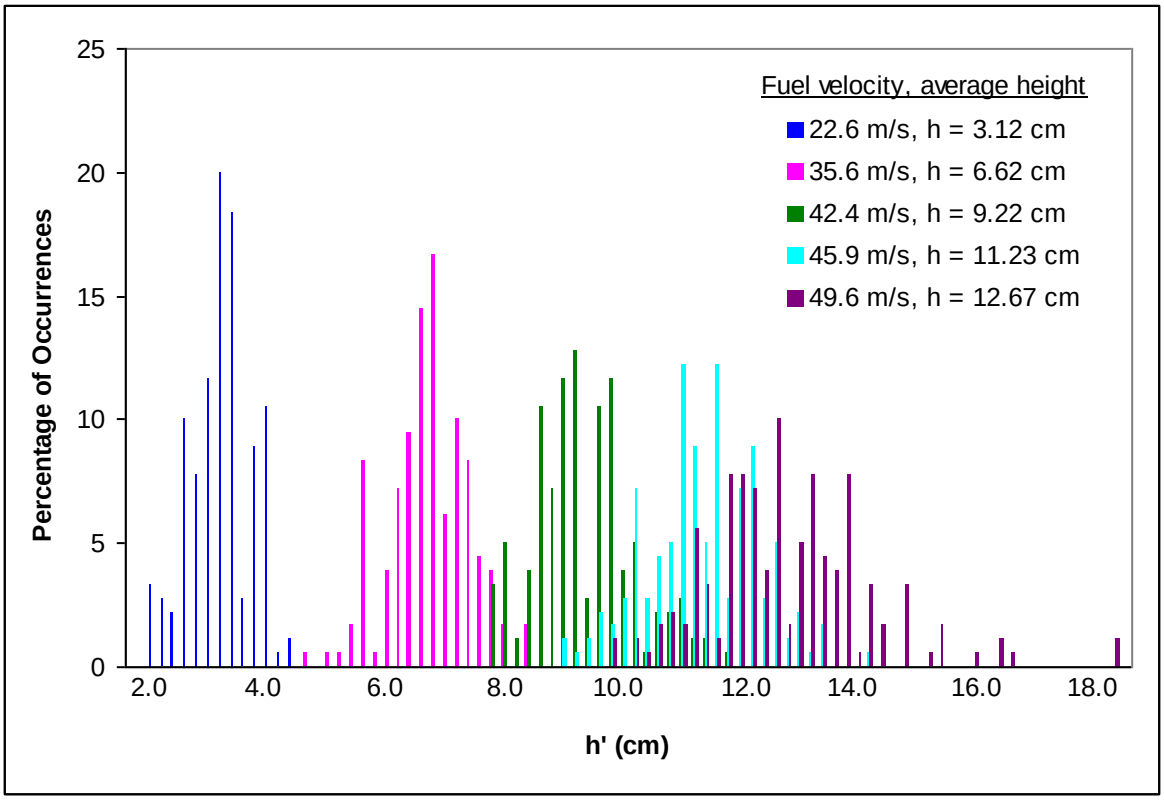

Figure 3.7 Histogram of height fluctuations for 5 cases with no co-flow present, 3.5 mm pipe diameter.

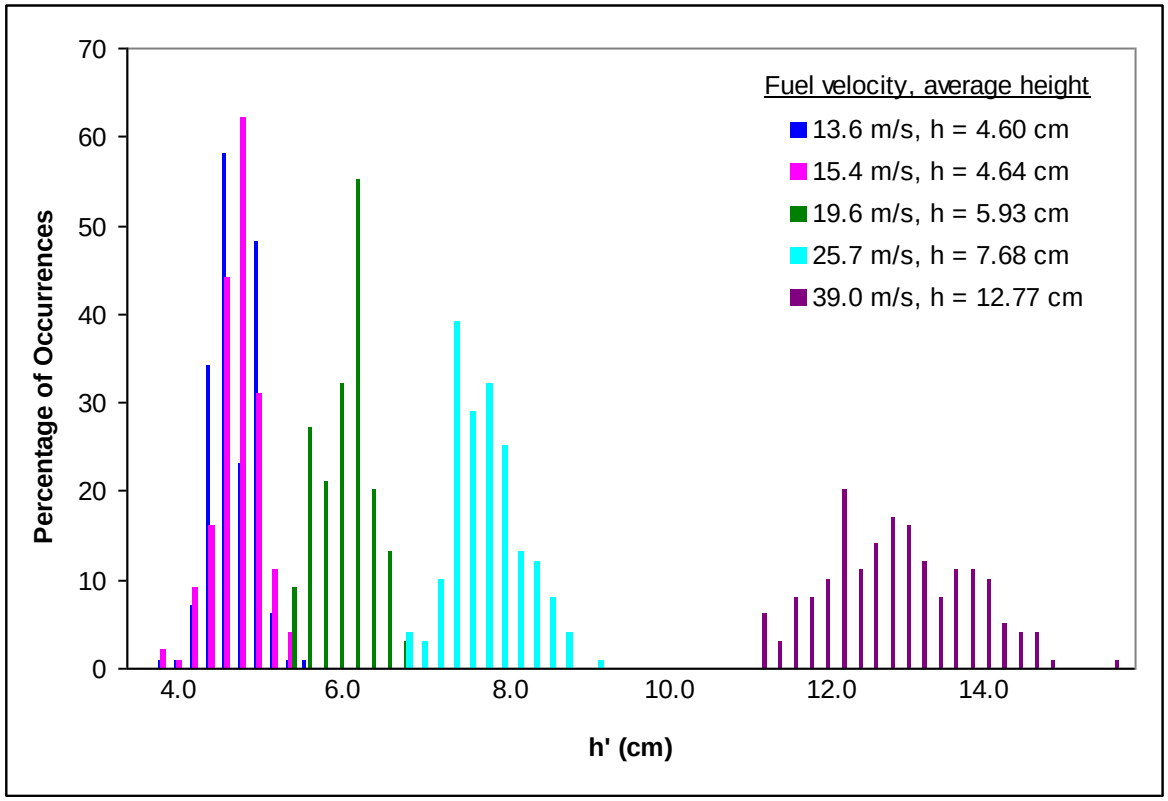

Figure 3.8 Histogram of height fluctuations for 5 cases with 0.35 m/s co-flow, 3.5 mm pipe diameter.

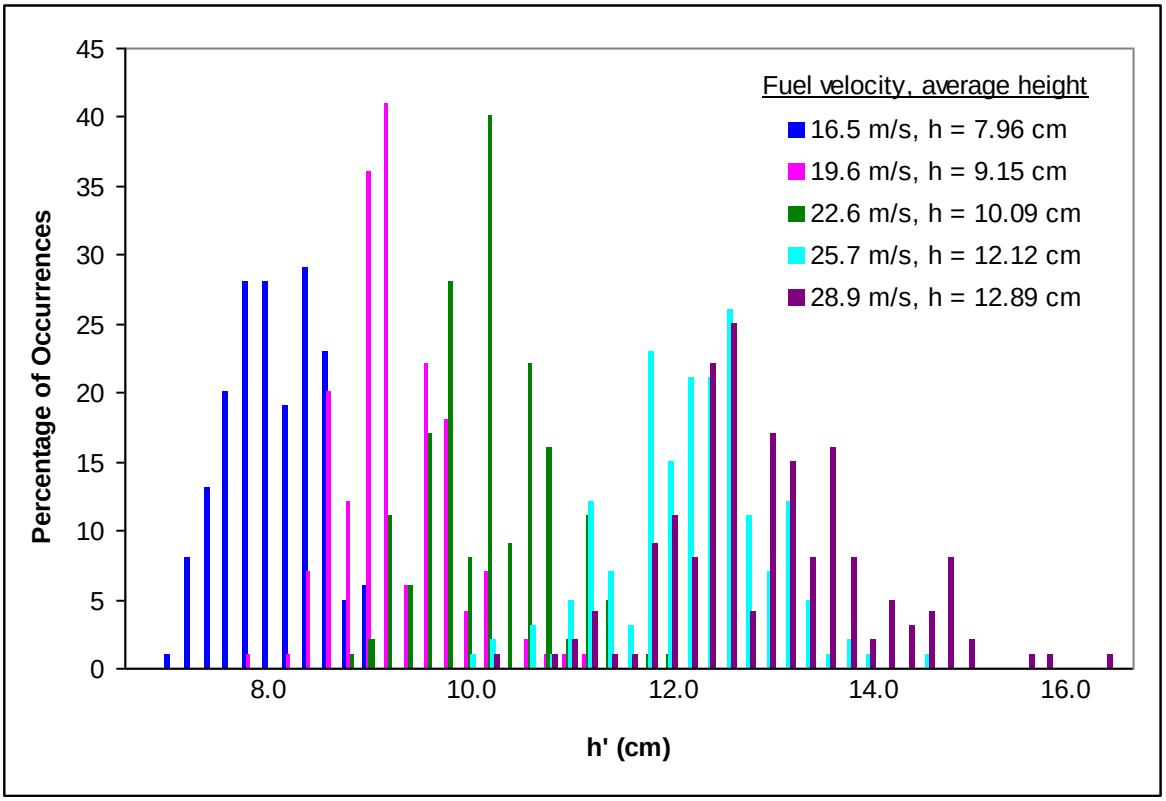

Figure 3.9 Histogram of height fluctuations for 5 cases with 0.52 m/s co-flow, 3.5 mm pipe diameter.

Knowing the extent to which turbulence influences flame height and fluctuations is vital to understanding the mechanisms controlling flame location. All of the cases reported in this chapter are in turbulent flow regimes, with the Reynolds numbers based on exit conditions ranging from around 2,800 to 10,700. Figure 3.10 shows that the normalized average heights, *h/d*, increase with increasing Reynolds number though the large pipe data produces lines with a smaller slope. Also, for comparable co-flow velocities, *h/d* is less when the large pipe is used. From the figure, a normalized height of 25 can be achieved by

flows with Reynolds numbers anywhere between 4,000 and 9,000. Thus, the same height with no co-flow present can also be achieved with a high co-flow velocity but lower Reynolds number. Since the Reynolds number is indicative of the amount of viscous dissipation, these results suggest that the downstream location at which a flame stabilizes is not strongly affected by the viscous dissipation. A certain amount of turbulence does not translate to the flame being far downstream as one would expect, but rather the flow velocities dictate the height.

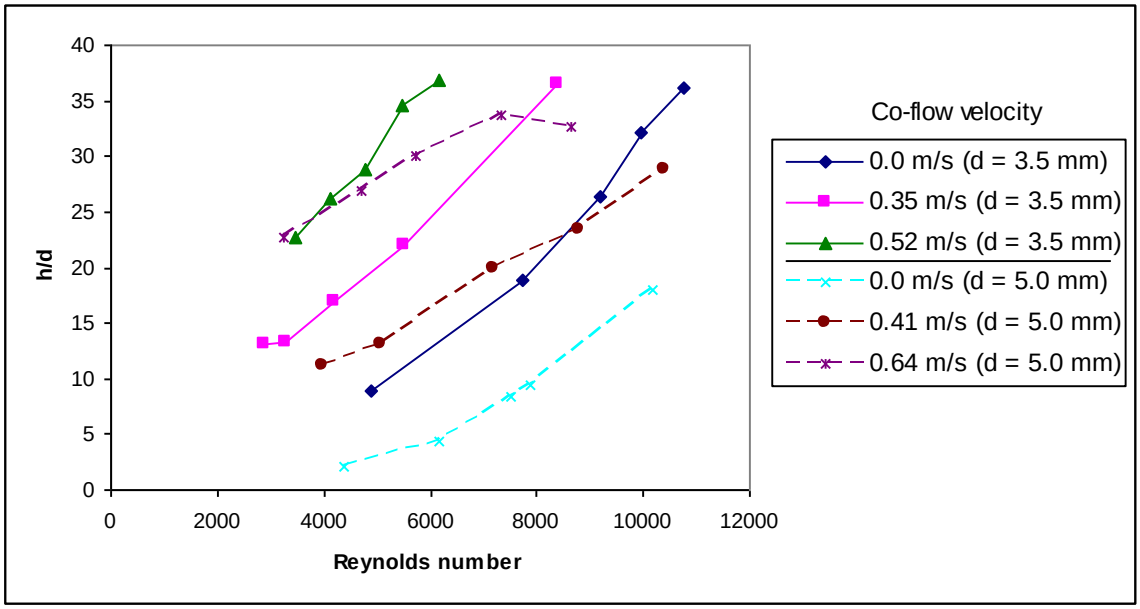

Figure 3.10 Average height normalized by the pipe diameter for each set of flow velocities. The smaller pipe data is indicated by solid lines and the larger pipe data by dashed lines.

Generally, as seen in Figure 3.10, the lifted height of a flame at a particular Reynolds number is not consistent. Thus, an effective jet velocity utilizing the density ratio helps to better relate the lifted height to flow velocities. As Montgomery *et al.* (1998) and Kumar *et al.* (2007) discussed, the effective jet velocity is calculated using a relation from Kalghatgi (1982) as:

$$U_{eff} = U_0 + C\sqrt{\rho_{cf}/\rho_0}\,U_{cf} \qquad 3.1$$

in which U_{eff}, U_0, and U_{cf} are the effective, fuel, and co-flow velocities, respectively, and ρ_{cf} / ρ_0 is the ratio of the co-flow to fuel densities. The constant C is chosen such that the data collapses to a linear relation. When C = 40 (the value also used in Kumar *et al.* (2007)), the height data from both size pipes collapses and allows for the prediction of the flame lifted height, as shown in Figure 3.11.

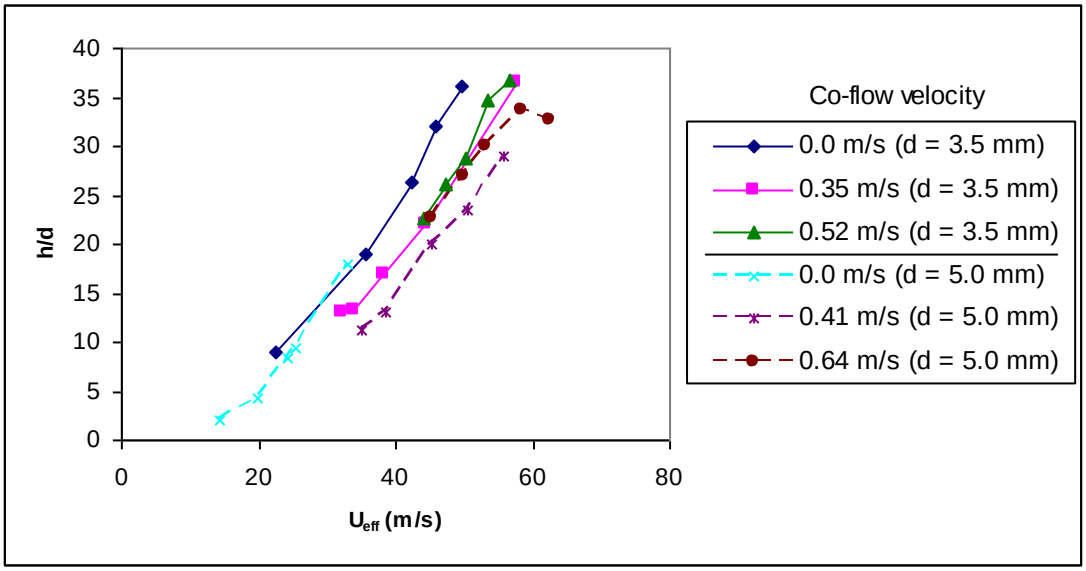

Figure 3.11 Normalized height plotted with the effective velocity, $C = 40$. The smaller pipe data is indicated by solid lines and the larger pipe data by dashed lines.

The height fluctuations, h', are normalized by the average height, h, and plotted against h/d in Figure 3.12. For each case, the maximum oscillation amplitude downstream is marked with a solid symbol and the maximum upstream is marked with the outline of the same symbol. Usually, the flame recessed further downstream than it propagated upstream, but this was not always observed. For flames stabilized at $h < 10d$, the fluctuations were generally above $0.3h$. Downstream of this region where the turbulence can be assumed to be fully developed, the oscillation behavior was more uniform with data showing $h' \leq 0.3h$. Approaching blowout ($h > 35d$) the fluctuations were not significantly greater except for the case with no co-flow present. However, results published by Hammer and Roshko (2000) of height fluctuations for several fuels at high Reynolds numbers showed that when normalized

by height, the height fluctuations increased with height and as blowout was approached. They also found that the ratio *h′/h* did not significantly change with pipe diameter, a finding supported by the current work.

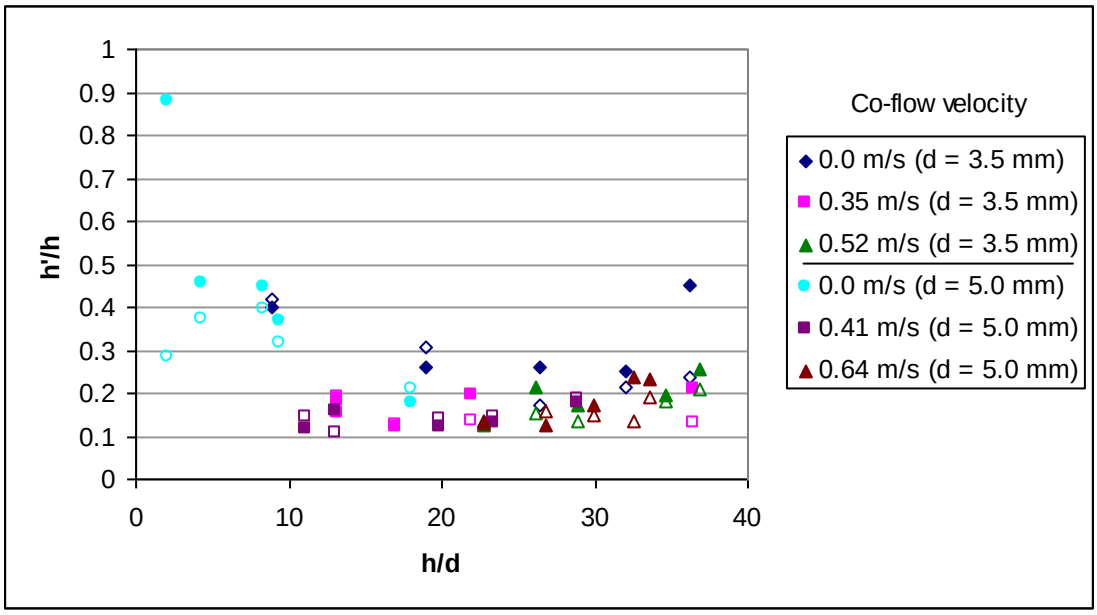

Figure 3.12 Height fluctuations normalized by the average height for each case. Because oscillation fluctuations are not generally symmetric about the average height, the greatest downstream *h′* (marked by a solid symbol) and the greatest upstream *h′* (marked by a symbol outline) for each case are shown.

3.3.1 Rate of Fluctuations

Using the heights from images taken during the thirty seconds of flame burning, the change in height with respect to time was examined. This oscillatory rate, *dh′/dt*, uses a lab

frame of reference and is positive for downstream recession. Because the radial flame position was not noted with the height, dh'/dt has only an axial component. The root mean square of dh'/dt (found with a backward differencing algorithm) was plotted with the Reynolds number for both fuel pipes to establish the relationship between the oscillatory rate and the amount of turbulence (Figure 3.13(a) and (b)). The data shows a mostly linear trend except that the data from the small pipe shows a sharp increase in dh'/dt above $Re = 8500$. This change is not seen as plainly in the large pipe data. While flames at $Re > 8500$ can be approaching blowout, Figure 3.10 shows that stabilized flames exist at $Re \geq 10{,}000$. Thus, the abrupt change of dh'/dt above $Re = 8500$ in Figure 3.13(a) is not necessarily explained by the flames' proximity to blowout.

Upatnieks *et al.* (2004) used cinema-PIV to study turbulent flames and found that the propagation of the flame base was close to the laminar flame speed. They surmised that streamline divergence at the flame front and not turbulence intensity is the primary factor in lifted height for conditions in which $Re < 8500$. Also, the propagation speed was not clearly linked to the passage of large eddies. Thus, the data of Upatnieks *et al.* (2004) and of the current study support the concept of edge-flames more strongly than turbulent flame propagation theories that are more likely relevant at $Re > 8500$.

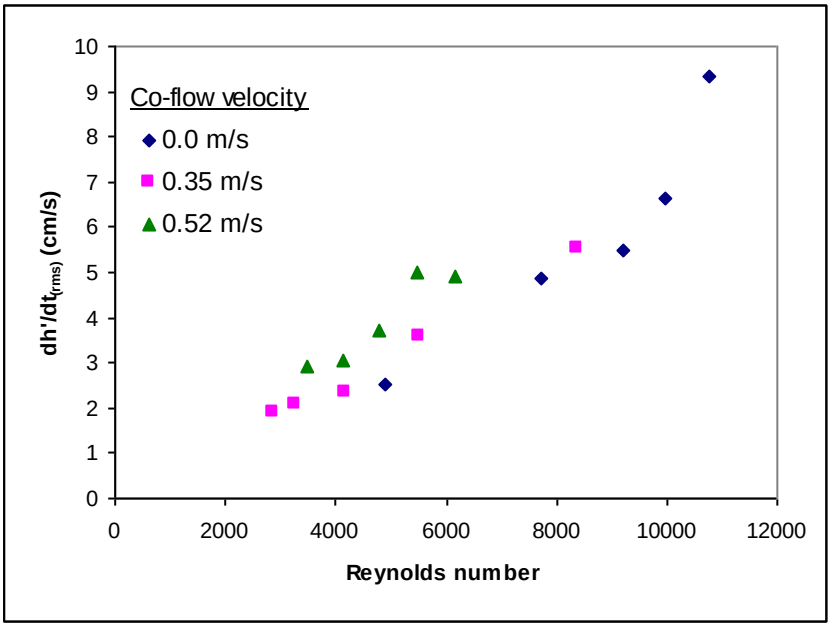

(a) 3.5 mm pipe diameter

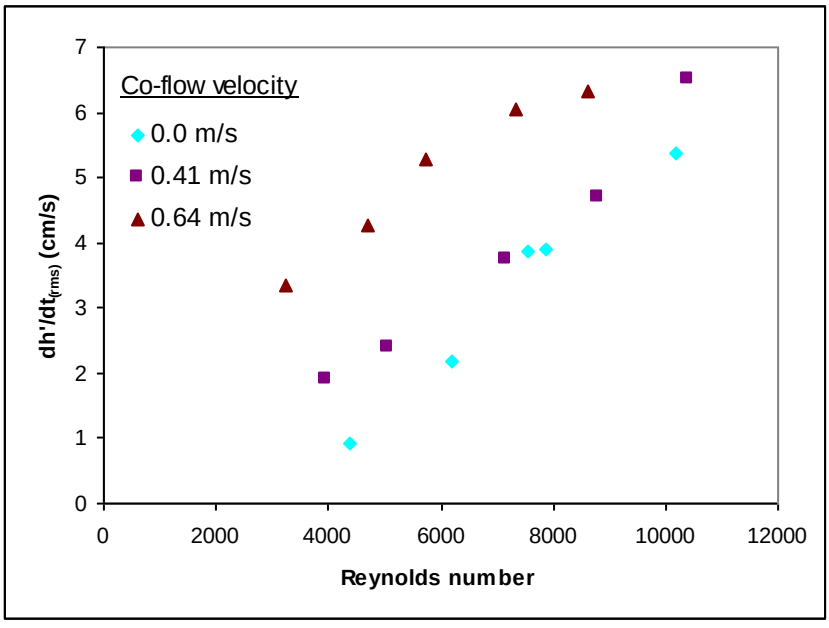

(b) 5.0 mm pipe diameter

Figure 3.13 RMS of *dh'/dt* for the (a) small pipe and (b) large pipe.

While the normalized amplitude of fluctuations appears to be independent of downstream location except in the areas near the burner and approaching blowout (as seen in Figure 3.12), the oscillatory rate is somewhat correlated with height. Figure 3.14 shows that the oscillatory rate increases as the normalized average height increases. However, at a given height, *dh'/dt* is less when co-flow is present; suggesting that the presence of co-flow has a greater effect on the oscillatory rate throughout the entire flowfield than it does on the normalized amplitude.

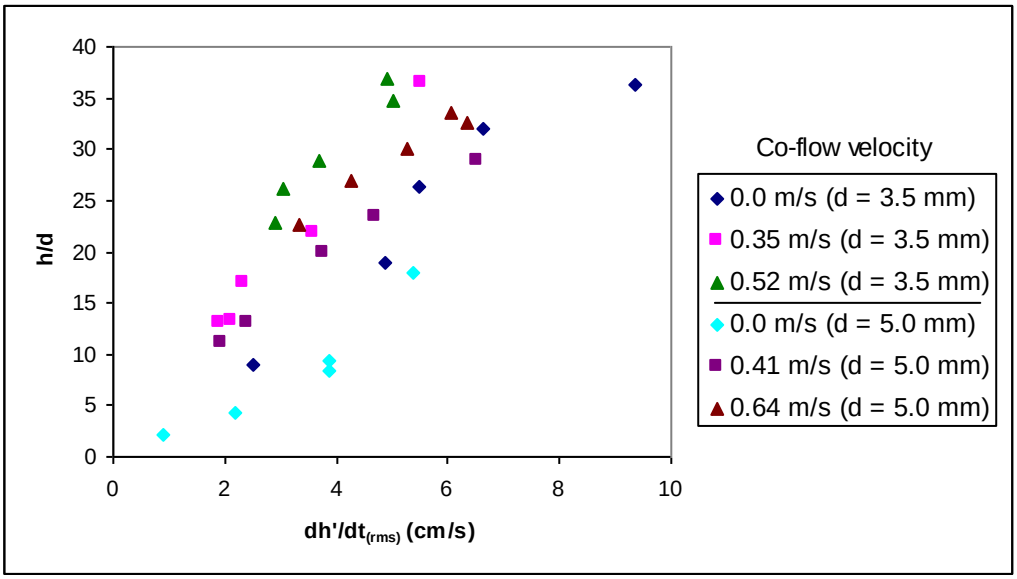

Figure 3.14 Change of *dh'/dt* with stable normalized height.

Applying the model that large scale structures dictate flame behavior leads to defining characteristics of these structures that can explain the data of the fluctuation amplitude and

oscillatory rate. The model theorizes that the stability mechanism is controlled by turbulent eddies whose passage causes a flame to be pushed downstream. These large-scale structures can produce high strain rates that result in the flame stabilizing at a greater height. Once the eddy is past the flame front, the flame can "jump" back upstream to a desirable location. The fluctuation amplitude and oscillatory rate increase with the flow velocity suggesting that the eddies must increase in size. With greater flow velocity, the eddies move downstream more quickly and move the flame further from its mean height. However Figure 3.12 indicates that due to the constancy of the normalized fluctuations with height in the fully turbulent region, these structures must develop in such a way that they are a constant size at a given height regardless of co-flow. This constant increase in eddies also explains the increase in oscillatory rate with the Reynolds number (see Figure 3.13).

The effective velocity can once again be applied to collapse the data into a linear relation useful for predicting the oscillatory rate for given fuel and co-flow velocities. Figure 3.15(a) and (b) show the root mean square of dh'/dt plotted with U_{eff} for the small and large pipes, respectively. The small pipe data correlated with the equation for U_{eff} when $C = 5.2$ (the value used in Montgomery *et al.* (1998)). For the large pipe data, $C = 15$ provided the best agreement. Montgomery *et al.* (1998) speculated that the constant, C, in the effective velocity equation takes into account chemical kinetics and burner characteristics. However, the oscillatory rate data does not collapse for the same value used previously with the normalized average height data (see Figure 3.11). Moreover, data from each pipe requires a different C value for optimal agreement.

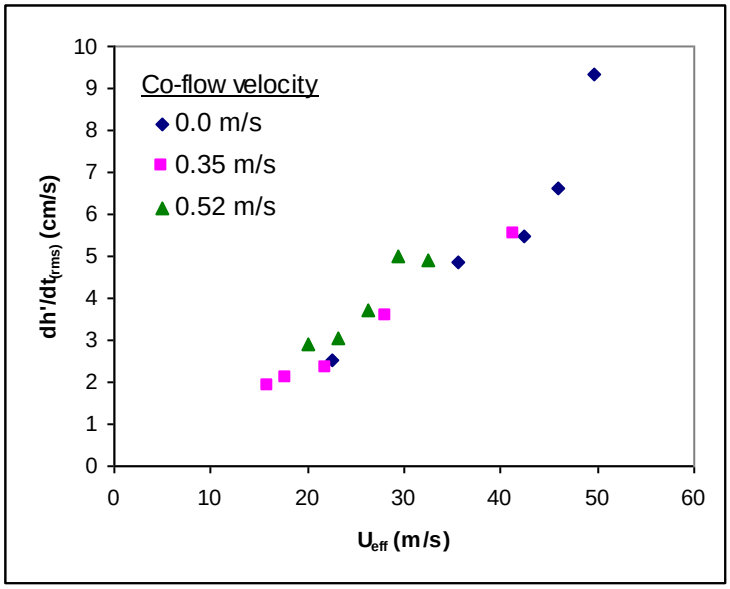

(a) small pipe with C = 5.2

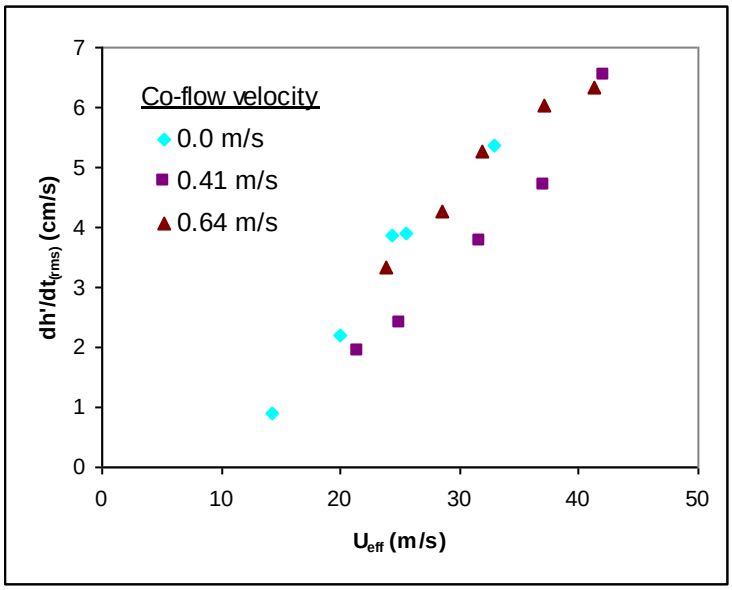

(b) large pipe with C = 15

Figure 3.15 RMS of *dh'/dt* for the (a) small pipe and (b) large pipe. Each pipe diameter requires a different value of C to linearize the data when plotted versus U_{eff}.

This use of the effective velocity with various characteristics of the same flame (i.e. no change in flow velocity) supports the conclusions put forth earlier in this paper that different mechanisms control the height and oscillatory rate. The location of the stabilized flame appears to be dictated by flow velocities but independent of the Reynolds number. The oscillatory rate increases with the Reynolds number and with height. Comparison of stable flames to unstable flames lends further insight into oscillatory behavior.

3.3.2 Fluctuations Preceding Blowout

At high flow velocities, a flame can be unable to sustain combustion and blows out. The blowout phenomenon has been regionalized to separate the pulsating behavior of the flame, similar to the fluctuations of stable flames, from the onset of receding that leads to blowout. However, instability of the flame in the pulsating region means that fluctuations are not always observed before blowout occurs (Chao *et al.*, 2000). A previous study observed flames for which the jet velocity was set high enough to cause the flame to blow out for three different co-flow velocities and a pipe diameter of 3.5 mm (Moore *et al.*, 2008). The flow velocities and average heights are shown in Table 3.2. Data from this study are plotted in Figure 3.16 with each curve tracing the downstream recession of a flame. In most cases, the flame lifted to a meta-stable position where the height fluctuated before extinguishing. Wu *et al.* (2006) also noted the existence of a pulsating region in which the flame becomes unstable and eventually extinguishes. The average height during fluctuations within the

pulsating region, defined to be bounded by the first and the last upstream propagation seen in the motion of the flame, was found to be more than 50d for each case.

Table 3.2 Velocities used to achieve blowout and the average height during the fluctuations prior to extinguishment.

Pipe diameter, d = 3.5 mm

Co-flow velocity (m/s)	Fuel velocity (m/s)	Average height (cm)
0.0	54.3	20.7
0.39	39.0	18.8
0.6	19.6	19.0

Figure 3.16 Downstream recession of the flame front for 10 different cases at three different conditions. (a) 0.0 m/s co-flow and 54.27 m/s fuel velocity. (b) 0.39 m/s co-flow and 38.98 m/s fuel velocity. (c) 0.6 m/s co-flow and 19.59 m/s fuel velocity. The time and height at which the diffusion flame is seen to disappear is marked for each case (see Chapter 4).

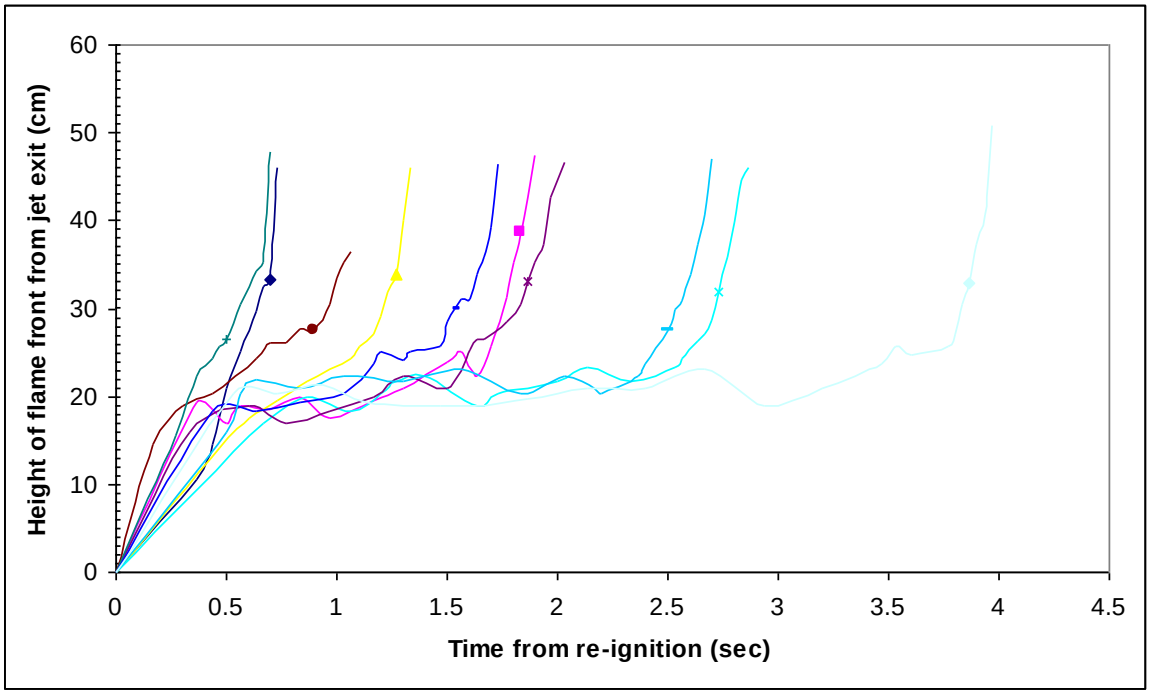

(a) 0.0 m/s co-flow

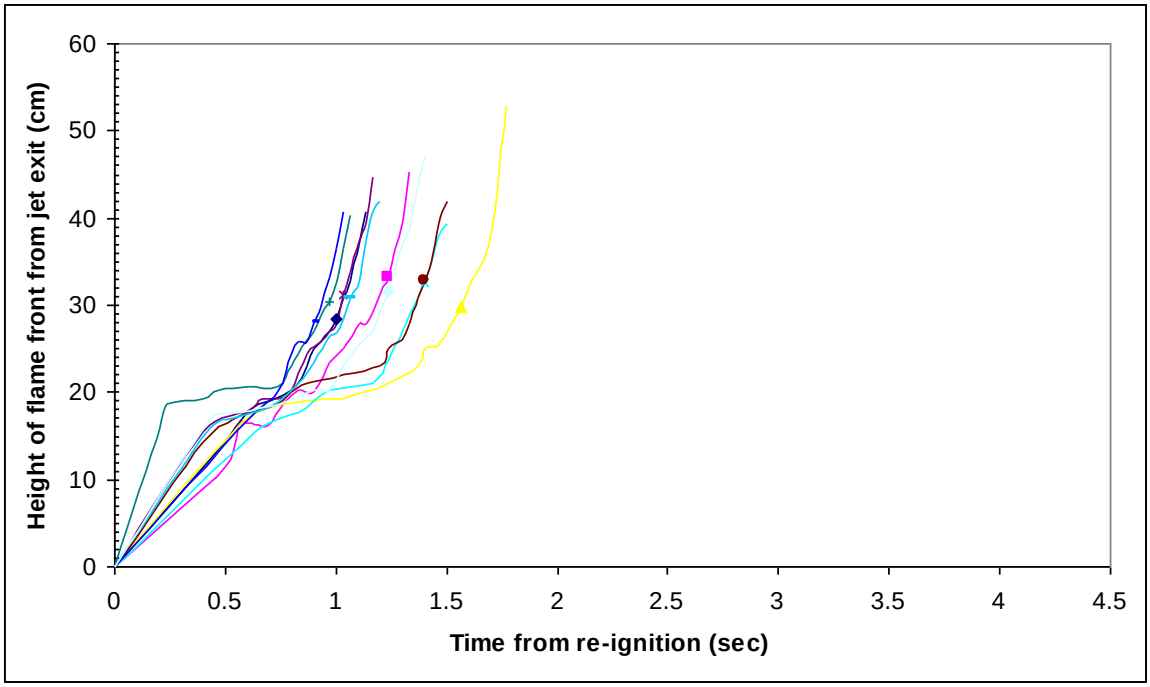

(b) 0.39 m/s co-flow

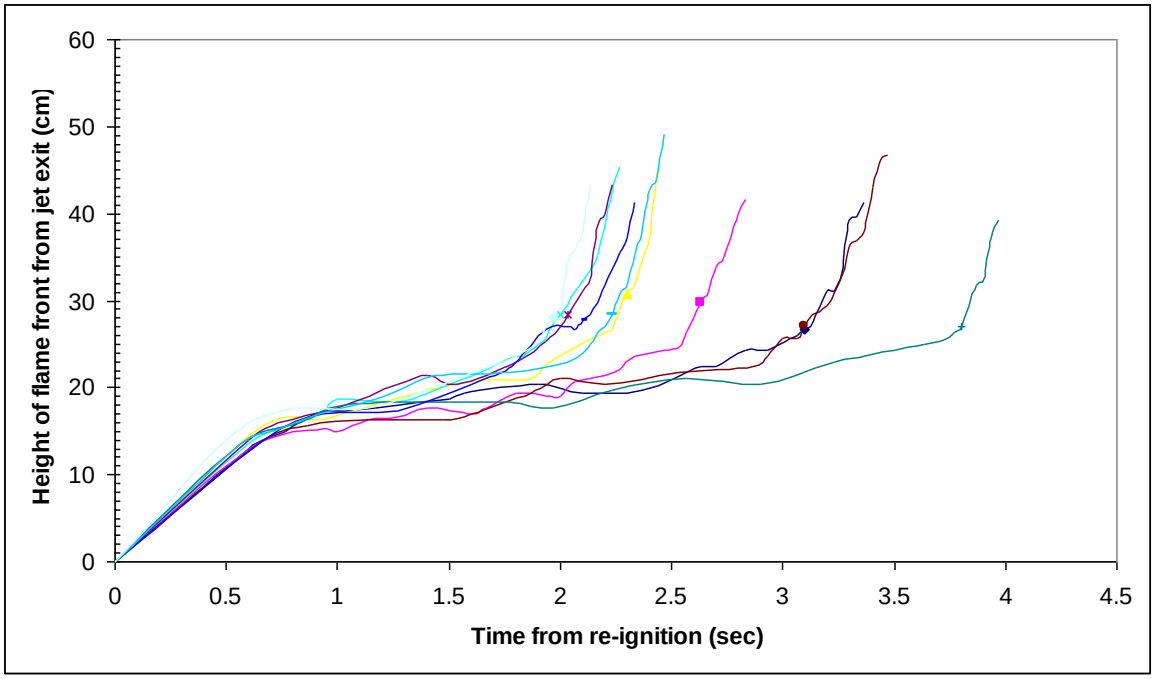

(c) 0.6 m/s co-flow

Figure 3.17(a), (b), and (c) allow direct comparison of the stable flames discussed previously (specifically in Figure 3.12, Figure 3.13(a) and Figure 3.14) and the three flames in the process of blowing out. Figure 3.17(a) shows the sharp increase in the normalized fluctuations for $h > 35d$, the region in which unstable flames fluctuate. Flames preceding blowout have $h' > 0.8h$. The oscillatory rates for the blowout cases are plotted versus the Reynolds number in Figure 3.17(b). While it is not necessary for the Reynolds number to be exceptionally high for blowout to occur, the oscillatory rates of the flames preceding blowout are about four times higher than their stable flame counterparts. In addition, the blowout flames show a change in behavior at Re = 8500 similar to that seen in the stable flames. The

relationship between the average heights and the oscillatory rates shown in Figure 3.17(c) indicates that a general trend is true for both stable and unstable flames; the height is proportional to the oscillatory rate, with a sharper increase in height occurring at low rates.

Figure 3.17 Comparison of stable and unstable flames. (a) Normalized height fluctuations. (b) RMS of *dh'/dt*. (c) Effect of height on *dh'/dt*.

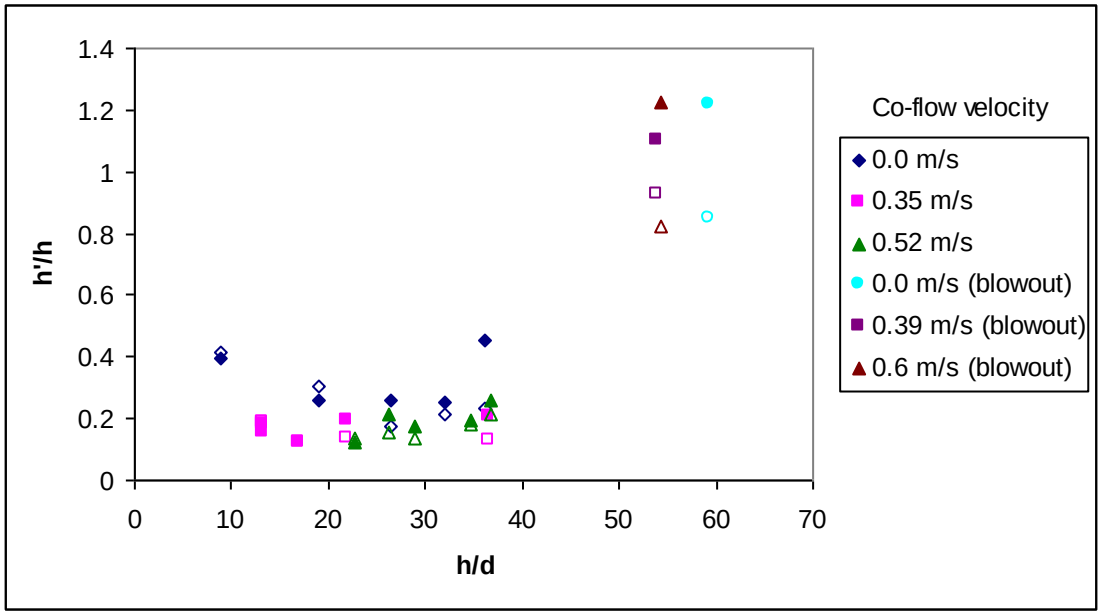
1.4
1.2
1
0.8
0.6
0.4
0.2
0
h'/h
0
10
20
30
40
50
60
70
h/d
Co-flow velocity
0.0 m/s
0.35 m/s
0.52 m/s
0.0 m/s (blowout)
0.39 m/s (blowout)
0.6 m/s (blowout)

(a)

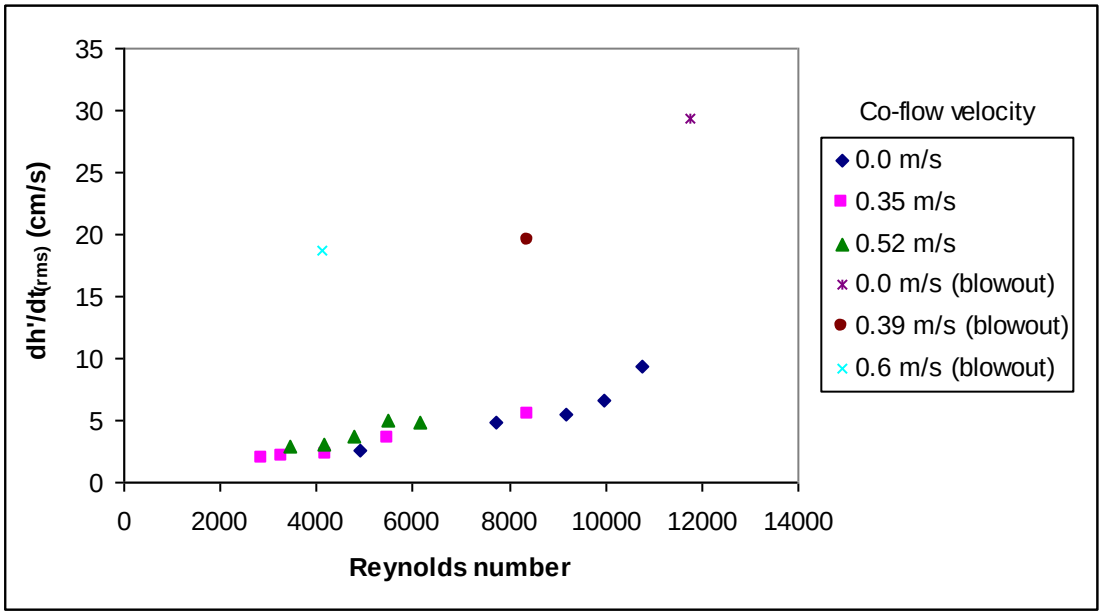
35
30
25
20
15
10
5
0
dh'/dt(rms) (cm/s)
0
2000
4000
6000
8000
10000
12000
14000
Reynolds number
Co-flow velocity
0.0 m/s
0.35 m/s
0.52 m/s
0.0 m/s (blowout)
0.39 m/s (blowout)
0.6 m/s (blowout)

(b)

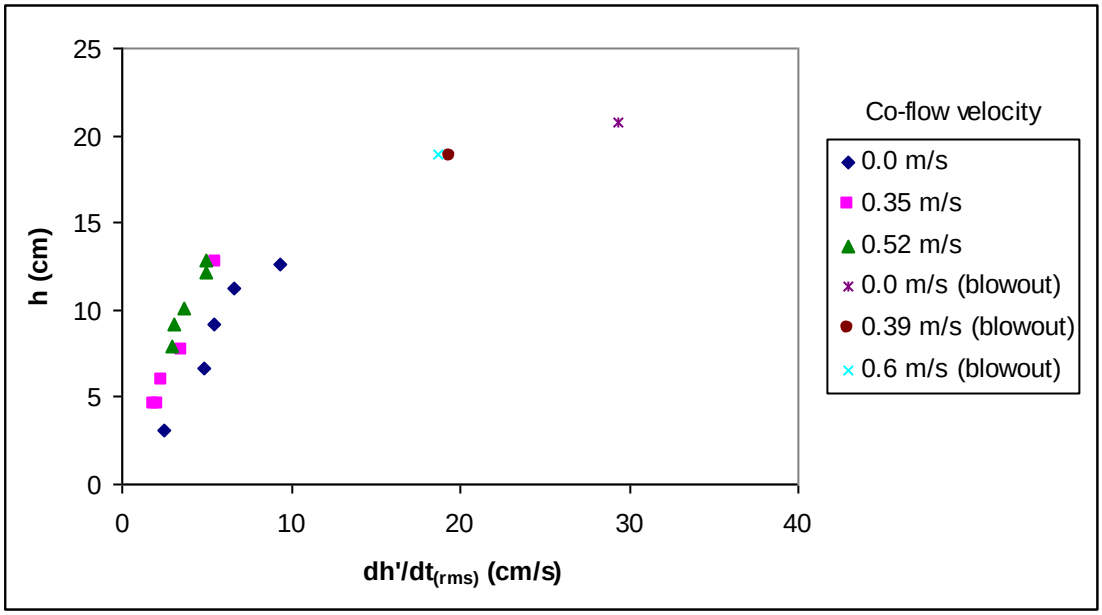

(c)

Because the oscillatory rate increases with the Reynolds number and with the normalized fluctuations, it could be concluded that a flame at a higher Reynolds number not only appears more turbulent from the size of its flame brush, but also acts more turbulent in that it fluctuates more rapidly. However when the rate of stable flames is compared to that of unstable flames approaching blowout, there is a gap in data between the two sets. The rate does not continue linearly from the stable flames to the blowout flames, as seen in Figure 3.17(b). This observation cannot be explained due to an extremely high Reynolds number for these flames. The turbulence in the flow for *Re* = 8000 is, therefore, not the cause for a flame to blow out. The three unstable flames have a greater height and oscillatory rate. Additionally, they have much greater normalized fluctuations. Thus, flames about to blow

out exhibit behavior markedly different from stable flames at comparable Reynolds numbers. The fluctuations of unstable flames occur at a greater rate and at a greater height. The role of large scale structures in blowout is therefore possible if there is a dramatic increase in their size far downstream in the region of instability.

3.4 Conclusions

Results from analysis of stable lifted turbulent methane-air flames in this study are intended to give a comprehensive view of flame height fluctuations in terms of fuel and co-flow exit velocities. Comparison of this data and data from the literature with new results on unstable flames approaching blowout reveals the role large-scale structures play in stability. The following conclusions have been drawn about the average height, the oscillation amplitude, and the oscillatory rate:

1. Observations about average height and fluctuations reveal the dependence (or lack thereof) of the Reynolds number on downstream location. Supported by the original data reported in this chapter, the Reynolds number is not a determining factor in the average height of a stable flame. Height increases with increasing Reynolds number but for a given *Re* value, the flame can be stable at multiple locations (or can be approaching blowout, depending on the regime). Also, it is reported for the first time, that the fluctuation amplitude increases with downstream location, but the normalized height fluctuations show little variation with height - except at locations very close to

the exit or approaching blowout far downstream. The consistency of the normalized fluctuations suggest that large eddies in the flow theorized as responsible for flame movement must be a constant size at a given height regardless of Reynolds number.

2. The trends in the data suggest that the amount of turbulence is not the cause for flame extinguishment. The oscillatory rate increases linearly with Reynolds number and with the normalized fluctuations. Flames about to blow out exhibit behavior markedly different from stable flames. The changes in unstable flame behavior can be explained by the theory of large-scale structures allowing for a significant increase in the size of large-scale structures far downstream.
3. The varying dependence of the average height, fluctuation amplitude, and oscillatory rate on turbulence is described by their relationship with the effective velocity. Plots of the height and the oscillatory rate with the effective velocity show that to best linearize the data, different values of the constant coefficient, *C*, must be used which leads to doubts about the characteristics dictating the coefficient's value. Also, the change in fuel pipe diameter requires a different *C* for the oscillatory rate but not for the height, suggesting that burner characteristics have more of an effect on oscillatory rate.

Applying the possible stabilization theories to the data presented herein lends support to the idea that various phenomena are at work and multiple models can be used to explain flame behavior. By comparing characteristics of fluctuations in stable and unstable flames, a better understanding of the causes of instability is possible. The results imply that while the

largest scales of turbulence may influence the lifted height, viscous dissipation plays a primary role in the oscillation behavior.

Chapter 4

Observations on Jet Flame Blowout

N. J. Moore, J. L. McCraw, and K. M. Lyons

Published in *International Journal of Reacting Systems*

Observations on Jet Flame Blowout

N. J. Moore, J. L. McCraw, and K. M. Lyons
North Carolina State University
Department of Mechanical and Aerospace Engineering
Raleigh, NC 27695-7910

Abstract

The mechanisms that cause jet-flame blowout, particularly in the presence of air co-flow, are not completely understood. This work examines the role of fuel velocity and air co-flow in the blowout phenomenon by examining the transient behavior of the reaction zone *at blowout*. The results of video imaging of a lifted methane-air diffusion flame at near blowout conditions are presented. Two types of experiments are described. In the first investigation, a flame is established and stabilized at a known, predetermined downstream location with a constant co-flow velocity, and then the fuel velocity is subsequently increased to cause blowout. In another, an ignition source is used to maintain flame burning near blowout and the subsequent transient behavior to blowout upon removal of the ignition source is characterized. Data from both types of experiments are collected at various co-flow and jet velocities. Images are used to ascertain the changes in the leading-edge of the reaction zone prior to flame extinction that help develop a physically-based model to describe jet-flame blowout. The data report a consistent predictor of blowout is the prior disappearance of the axially-oriented flame branch. This is witnessed despite a turbulent flame's inherent variable behavior. Interpretations are also made in light of analytical mixture fraction expressions from the literature that also support the notion that flame blowout occurs when the leading-edge reaches the vicinity of the lean-limit contour, which coincides approximately with the conditions for loss of the axially oriented flame structure.

Keywords:

Combustion; Jet Flame; Blowout; Flame Propagation

Corresponding Author, Email: Lyons@eos.ncsu.edu

4.1 Introduction

At a particular fuel velocity, a gaseous hydrocarbon jet-flame will detach from the burner and stabilize at some axial distance downstream. The reaction zone consists of a leading partially-premixed flame front and a trailing diffusion flame created at the vertically-oriented interface of the residual fuel not consumed by the leading flame front and air. A diffusion flame has no burning velocity so it is the premixed flame front that is generally assumed to act as a stabilizing anchor. Many studies, like that of Muñiz and Mungal (1997) and Watson *et al.* (2000, 2002, 2003), have investigated stable lifted flame reaction zone structures that settle at moderate downstream positions. If the reaction zone moves further downstream, it eventually enters a region that can no longer support combustion due to the low fuel concentration and all reaction abruptly ceases, a condition known as flame blowout (Kalghatgi, 1981; Pitts, 1988; Coats, 1996; Chao *et al.*, 2000, 2004). The term "blowout" seems more physically descriptive than the sometimes used "blowoff", since the global reaction zone does not seem to blow off the downstream end of the jet, but rather, to locally cease (Liñán and Williams, 1993). Since the blowout phenomenon happens typically in an abrupt and unpredictable manner, its transient characteristics are difficult to study experimentally. Additionally, the large width of the fuel jet, the small gradients in the scalar and velocity fields and the relatively low values of fuel concentration make the situation, in

many ways, more challenging to fully characterize than the situations described in the studies of Watson *et al.* (2000, 2002, 2003).

Theories have been developed to determine the mechanism controlling blowout. For a laminar propane jet flame, Savas and Gollahalli (1986) studied the shape of the flame front and found that near blowout, the flame front became flat (an axially-centered disk) and the chemi-luminescence weakened. The blowout conditions were determined to be dependent on the fuel and oxidizer properties and the burner geometry. Chung and Lee (1991) showed similar phenomena, also in laminar jet flames. For turbulent flames, Broadwell *et al.* (1984) proposed that at the blowout velocity, the combustion ceases because there is not enough time for ignition of incoming fuel/air mixtures by entrained hot products. This work and others (Miake-Lye and Hammer, 1988) point to the primary role of large scale structures in facilitating hot product transport. Similarly, Dahm and Dibble (1988) applied a blowout parameter from Broadwell *et al*. (1984) for turbulent jets in co-flow and showed that an increased co-flow velocity decreased the jet blowout velocity. The blowout parameter, based on characteristic ignition time and mixing time ratios, predicts blowout trends correctly. More recently, Han and Mungal (2000) also offered observations on flame blowout, but focused their explanation on the inability of the reaction zone to counter-propagate against incoming reactants at blowout. Burgess and Lawn (1999), Brown *et al*. (1999), Dahm and Mayman (1990) and Montgomery *et al*. (1998) discussed related elements of flame blowout; a recent overview of this previous research in blowout is contained in Chao *et al*. (2004). More recently, Wu *et al.* (2006) report on lifted flames near blowout, with detailed comments

on triple flames in the pulsating region and describe a proposed mechanism of flame pulsation and blowout.

The current paper discusses an experimental study of the blowout phenomenon for a lifted methane-air diffusion flame in various co-flow conditions. Rather than focus on detailed instantaneous images of reaction zones, as has been our tact in the past, this effort has utilized time sequences of the reaction zone at blowout. The main focus is to investigate the transient behavior leading to global blowout. Instantaneous measurements at blowout prove to be quite difficult with the limitations of single-shot experimental techniques due to the abrupt onset of blowout. Two types of experiments are described that attempt to clarify the characteristics of flames during the blowout process, focusing on the behavior of the leading-edge reaction zone and the trailing diffusion flame at blowout. Sequences of digital images of the lifted reaction zone are provided along with details of the flame movement for different combinations of fuel and co-flow velocities. Interpretations of the data are discussed, utilizing a relation for the stoichiometry from Tieszen *et al*. (1996). This allows for the assessment of past theories and the development of a physically-based concept of flame blowout in turbulent jets, along with proposing a new signature which indicates the imminence of flame blowout.

4.2 Experimental Setup

The experiments were performed at the Applied Energy Research Laboratory on the campus of North Carolina State University. A vertical jet flame burner with a fuel pipe of 3.5 millimeters (mm) diameter was used to deliver 99% pure methane. The apparatus provides a "top-hat" velocity profile at the pipe's exit. As shown in the schematic in Figure 4.1, the fuel pipe is surrounded by an annulus of co-flowing air with a diameter of 150 mm. Care was taken to minimize the effects of room currents on the flame apparatus by turning off laboratory ventilation during the recording of data and limiting activity near the burner. The height of the lifted flame, *h*, is the distance from the lowest part of the flame front to the burner.

For this investigation, images of chemiluminescence (Lyons and Watson, 2000) from the methane jet near blowout conditions were obtained with a Panasonic Model PV-GS120 camera producing thirty frames per second (60 interlaced fields). The colors of the images were enhanced using Adobe Photoshop. A rotameter measured the fuel velocity, and the co-flow velocity was measured using a TSI Veloci-calc model 8345 anemometer. The minimum and maximum co-flow velocities used were 0.0 m/s and 0.65 m/s, respectively.

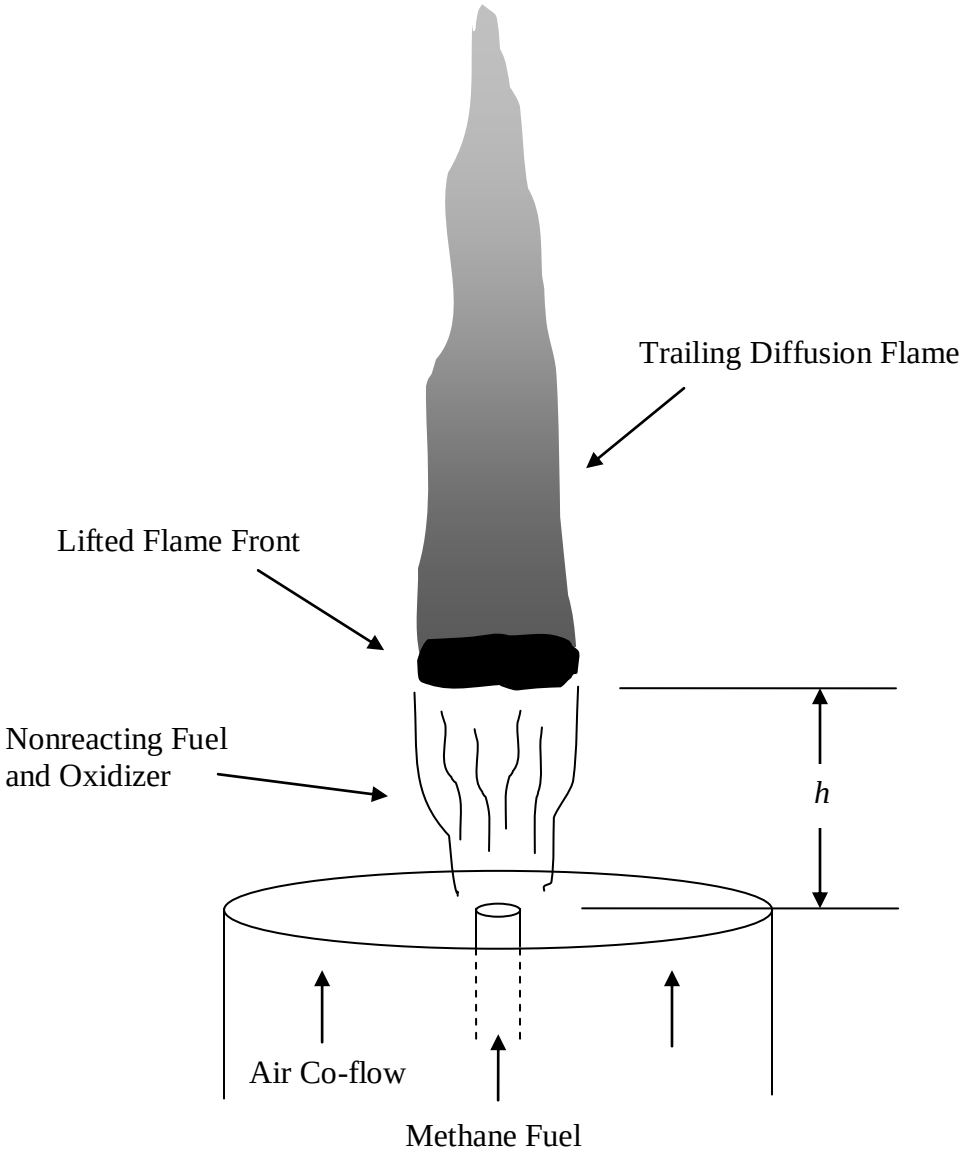

Figure 4.1 Methane is delivered from the nozzle that is surrounded by co-flowing air. The conditions allow the flame to lift to some downstream position where there exists the lifted flame front and the trailing diffusion flame, before proceeding to blowout. *h* is the distance from the fuel nozzle to the lifted flame front.

4.3 Results and Discussion

Images of blowout of a methane flame were obtained at various conditions during two different types of experiments. In the first series of experiments, blowout was brought about by a change in the flow conditions of a stable lifted flame. For a constant co-flow velocity, the initial fuel velocity was set to allow the flame to stabilize at a lifted height of approximately 14.0 cm (or 40 nozzle diameters) above the nozzle. The same stable height was used throughout the first experiments and was chosen because a reaction zone at that height is stable (i.e. will not spontaneously blowout) and turbulent for each co-flow velocity tested. The fuel velocity was then increased slightly until blowout occurred. The procedure was repeated multiple times to determine the lowest jet velocity at which the flame would consistently blow out. Table 4.1 contains examples of conditions that were digitally recorded, with the fuel velocities being the averaged values.

Table 4.1 Flow conditions for flame from stable lifted positions (a) to blowout (b).

Co-flow velocity (m/s)	*Lifted* 14.0 cm *(a)*		*Blowout (b)*	
	Fuel velocity (m/s)	Reynolds number	Fuel velocity (m/s)	Reynolds number
0.0	46.6	10114	50.4	10929
0.3	36.9	8013	41.7	9050
0.4	31.6	6848	35.6	7716
0.5	27.0	5855	31.6	6848

The data of Table 4.1 shows that with increasing co-flow, decreasing values of the methane jet velocity are needed for blowout to occur. Dahm and Dibble (1988) proposed that this reduction in fuel velocity at blowout was due to the local molecular mixing rate. In experiments by Brown *et al.* (1999), changing the co-flow velocity had a greater effect on a flame the further downstream the flame was stabilized and resulted in lower jet velocities for flame blowout. Additionally, the findings of Brown *et al.* (1999) confirmed the data of the current study which show that for a given co-flow velocity, the flame can on occasion extinguish at a slightly lower fuel velocity than the experimentally-determined average blowout velocity. In this regime (as witnessed in the current study), the co-flow so dominates that it tends to be comparable to the jet velocity and the bulk co-flow velocity carries the reaction zone downstream. As discussed elsewhere, it is proposed that at this downstream location the flame blows out as the lean-limit is reached.

Images from these experiments were examined to determine the effect of co-flow on the mechanism of blowout. Figure 4.2 shows two sequences of images of the flame proceeding to blowout. The images in Figure 4.2(a) are from a flame with 0.3 m/s co-flow, corresponding to the data on the second line of Table 4.1. The sequence begins after the fuel velocity was increased from 36.9 m/s to 41.7 m/s. The image at time zero is the last one of the flame at the stable lifted height, immediately after which the flame begins moving downstream. The flame transitions from a stable lifted flame to a quasi-stable flame on the threshold of blowout. During this transition, the length of the diffusion flame decreases as the leading-edge of the flame front drops downstream. The contrast in color for this

sequence has been increased due to the faint chemiluminescence of the actual flame. The blue flame consists of a leading-edge flame front that anchors the trailing diffusion flame. Blowout occurs 1.50 seconds after the change in fuel velocity causes downstream movement of the flame.

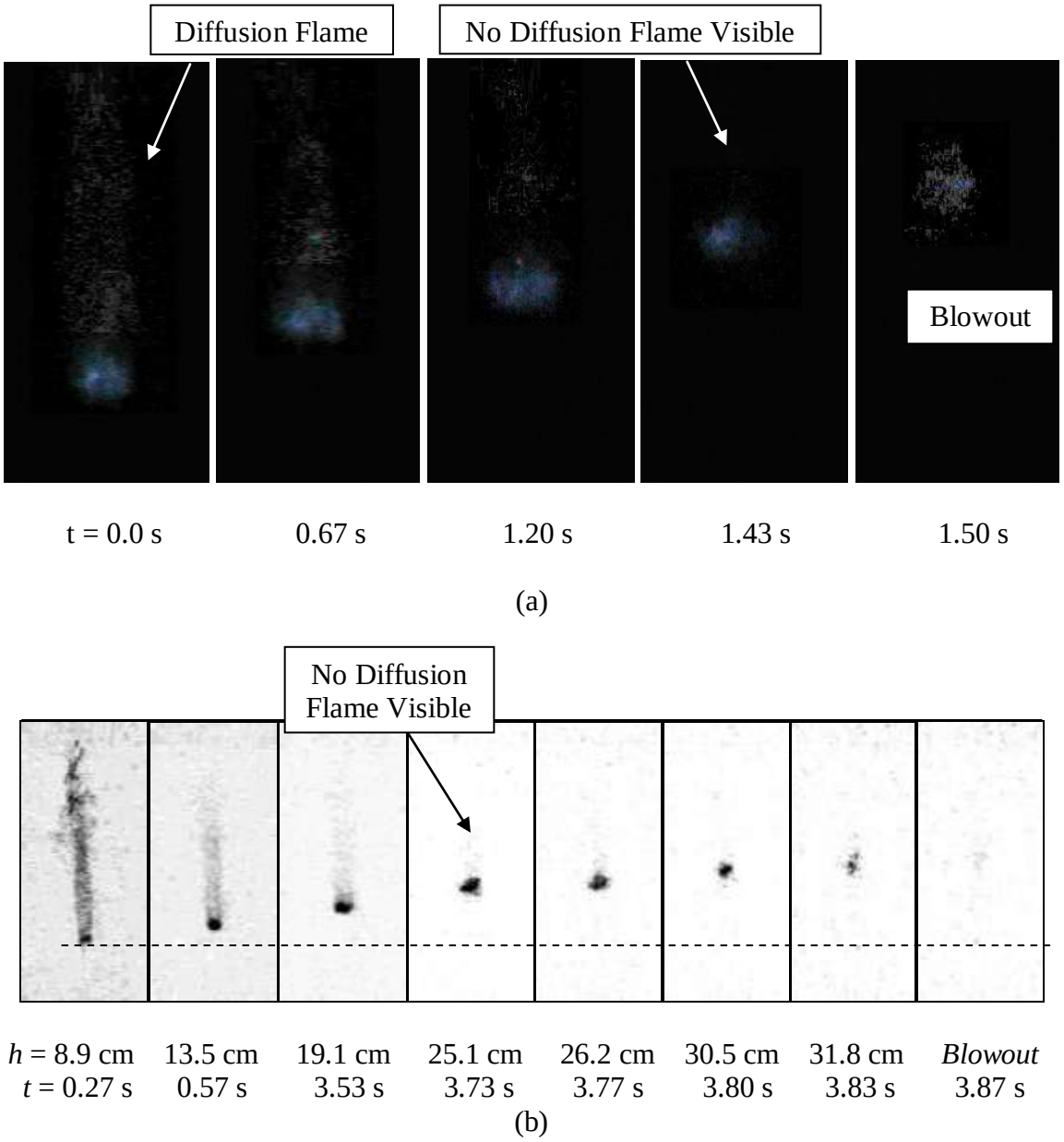

Figure 4.2 (a) Enhanced images of the flame receding downstream for 0.3 m/s co-flow. The fuel velocity was increased from 36.9 to 41.7 m/s to cause blowout (line 2, Table 4.1). The entire flame is blue in color. (b) Inverted images of the flame after being re-ignited at time zero, with 34.3 m/s fuel velocity and 0.55 m/s co-flow (line 4, Table 4.2). The distance, *h*, from the fuel nozzle to the lifted flame front is measured for each.

In the second series of experiments, the fuel velocity was set at blowout conditions, predetermined by multiple tests, for a particular co-flow velocity. With the fuel and co-flow velocities held constant, the flame was re-ignited at the fuel nozzle and allowed to move downstream and eventually extinguish. Section 3.3.2 also includes data from these experiments. Figure 4.2(b) shows one sequence of images from these experiments with the colors inverted and enhanced to counteract the faintness of the flame. The larger field of view includes the nozzle but it is not visible in the enhanced images. For this sequence, the flame was re-ignited from the nozzle with 0.55 m/s co-flow and 34.3 m/s fuel velocity. After 3.53 seconds, the chemiluminescence witnessed from the trailing diffusion flame has been significantly reduced and the leading-edge of the flame front has moved 19.1 cm downstream. At 25.1 cm and 3.73 seconds, the diffusion flame is no longer visible. In the remaining 0.14 seconds until the flame entirely extinguishes, the flame front moves 6.7 cm. Thus, the flame moves farther downstream much more rapidly in the absence of the trailing diffusion flame compared to when it is present. The last image in the series shows that complete blowout was achieved 3.87 seconds after re-ignition.

Data from repeated tests for each of the flow conditions revealed no trend in the amount of time needed from re-ignition to blowout. However, similar characteristics of the flame were noticed regardless of the presence or magnitude of the co-flow velocity or by which method blowout was achieved. At downstream locations, the flame front is witnessed to decrease its recession speed downstream as the diffusion flame diminishes. After the chemiluminescence from the trailing diffusion flame is no longer detected, the small region

of flame at the leading-edge (a "blue" flame ball) increases its recession speed downstream until all reaction is completely extinguished. Importantly, as Figure 4.2 shows and other experiments verify, blowout is not witnessed while the axially-oriented diffusion flame is present.

As suggested by Han and Mungal (2000), the velocity of the stoichiometric contour can be estimated and used to approximate the amount of mixing between the fuel jet and the surrounding air. This velocity, U_S, can be calculated from

$$U_S = Z_S U_0 + (1 - Z_S) U_{cf} \qquad 2.1$$

where Z_S is the stoichiometric mixture fraction (0.055), U_0 is the nozzle exit velocity, and U_{cf} is the co-flow velocity. To test for blowout dependence on the stoichiometric contour velocity, the co-flow and fuel velocities were varied such that U_S remained the same, beginning with 0.50 m/s co-flow and 35 m/s fuel giving U_S = 2.4 m/s, as seen in Table 4.2. Despite starting at a blowout condition and keeping U_S constant, the flame's behavior was not consistent. At the lowest co-flow velocity, the flame stabilized and was not seen to blowout for an extended amount of time, in spite of being at a higher fuel velocity than a comparable flame in Table 4.1. Added to the unpredictable nature of blowout, a difference in experimental procedures cannot be ruled out as a cause of some discrepancy. Blowout occurred in one second at the highest co-flow velocity. These variations in behavior predict a lack of dependence of blowout on U_S. As implied in previous studies by Han and Mungal (2000) and Watson *et al*. (2002), U_S is a useful quantity for estimating the axial velocity at

the stoichiometric contour of the *already* established portions of the flame; the leading-edge of the flame has been found to favor lower speed regions (S_L to 3 S_L) typically less than U_S.

Table 4.2 Fuel velocity, U_0, and co-flow velocity, U_{cf}, for a given stoichiometric contour velocity, U_S. Times given are from re-ignition to blowout based on digital images.

U_0 (m/s)	U_{cf} (m/s)	U_S (m/s)	Time to blowout (sec)
36.9	0.4	2.4	*No blowout after 60 sec*
36.0	0.45	2.4	20.5
35.0	0.5	2.4	2.47
34.3	0.55	2.4	3.87
33.5	0.6	2.4	2.03
32.6	0.65	2.4	1.00

4.4 Analysis of the Scalar Field

An analysis of the scalar field for the turbulent methane jet flame indicates a correlation between the downstream appearance of the flame and the value of the local mixture fraction. The scalar field of methane issuing into quiescent air is determined from the method used by Tieszen *et al*. (1996). The time-averaged mass fraction of fuel, *Y*, into air with no co-flow present is represented as:

$$Y = 10 \cdot \left(\frac{\rho_0}{\rho_\infty} \right)^{1/2} \left(\frac{r_0}{z} \right) \exp\left\{ -57 \left(\frac{r}{z} \right)^2 \right\}. \qquad 1.4$$

This equation, a function of the ratio of the densities of methane, ρ_0, and air, ρ_∞, and the nozzle diameter r_0, is used to estimate the fuel concentration at a particular downstream location z for a given radial position r. It assumes self-similarity and is derived from the concentration profile developed by Dowling and Dimotakis (1990), thus a lack of dependence on the jet velocity. The stoichiometric contour and those indicating the 5 and 15% flammability limits of methane generated from this approach are shown in Figure 4.3. Also shown in Figure 4.3 are the axial locations of the flame front as the flame progresses downstream for two different cases. Because Equation 1.4 is strictly valid only when no co-flow is present, both cases have zero co-flow velocity but slightly different fuel velocities, as each was achieved by one of the two different techniques explained above. For Case 1, the flame is at a stable lifted position before the velocity is increased from 46.6 to 50.4 m/s to induce blowout. For Case 2, the flame was re-ignited at the nozzle with the fuel velocity kept constant at 54.3 m/s. Blowout occurs at 33.8 cm for Case 1 and 38.9 cm for Case 2.

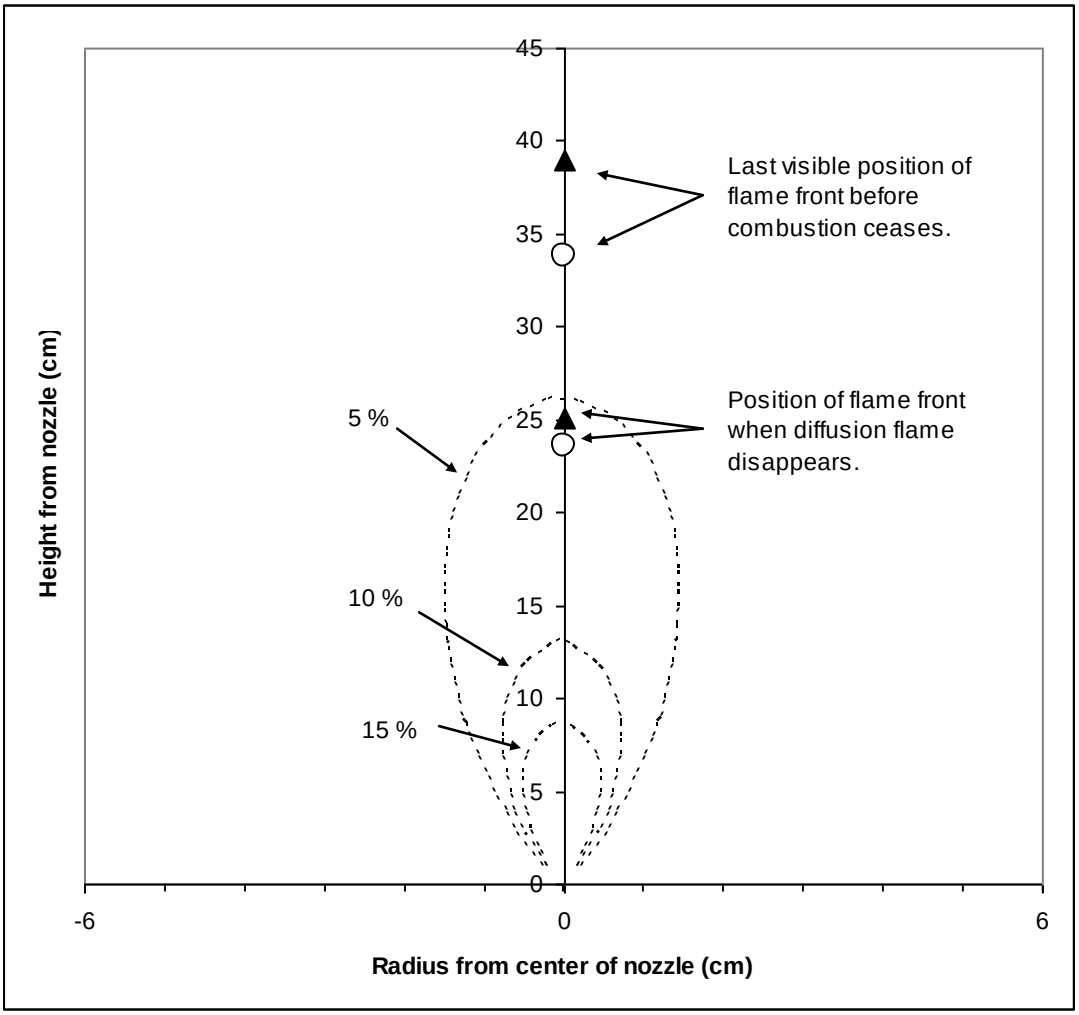

Figure 4.3 Position of the flame leading-edge relative to the mean fuel concentration as calculated from the approach of Tieszen *et al*. (1996) for two cases without co-flow. For Case 1 (circles), the fuel velocity is increased from 46.6 m/s to 50.4 m/s (line 1, Table 4.1) from the first series of experiments. For Case 2 (triangles), the fuel velocity is 54.3 m/s from the second series. What is notable is that the position where the axial oriented flame is lost corresponds to the approximate position of the lean limit.

For both cases, the downstream location of the flame front when the diffusion flame disappeared was determined from the images. As seen in Figure 4.3, the location for Case 1

is 23.6 cm and for Case 2 is 25.1 cm. The location for both is just within the 5% methane contour, implying that the mixture fraction at the leading-edge is found to be approaching the mean lean flammability limit contour (and moving downstream in a direction of decreasing mixture fraction) when the diffusion flame is witnessed to disappear and the flame to subsequently blow out. Data from multiple tests confirm that the disappearance of the diffusion flame occurs near the 5% methane contour. Tests conducted with co-flowing air gave similar results; however, a more accurate representation for the flammability limits with co-flow present is necessary before the results can be confirmed.

Equations for the time-averaged velocity profile of the flame (also from Tieszen *et al.*, 1996) have been examined to verify the validity of Equation 1.4 in this study (see Appendix). Data from numerous experiments utilizing particle image velocimetry to determine the velocity of the stabilized flame were compared to the estimates provided by the Tieszen velocity relation (Watson *et al.*, 2002; Su *et al.*, 2006; Muñiz and Mungal, 1997). The published PIV measurements for each agree with the estimated velocities, especially as the flame stabilizes further downstream. Each of these experimental studies used planar laser-induced fluorescence to determine the axial and radial location of the flame edge. Watson *et al.* (2002) used the CH radical to locate the flame edge; thus the PIV measurements were greater than one could expect from using OH, due to the tendency of the CH zones to lie towards the centerline. To account for this, the locations of the rich flammability limits were used to estimate the velocities for these data sets and good general agreement was found, with better results further downstream. The agreement of the velocity

estimates despite the presence of co-flow supports the use of the similarly derived Tieszen relation (Equation 1.4) for the mass fraction.

These findings support the earlier interpretations based on the digital images, namely that the reduction and eventual disappearance of the diffusion flame indicates the onset of blowout. In addition, once the trailing diffusion flame is absent, the flame front is shown to move into a downstream region in which the mixture fraction is below 5%, and stable combustion is no longer possible. Blowout is found to be imminent for these conditions.

4.5 Conclusions

From the images generated by the two types of experiments, general conclusions can be drawn. As shown in Figure 4.4(a), a stable lifted flame consists of a premixed flame front and a diffusion flame. When the flame front moves downstream, due to the fuel being at the blowout velocity, the diffusion flame length begins to shorten, Figure 4.4(b). Once this trailing flame has disappeared, Figure 4.4(c), the reaction zone progresses downstream, being unable to stabilize, and eventually extinguishes, Figure 4.4(d).

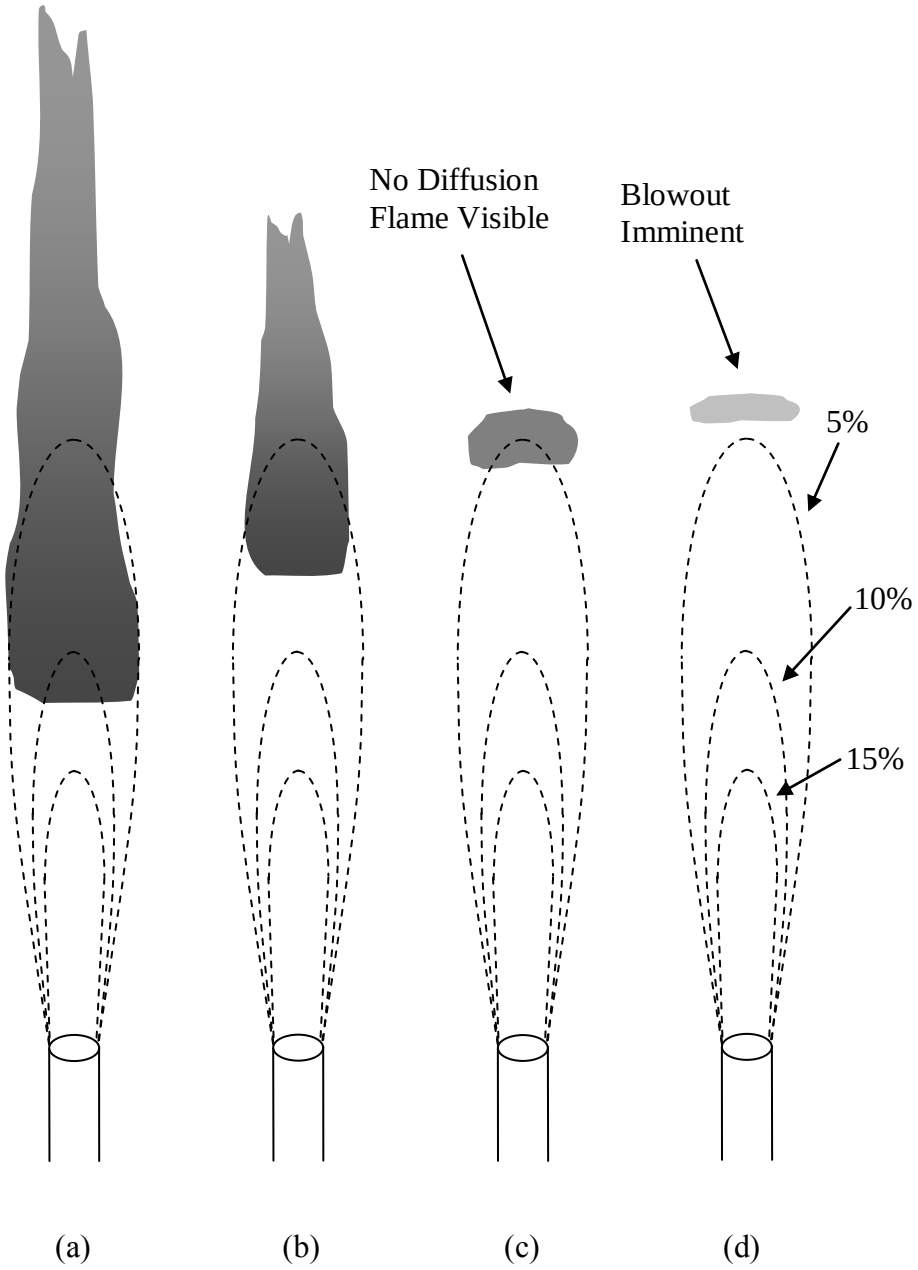

Figure 4.4 Schematic of the blowout mechanism relative to the flammability limits of methane. (a) A stable lifted flame. (b) The unstable flame has recessed downstream and the diffusion flame has shortened. (c) The diffusion flame has disappeared. (d) Blowout occurs.

The results of the study suggest that the trailing diffusion flame, specifically its disappearance, plays a useful function as a flame extinction precursor signature. The loss of the chemiluminescence from the trailing diffusion flame functions as an indicator of blowout being imminent. Only after the diffusion flame disappears does blowout occur for all of the regimes studied.

It is concluded from the analysis that blowout occurs when the leading-edge of the reaction zone moves to a downstream region where most of the fuel that is consumed is burnt locally near the leading-edge, leaving little in the way of fuel-rich gases to feed the trailing diffusion flame, only large volumes of very fuel-lean gases. In this sense, blowout may be viewed for the cases studied as a lean-limit phenomenon (Williams, 1977, especially Glassman comments) and this simple analysis supports this conjecture, as well as the paper of Wu *et al.* (2006), as shown in Table 4.3. The explanations in this paper do not explicitly address the mixing effects (Dahm and Dibble, 1988) or the velocity field considerations (Han and Mungal, 2000), nor do they contradict them, but rather offer an alternative way based on lean limits to describe blowout and report a new visually observable indicator that is compatible with concepts developed from the general approach of Broadwell *et al.* (1984).

Table 4.3 Comparison of theories on blowout from past publications.

	Blowout Concepts Supported	*Proposed Blowout Mechanism*
Broadwell *et al.* (1984)	Large-scale structures move hot product to flame leading-edge	Mixing between hot products and unburned fuel allows insufficient time for combustion to occur
Dahm and Dibble (1988)	Molecular mixing rate	Reduction in the fuel velocity with increasing co-flow velocity corresponds to a consistent blowout parameter
Tieszen *et al.* (1996)	Local flow velocity exceeds turbulent flame speed	Turbulent flame propagation on outside of reaction zone stabilizes flames near blowout
Han and Mungal (2000)	Flame propagation against incoming reactants	Flame base moves into a higher velocity region due to a change in the stoichiometric velocity of the flame surface
Wu *et al.* (2006)	Triple flames/flame pulsation	Lessening of stoichiometric branch of triple flame leads to downstream recession and eventual blowout

4.6 Acknowledgements

The research reported in this paper has been supported by the U. S. Army Research Office (Contract W911NF0510045).

4.7 References

Broadwell, J. E., Dahm, W. J. A., and Mungal, M. G., (1984) Blowout of Turbulent Diffusion Flames, *Proceedings of the Combustion Institute,* The Combustion Institute, Pittsburgh, 20, pp. 303-310.

Brown, C. D., Watson K. A. and Lyons, K. M., (1999) Studies on Lifted Jet Flames in Co-flow: The Stabilization Mechanism in the Near- and Far-Fields, *Flow, Turbulence and Combustion,* 62, pp. 249-273.

Burgess, C. P. and Lawn, C. J., (1999) The Premixture Model of Turbulent Burning to Describe Lifted Jet Flames, *Combustion and Flame,* 119, pp. 95-108.

Chao, Y.-C., Chang, Y.-L., Wu, C. Y., and Cheng, T. S., (2000) An Experimental Investigation of the Blowout Process of a Jet Flame, *Proceedings of the Combustion Institute,* The Combustion Institute, Pittsburgh, 28, pp. 335-342.

Chao, Y.-C., Wu, C. Y., Lee, K.-Y., Li, K.-Y., Li, Y. H., Chen, R.-H. and Cheng, T.-S., (2004) Effects of Dilution on Blowout Limits of Turbulent Jet Flames, *Combustion Science and Technology,* 176, pp. 1735-1753.

Chung, S. H. and Lee, B. J., (1991) On the Characteristics of Laminar Lifted Flames in a Nonpremixed Jet, *Combustion and Flame,* 86, pp. 62-72.

Coats, C. M., (1996) Coherent Structures in Combustion, *Progress in Energy and Combustion Science,* 22, pp 427-509.

Dahm, W. J. A. and Dibble, R. W., (1988) Co-flowing Turbulent Jet Diffusion Flame Blowout, *Proceedings of the Combustion Institute*, The Combustion Institute, Pittsburgh, 22, pp. 801-808.

Dahm, W. J. A. and Mayman, A. G., (1990) *AIAA Journal* 28 (7), pp. 1157-1162.

Dowling, D. R. and Dimotakis, P. E., (1990) Similarity of the Concentration Field of Gas-Phase Turbulent Jets, *Journal of Fluid Mechanics* 218, pp. 109-141.

Han, D. and Mungal, M. G., (2000) Observations on the Transition from Flame Liftoff to Flame Blowout, *Proceedings of the Combustion Institute*, The Combustion Institute, Pittsburgh, 28, pp. 537-543.

Kalghatgi, G. T., (1981) "Blowout Stability of Gaseous Jet Diffusion Flames. Part 1: In Still Air," *Combustion Science and Technology*, Vol. 26, pp. 233-239.

Liñán, A., and Williams, F. A., (1993) *Fundamental Aspects of Combustion*, Oxford University Press, New York.

Lyons, K.M and Watson, K. A. "Partially Premixed Combustion in Lifted Turbulent Jets," *Combustion Science and Technology*: 97 - 105 (2000).

Miake-Lye, R. C., and Hammer, J. A., (1988) Lifted Turbulent Jet Flames: A Stability Criterion Based on the Jet large-scale Structure, *Proceedings of the Combustion Institute*, The Combustion Institute, Pittsburgh, 22, pp. 817-824.

Montgomery, C. J., Kaplan, C. R. and Oran, E. S., (1998) The Effect of Co-flow Velocity on a Lifted Methane-Air Jet Diffusion Flame, *Proceedings of the Combustion Institute*, The Combustion Institute, Pittsburgh, 27, pp. 1175-1182.

Muñiz, L., and Mungal, M. G., (1997) "Instantaneous Flame-Stabilization Velocities in Lifted-Jet Diffusion Flames," *Combustion and Flame*, Vol. 111, pp. 16-31.

Pitts, W. M., (1988) Assessment of Theories for the Behavior and Blowout of Lifted Turbulent Jet Diffusion Flames, *Proceedings of the Combustion Institute*, The Combustion Institute, Pittsburgh, 22, pp. 809-816.

Savas, O and Gollahalli, S. R., (1986) Stability of Lifted Laminar Round Gas-Jet Flame, *Journal of Fluid Mechanics*, 165, pp. 297-318.

Su, L.K., Sun, O. S. and Mungal, M. G., Experimental Investigation of Stabilization Mechanisms in Turbulent, Lifted Jet Flames, *Combust. Flame*, **144**, 494-512 (2006).

Tieszen, S. R., Stamps, D. W., and O'Hern, T. J., (1996) A Heuristic Model of Turbulent Mixing Applied to Blowout of Turbulent Jet Diffusion Flames, *Combustion and Flame*, 106, pp. 442-466.

Watson K. A. and Lyons, K. M., Donbar, J. M. and Carter, C. D., (2000) "Simultaneous Rayleigh Imaging and CH-PLIF Measurements in Lifted Jet Diffusion Flames", *Combustion and Flame* 123: 252 - 265.

Watson, K. A., Lyons, K. M., Donbar, J. M. and Carter, C. D, (2002) Simultaneous Two-Shot CH-PLIF and Particle Image Velocimetry Measurements in Lifted CH_4-Air Diffusion Flames, *Proceedings of the Combustion Institute*, The Combustion Institute, Pittsburgh, 29, pp 1905-1912.

Watson K. A. and Lyons, K. M., J. M. Donbar and C. D. Carter, (2003) "On Scalar Dissipation and Partially Premixed Flame Propagation", *Combustion Science and Technology* 175 (4) 649-664.

Williams, F. A., (1977) Mechanisms of Fire Spread, *Proceedings of the Combustion Institute*, The Combustion Institute, Pittsburgh, 16, pp. 1281-1294 (and Comment by I. Glassman p. 1292).

Wu, C.-Y., Chao, Y.-C., Cheng, T.-S., Li, Y.-H., Lee, K.-Y., and Yuan, T., (2006) The Blowout Mechanism of Turbulent Jet Diffusion Flames, *Combustion and Flame*, 145, pp. 481-494.

Chapter 5

Investigation of the Lean-Limit Phenomenon

5.1 Introduction

The effect of diluents on blowout has been studied in multiple configurations. Karbasi and Wierzba (1998) looked at blowout velocities for flames in which the fuel jet contained a diluent and in which the co-flowing stream contained a diluent. The diluted co-flow had a greater effect on the blowout limit than when the same concentration existed in the jet. Dahm and Mayman (1990) experimented with methane and ethylene diluted with carbon dioxide or air. They devised a "flip" experiment in which the separate fuel and diluent streams could be switched such that either could issue from the center nozzle and the other from a surrounding nozzle. Their results showed that the blowout velocities from both configurations were almost equal, demonstrating that the blowout behavior is determined by mixing that occurs in the far-field.

The findings of Chapter 4 revealed that further investigation into the relationship between a flame's behavior and the lean flammability limit was necessary. The estimate of the scalar field based on Tieszen's relation (Tieszen *et al.*, 1996) does not account for the presence of co-flow so analysis is limited. Therefore, experiments with nitrogen-diluted methane were performed to determine if the disappearance of the diffusion flame that is consistently observed prior to blowout is related to the value of the local mixture fraction.

Additionally, the velocities of methane, nitrogen and co-flowing air at blowout have been studied to determine a predictive parameter for various cases. Multiple studies have attempted to quantify blowout limits using a model based on fuel properties and a relation for the flow exit velocity (Broadwell *et al.*, 1984; Kalghatgi, 1981; Dahm and Dibble, 1988). Analysis of this model is applied to the current research to describe the physical reasons for the blowout velocities recorded.

5.2 Derivation of the Scalar Field Estimate

The general similarity profile of the mean concentration of jet fluid is

$$\bar{C}(r,z) = K\frac{C_0 d}{z - z_0} g\left(\frac{r}{z - z_0}\right) \qquad 5.1$$

for nozzle exits that give a top-hat velocity profile and density ratios of one (Dowling and Dimotakis, 1990). C_0 is the jet exit concentration and $g(\ )$ is a smoothing function determined from experimental results. d is the nozzle exit diameter, z_0 is the virtual origin,

and *(r,z)* is the radial and axial distance from the nozzle. *K* is a constant determined experimentally.

Chen and Rodi (1980) offer that the concentration ratio is equal to

$$\frac{C(r,z)}{C_0} = \exp\left[-K_c\left(\frac{r}{z}\right)^2\right] \qquad 5.2$$

where

$$K_c = \frac{\ln(2)}{(\dot{Y}_{0.5c})^2} \qquad 5.3$$

and $\dot{Y}$ is the rate of spread determined experimentally to be within 0.084 and 0.117. Tieszen *et al.* (1996) used the exponentially decaying term of Equation 5.2 for the smoothing function of Equation 5.1. This derivation assumes that the ratio of inertial to buoyant forces, or the Froude number, is at infinity meaning the fuel is a pure jet and non-buoyant and that the density ratio is one.

Using the approximations above, the time-averaged mass fraction of fuel, *Y*, into air with no co-flow present is represented as

$$Y = 10 \cdot \left(\frac{\rho_0}{\rho_\infty}\right)^{1/2}\left(\frac{r_0}{z}\right)\exp\left\{-57\left(\frac{r}{z}\right)^2\right\} \qquad 1.4$$

(Tieszen *et al.*, 1996). By choosing 0.11 for $\dot{Y}$ in Equation 5.3, K_c = 57 which is the value Chen and Rodi (1980) recommend and Tieszen *et al.* (1996) use. *K* in Equation 5.1 was determined experimentally to be 10.

Equation 1.4, first given in Section 1.3.2, takes into account a change in density. If the density ratio is approximately one, then Equation 1.4 closely resembles the earlier approximations. The effect of a ratio other than one is lessened by taking the square root of the ratio. As Chen and Rodi (1980) state, the constants in the equation are only valid for downstream similarity regions where the density ratio is unity; however, a large change in density does not significantly change the behavior so the constants can be used for the entire downstream area. The similarity region begins at about twenty nozzle diameters downstream (Dowling and Dimotakis, 1990).

Equation 1.4 is only valid for a jet issuing into quiescent air. The presence of concurrent co-flow would change the rate of spread of the jet and narrow the spread angle such that the exponential coefficient of Equation 5.3 would be less. Results in Chapter 4 on blowout suggest that the co-flow velocity lowers the position at which the diffusion flame disappears so the flammability limits established by Equation 1.4 should exist further upstream for these cases.

5.3 Experiments with Diluted Methane

The scalar field established by Equation 1.4 accounts for dilution in the fuel stream. The density at the jet exit, ρ_0, is the density of the fuel mixture. Experiments were performed with diluted methane flames at blowout conditions. A second rotameter was used to regulate the flow rate of nitrogen such that the amounts of methane and nitrogen issuing from the fuel

pipe could be independently controlled. For each test, a butane lighter was used as the ignition source and was placed at the fuel pipe exit to ignite the jet after flow rates were set.

After several tests were made, the flow rate of methane necessary to cause the flame to blow out within approximately thirty seconds was determined. With the flow rate held to that blowout velocity, the flame was lit at the jet exit and allowed to blow out ten times. The recorded images of these flames from a Panasonic Model PV-GS300 camera were used to determine the height of the flame front at which the diffusion flame disappeared. Having established the limiting case, the flow rate of nitrogen was varied between 5.9 and 9.9 m/s and several tests were used to determine the flow rate of methane to ensure blowout. No flame could be established with a nitrogen velocity greater than 9.9 m/s. Table 5.1 provides the blowout velocities of methane and nitrogen, so called because a lower velocity of either gas would not produce a flame that blows out. Table 5.1 also gives the average height of diffusion flame disappearance for each case as observed from digital images.

Table 5.1 Flow rates of nitrogen and methane used to cause blowout.

Nitrogen velocity (m/s)	Methane velocity (m/s)	Average height at diffusion flame disappearance (cm)	Lean flammability limit	Height of lean flammability limit (cm)
0.0	65.7	28.3	5.0%	26.1
5.9	57.4	26.9	5.5%	24.9
8.1	49.6	27.1	5.8%	24.2
8.7	16.5	18.4	7.6%	19.9
9.2	35.6	24.7	6.3%	23.0
9.9	28.6	22.9	6.7%	22.0

Images of the flame from ignition to blowout are shown in Figure 5.1 for the case with the methane velocity, U_{CH_4}, at 28.6 m/s and the nitrogen velocity, U_{N_2}, at 9.9 m/s (Table 5.1, bottom row). Blowout occurs 2.97 seconds after ignition at the burner. The diffusion flame is clearly seen until 2.83 seconds. The flame moves quickly downstream to blowout after the diffusion flame disappears. Figure 5.2 shows images similarly obtained for U_{CH_4} = 49.6 m/s and U_{N_2} = 8.1 m/s (Table 5.1, third row). For this case, the diffusion flame disappears after 1.67 seconds and blowout occurs at 1.8 seconds. As stated in the previous chapter, extensive testing of flames at blowout reveal no trend in the time needed for a flame at blowout conditions to proceed from ignition to extinguishment.

Figure 5.1 Images of flame for U_{CH_4} = 28.6 m/s, U_{N_2} = 9.9 m/s.

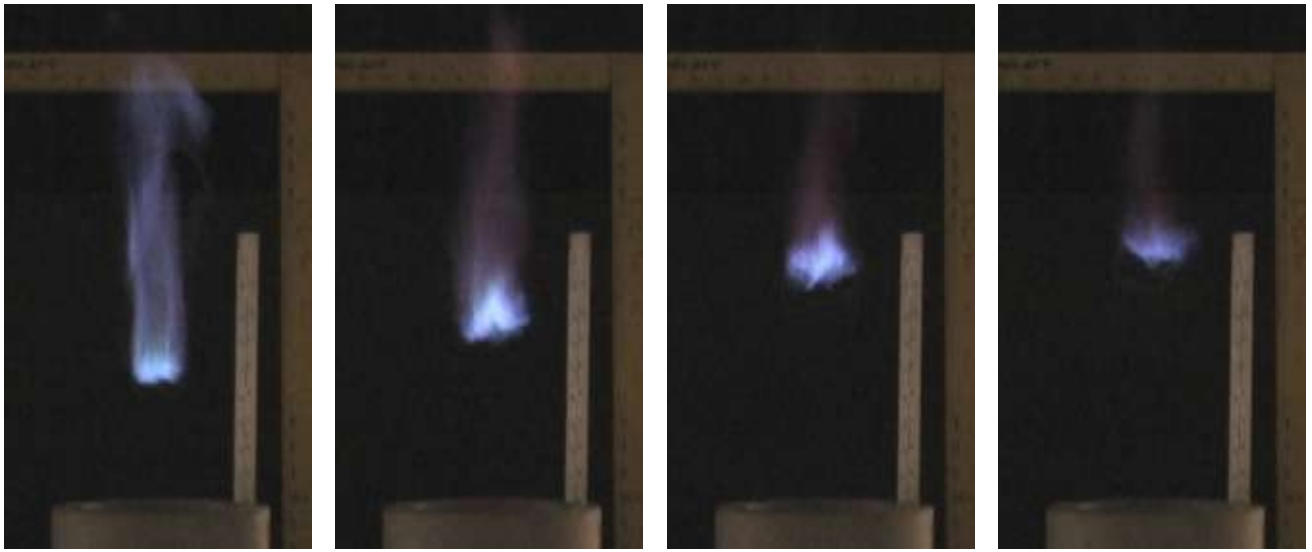

(a) h = 10.7 cm
t = 0.73 s

(b) h = 14.2 cm
t = 2.17 s

(c) h = 19.1 cm
t = 2.77 s

(d) h = 20.8 cm
t = 2.8 s

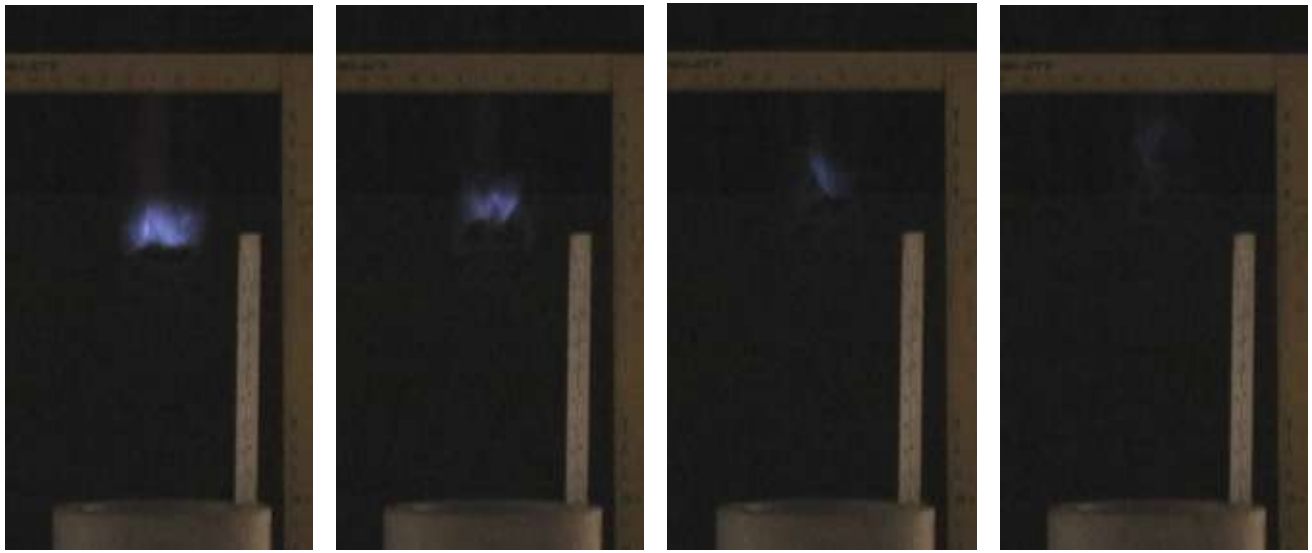

(e) h = 22.7 cm
t = 2.83 s

(f) h = 25.2 cm
t = 2.87 s

(g) h = 27.4 cm
t = 2.9 s

(h) h = 30.0 cm
t = 2.93 s

Figure 5.2 Images of flame for U_{CH_4} = 49.6 m/s, U_{N_2} = 8.1 m/s.

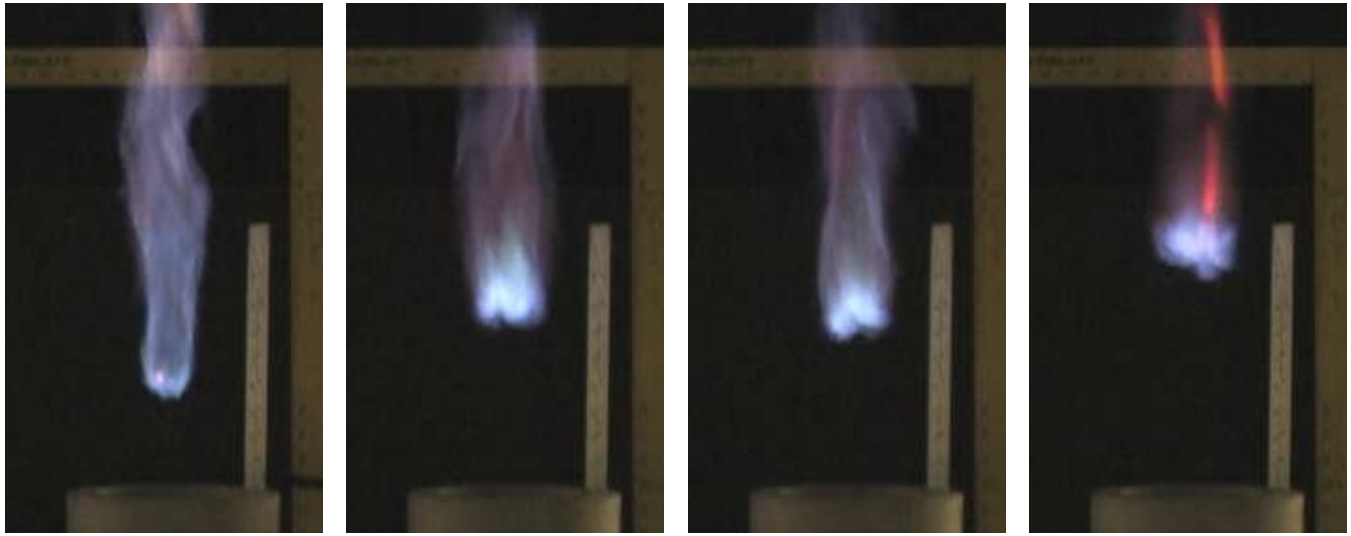

(a) h = 8.8 cm
t = 0.37 s

(b) h = 15.1 cm
t = 0.8 s

(c) h = 13.9 cm
t = 1.27 s

(d) h = 19.5 cm
t = 1.43 s

(e) h = 23.2 cm
t = 1.6 s

(f) h = 27.4 cm
t = 1.67 s

(g) h = 31.3 cm
t = 1.7 s

(h) h = 35.7 cm
t = 1.73 s

As first proposed in Chapter 4, the height of the flame front at which the diffusion flame disappears is theorized to occur at the lean limit of the fuel mixture. Flammability limits of fuels in air have been determined experimentally and are believed to be due to heat loss from the flame, flame stretch, and flame instabilities (Strehlow, 1984). The flammability limits for a mixture can be calculated using Le Chatelier's principle, which is fairly accurate for mixtures containing hydrocarbons (Strehlow, 1984). The heating value of a fuel, *Q*, multiplied by its lean limit as a percent of volume, *L*, is about constant so the relation

$$Q_1 L_1 = Q_m L_m \tag{5.4}$$

is true for subscript *1* representing a particular fuel and *m* representing a mixture. For a mixture consisting of *J* number of fuels,

$$Q_m = \sum_{j=1}^{j=J} x_j Q_j \tag{5.5}$$

where *x* is the volume fraction. Thus, using Equations 5.4 and 5.5,

$$\frac{\sum_{j=1}^{j=J} x_j Q_j}{Q_m} = 1 = \frac{\sum_{j=1}^{j=J} x_j L_m}{L_j} \tag{5.6}$$

and

$$L_m = \frac{1}{x_1 / L_1 + x_2 / L_2 + \cdots + x_J / L_J} \tag{5.7}$$

(Weinberg, 1963). So the lean limit of a mixture of methane and nitrogen can be calculated from the volume fraction of methane by

$$L_m = \frac{1}{x_{CH_4} / 5.0 + 0} = \frac{5.0}{x_{CH_4}}, \tag{5.8}$$

assuming an ideal gas (Strehlow, 1984). The calculated lean limits for the five mixtures are shown in Table 5.1.

The mass fraction of the mixture was calculated from Equation 1.4 by determining the density of the mixture. The flow velocities of methane and nitrogen set by the rotameter of each were, along with the gas densities, used to determine the mass flow rate of each gas. The density of the mixture was then calculated by

$$\rho_0 = Y_{CH_4}\rho_{CH_4} + Y_{N_2}\rho_{N_2} \tag{5.9}$$

where Y is the mass fraction determined by

$$Y_i = \frac{\dot{m}_i}{\dot{m}_i + \dot{m}_j} \tag{5.10}$$

for a mixture of i and j with the mass flow rate $\dot{m}$.

Figure 5.3 shows the graphical results of these experiments. For each fuel velocity, the height at which the diffusion flame disappears is plotted with the average of the data and the estimated height of the lean limit. In each case, the diffusion flame disappears within 3 cm of the lean flammability limit. This data supports the conclusion first put forth from data in Figure 4.3 that during blowout the reaction zone at the flame front moves to a downstream location at which all fuel is burnt locally. Burning at the lean limit does not leave enough

fuel-rich gases to support a diffusion flame. Blowout occurs quickly after the diffusion flame disappears and at a location slightly beyond the location of the lean limit.

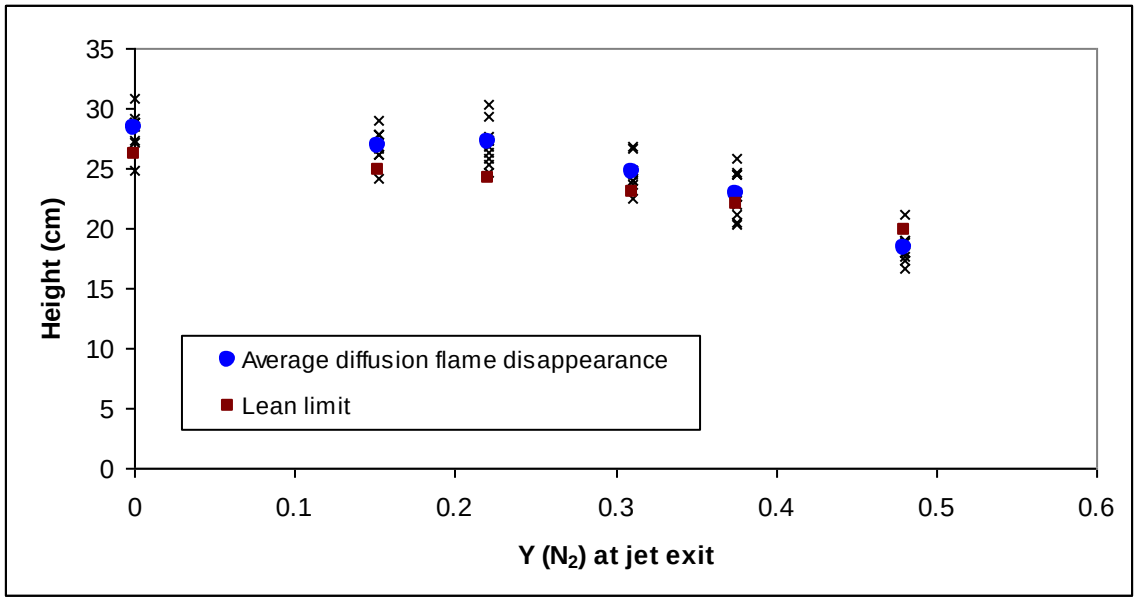

Figure 5.3 Height of the disappearance of the diffusion flame and the lean limit for each case (x) and the average.

5.4 Blowout Parameter

As first discussed in Section 1.3.2, Broadwell *et al.* (1984) defines a blowout criterion as the ratio between the mixing time and the chemical time. The molecular mixing between the fuel and entrained air is caused by inviscid motions scaled with the local jet diameter, δ, and associated with time

$$t_m = \frac{\delta}{u} \tag{5.11}$$

where u is the local velocity. The fluctuations eventually reach the Kolmogorov scale. Diffusion at this scale is associated with time, t_λ,

$$t_\lambda = \frac{\delta}{u}\left(\frac{Sc}{\mathrm{Re}}\right)^{1/2} \tag{5.12}$$

where *Sc* is the Schmidt number and *Re* is the Reynolds number. At high Reynolds numbers like those seen at blowout, the small scale diffusion can be neglected and the mixing time is approximated as Equation 5.11. Thus, the critical parameter, ε, is

$$\varepsilon \equiv \frac{t_m}{t_c} \propto \frac{\delta/u}{\kappa/S_L^{\,2}} \tag{1.3}$$

which can be rewritten as

$$\varepsilon = \frac{dS_L^2\psi^2\left(\rho_0/\rho_\infty\right)^{1/2}}{u\kappa}. \tag{5.13}$$

Equation 5.13 uses conservation of momentum and similarity to put ε in terms of the fuel pipe diameter, d, and properties of the fuel (Broadwell *et al.*, 1984). Kalghatgi (1981) provides the values used by Broadwell *et al.* (1984): ψ (stoichiometric air to fuel ratio) = 17.2, S_L (laminar burning velocity) = 0.39 m/s, and κ (thermal diffusivity) = 4.56 x 10^{-4} m^2/s. Including the density ratio for fuel to air, these values are defined as

$$A = S_L^2\psi^2\left(\rho_0/\rho_\infty\right)^{1/2}\kappa^{-1} \tag{5.14}$$

so A = 73,520 s^{-1} for a methane jet-flame.

The velocity in Equation 5.13 can be approximated as the jet exit velocity at blowout in order to determine the critical value of ε at blowout. Because the jet exit diameter was the same for all experiments (in Chapter 4 and Chapter 5), Equation 5.13 is rewritten as

$$\varepsilon = \frac{257.2 m/s}{u} \tag{5.15}$$

and so a constant value of ε requires a constant u. Broadwell *et al.* (1984) found $\varepsilon \approx 4.6$ for methane, and Dahm and Dibble (1988) found $\varepsilon \approx 4.3$ for methane with co-flow. To calculate this parameter for the flames with co-flow analyzed in Chapter 4, an effective velocity is used

$$U_{eff} = U_0 + C\sqrt{\rho_{cf}/\rho_0}\,U_{cf} \tag{3.1}$$

where C = 40 (Kumar *et al.*, 2007). Using this velocity in Equation 5.15 gives a range of ε from 3.9 to 4.9 and an average ε of 4.35 a value in good agreement with the previous studies. Table 5.2 provides the data from experiments and the effective velocities calculated, and Figure 5.4 plots the blowout velocities. For ε < 4.35, the flow velocities are such that blowout is predicted to occur.

Table 5.2 Blowout velocities for flames with co-flow.

Methane velocity (m/s)	Co-flow velocity (m/s)	U_{eff} (m/s) – Equation 3.1	ε
65.7	0.0	65.7	3.9
42.4	0.35	61.2	4.2
39.0	0.39	59.9	4.3
32.2	0.49	58.5	4.4
19.6	0.6	51.8	4.9

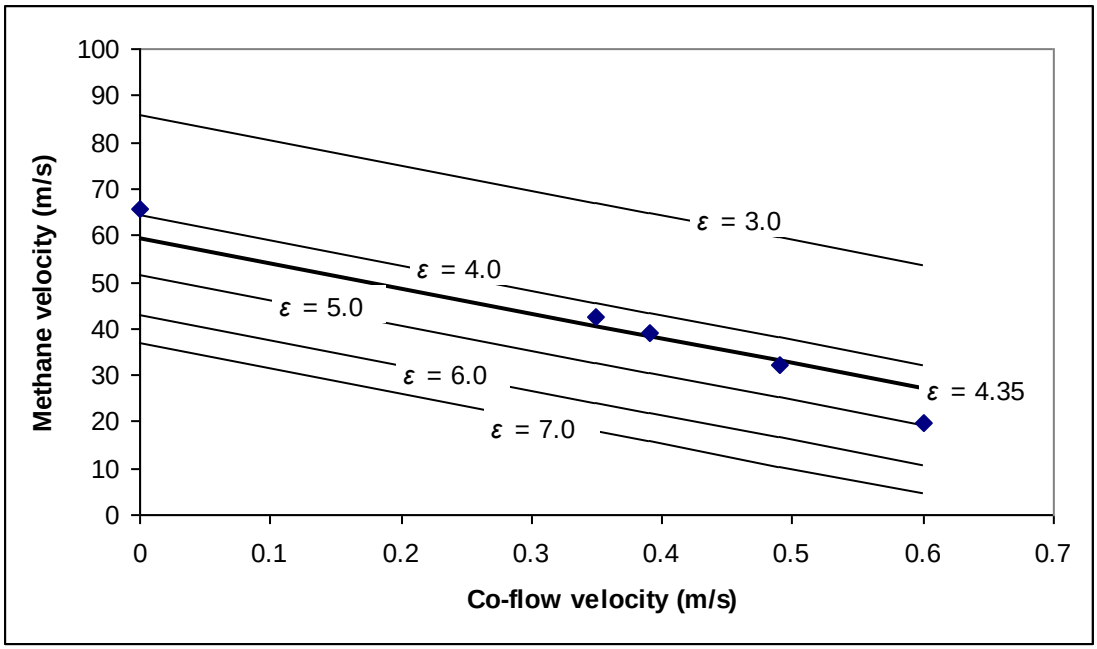

Figure 5.4 Velocities required for blowout shown with ε contours.

Figure 5.5 shows that the relationship between the amount of methane and nitrogen in a blowout mixture is nonlinear, which is an obvious departure from the behavior of Figure 5.4. The dashed line delineates the fuel and nitrogen velocities that will result in blowout and

those that will not. A flowrate of about 10 m/s or higher of nitrogen will most likely result in blowout. At high enough velocities of either gas, ignition may not result in anything but localized combustion.

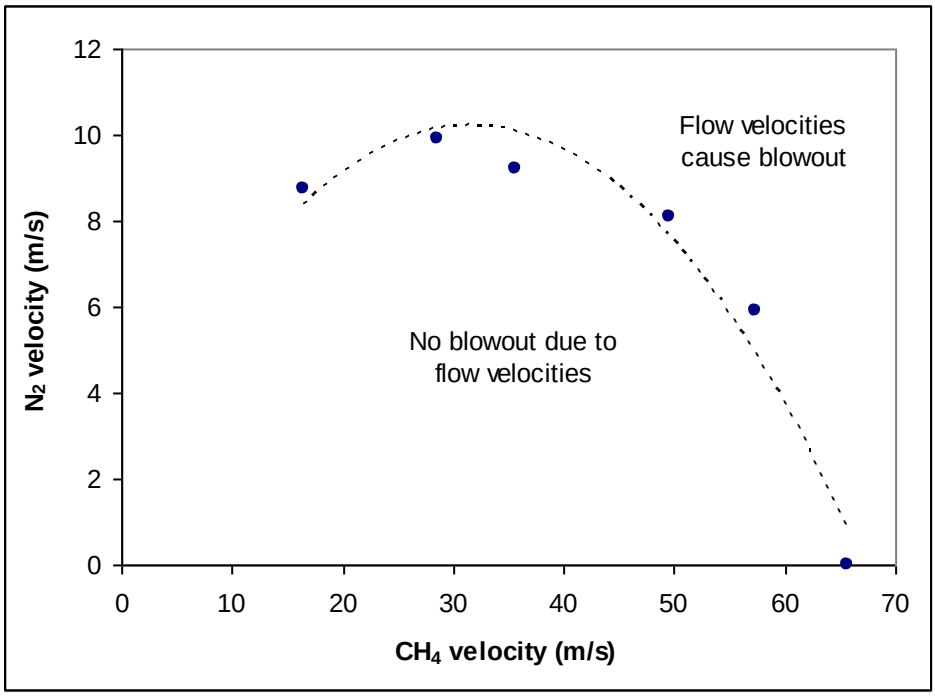

Figure 5.5 Methane and nitrogen velocities for flame blowout.

The velocity of the fuel decreases linearly as the diluent concentration increases, as seen in Figure 5.6. The change in the diluent velocity however creates a parabola when plotted with the concentration. The combined velocity is the total jet exit velocity issuing

from the fuel pipe. Dahm and Mayman (1990) modified Equation 5.13 to correct for large diluent concentrations. Thus, ψ is replaced by φ where

$$\phi = (1 - Y_{N_2})\psi . \tag{5.16}$$

Equation 5.13 then becomes

$$\varepsilon = \frac{dS_L^2 (1+\phi)^2 \left(\rho_0 / \rho_\infty \right)^{1/2}}{u\kappa} . \tag{5.17}$$

As shown in Table 5.3, using the combined velocity in Equation 5.17 and the mixture density results in a range of ε from 3.4 to 4.0 and an average ε of 3.59. This value is slightly lower than that found by Weiland and Strakey (2009) of ε = 4.92 for confined nitrogen-diluted hydrogen flames. The discrepancy can be due to differences in defining the velocity or in the gas properties used. The data shown in Figure 5.5 is consistent with studies of other diluted flames and this behavior provides insight into the blowout phenomenon.

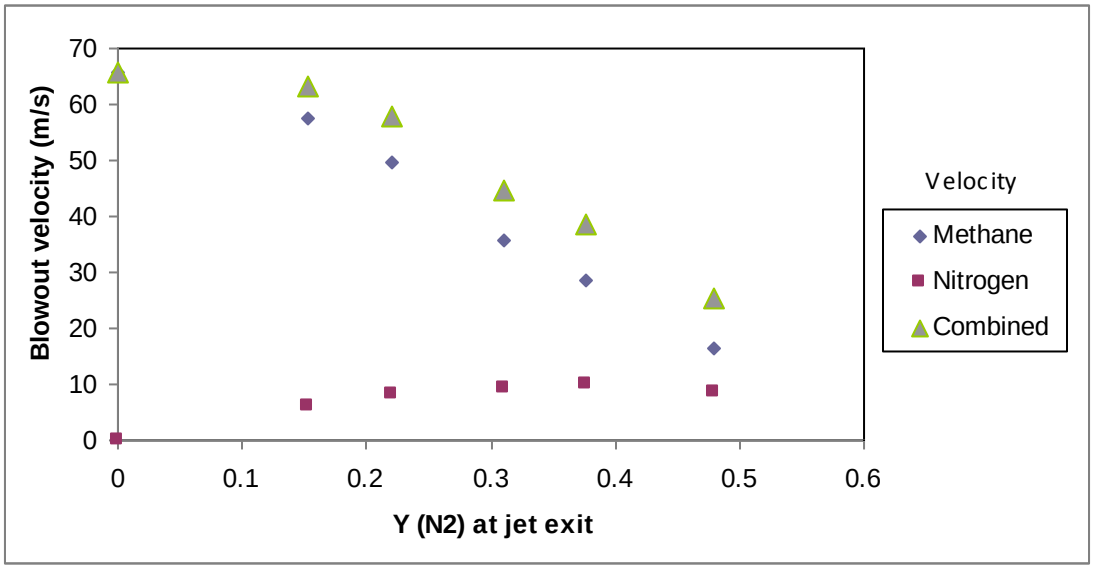

Figure 5.6 Flow velocities for each diluent concentration tested.

Table 5.3 Blowout velocities for diluted flames.

Methane velocity (m/s)	Nitrogen velocity (m/s)	Combined velocity (m/s)	ε
57.4	5.9	63.3	3.5
49.6	8.1	57.7	3.4
35.6	9.2	44.8	3.6
28.6	9.9	38.5	3.5
16.5	8.7	25.3	4.0

5.5 Conclusions

Further analysis of the blowout phenomenon has helped to verify the importance of the diffusion flame and establish a parameter for predicting blowout. Data from both flames with co-flow and diluted flames show that the calculation of the blowout criterion is highly dependent on the method used to determine the velocity of the jet mixture downstream. For diluted flames, this parameter is about 3.59. For flames with co-flow, it is about 4.3.

The parabolic relationship between the methane and nitrogen velocities results in the nitrogen concentration decreasing with increasing methane velocity. At the greatest nitrogen velocity, the concentration is 0.38. To achieve a higher concentration the rate of nitrogen must be decreased. This behavior is markedly different from flames of pure methane in the presence of co-flow where the velocities have a linear relationship. Dahm and Mayman (1990) also found a parabolic relationship between fuel and diluent velocities using air as the diluent. Thus, despite blowout occurring far downstream, it is affected by the mixing that occurs at the burner, since a jet of fuel/air has different blowout limits than a fuel jet surrounded by co-flowing air.

There exists (within the range where combustion is possible) two different fuel velocities at which blowout will occur for a given diluent velocity. Blowout is therefore not dependent on diluent concentration or, as noted in previous chapters, on the amount of turbulence as defined by the Reynolds number. The disappearance of the diffusion flame

remains, however, a consistent indicator that blowout is imminent. Regardless of the diluent concentration, the disappearance occurs at the lean flammability limit.

Chapter 6

Summary

6.1 Conclusions

The changes in the reaction zone of turbulent flames, documented with images and recorded data, have been used to determine characteristics of flame stability and predict the onset of instability. Experiments of methane flames with co-flowing air and without were performed to deduce causes for the change in behavior which defines laminar and turbulent stable flames and unstable flames. Further experiments with diluted-methane flames were done to lend support to previous analysis. Conclusions from each set of experiments have been discussed in detail in Sections 2.5, 3.4, 4.5, and 5.5.

Results from studies of flames close to the burner illuminated the role of flow velocity on hysteretic behavior. The amount to which co-flow affects a flame's location depends on its velocity. At low velocities, a flame's height will decrease between lift-off and reattachment. However, at high velocities, a local minimum occurs and the height immediately prior to reattachment can exceed that at lift-off. A critical point based on the

normalized co-flow velocity was determined at which a local minimum is observed. The existence of this local minimum indicates the competing effects of the axial velocity field and of a shift in the location of the flammable region.

Within the fully developed turbulent region, stable lifted flames fluctuate in a temporally irregular manner. The location and flow velocity have different influences on the fluctuation characteristics identified. The normalized fluctuation amplitude is found to be unaffected by downstream distance but the oscillatory rate does vary with distance. Fluctuation behavior from flames about to blow out shows a discernible difference from that of stable flames which implies a significant increase in the size of large-scale structures far downstream. The data suggest that the largest scales of turbulence may influence the lifted height but that viscous dissipation plays a primary role in fluctuations.

At high enough flow velocities, flames move downstream, become unstable, and blow out. While experiments proved that the amount of time from ignition to blowout was unpredictable, the disappearance of the diffusion flame is a precursor to blowout and indicates that extinguishment is imminent. An estimate of the location of the flammability limits for diluted and nondiluted flames without co-flow was used to determine that the disappearance occurs near the lean limit. The role of the diffusion flame was verified by noting that the velocity of the flame front increased significantly after the diffusion flame was witnessed to disappear. Blowout velocities for diluted flames and flames with co-flow were used to calculate a parameter which can be used to predict the flow velocities at which blowout will occur.

Defining the mechanisms for stability requires understanding the behavior of flames in any flammable region, from the jet exit to the lean flammability limit. This work has established the significant role of co-flow on flame behavior near the burner, defined fluctuations of stable lifted flames in terms of amplitude and oscillatory rate, and discovered a visual indicator of blowout for unstable flames far downstream.

6.2 Future Work

While results from the current research have led to important observations on the mechanisms of stabilization, more work in the area is warranted to gain a better understanding of the phenomena described in the current paper. The reasons for the pronounced effect of co-flow on flames in hysteresis could be better understood by studying the velocity field of the incoming flow. Also, to determine if diffusion flame disappearance is a consistent precursor to blowout, experiments should be performed with other hydrocarbon fuels, both diluted and undiluted. Ethylene and propane are reasonable choices because the chemistries of these fuels are comparatively well-known.

To determine the velocity field and acquire concentration measurements, the use of particle image velocimetry (PIV) and planar laser-induced fluorescence (PLIF) is required. PIV involves seeding the flow with tracking particles and illuminating the particles to find the instantaneous velocity field throughout the laser sheet. PLIF can determine the instantaneous population densities of atoms or molecules and is especially useful for

turbulent flames. CH or OH radical fields are used to mark the relative location and thickness of the flame. These techniques have been used simultaneously in a number of studies (Frank *et al*., 1996; Han and Mungal, 2003; Carter *et al*.. 1998) and an extensive explanation of these procedures can be found in Watson (2002) and Watson *et al*. (1999). Those studies examined the leading-edge flame structure and found the significance of large-scale structures on flame extinction.

6.2.1 Experiments on Jet Confinement

Little experimental work has been done thus far in the combustion field on confined jets. The research that has been conducted indicates that flame stabilization can be greatly influenced by confinement. Thus, knowledge of liftoff, blowout, and local extinction in free jets does not lend itself immediately to a model of confined behavior. A better understanding of flame behavior in confined jets can lead to better design of combustion chambers, micro-jets, and other devices, as well as aid in the understanding of fundamental concepts of flame behavior.

The change in the flow field of confined jets compared to free jets affects flame behavior. Jet confinement is an important issue because it denies radial entrainment. The entrainment ratio and mixing of a confined jet differs markedly from that of a free jet since there is no continual radial entrainment. Mass is conserved in the axial direction for a confined jet. However, momentum is not conserved due to friction caused by the walls of confinement (Cha and Chung, 1996).

Some research has been done with confined jets to determine the effect of confinement on flame characteristics. Brookes *et al.* (1999) studied methane diffusion flames confined in a Pyrex cylinder. Their data was used to create a model of soot production and thermal radiation based on the behavior of flames at one and three atmospheres pressure. A study by Cha and Chung (1996) investigated the effect of the flow field on the liftoff height of nonpremixed turbulent flames. Using propane fuel, the nozzle and cylinder diameters were changed to determine trends. Cha and Chung (1996) found that the liftoff height of a free jet has no dependence on the nozzle diameter. Figure 6.1 shows their experimental data for the various nozzle and cylinder diameters. This linear relationship was not seen in the confined jet. A 150 millimeter long cylinder was placed over the burner to get data on confinement effects. The data indicated that the liftoff height had a linear dependence on the nozzle diameter as well as the jet exit velocity; hence, the liftoff height is proportional to the Reynolds number and can be represented by the following:

$$\frac{H_L}{d} = U_0\left(1.02 + \frac{0.0976}{D - 0.35}\right) \qquad 6.1$$

where H_L is the liftoff height, d the nozzle inner diameter, U_0 the fuel jet exit velocity, and D the diameter of the confining cylinder. It was also found that within a cylinder of less than 35 cm diameter, flames are unable to liftoff and blowout directly. Cha and Chung (1996) hypothesized that the confinement restricts the entrainment to the area near the nozzle, given the same co-flow condition as a free jet, which enhances nozzle cooling and promotes liftoff. They also looked at the height at which blowout occurred and the blowout velocity. The

ratio of blowout height to nozzle diameter is nearly constant for both the confined and free jets, and the blowout velocity is independent of the diameter for confined jets (see Figure 6.2). These results indicate the importance of studying confined jets.

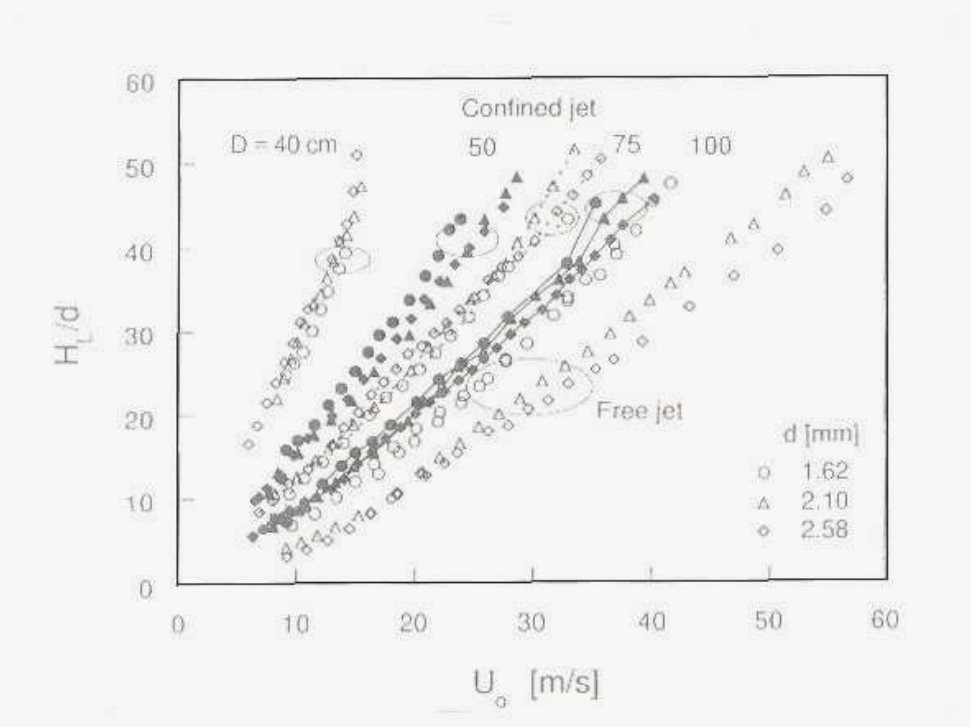

Figure 6.1. Liftoff height, H_L, nondimensionalized by the nozzle diameter, d, versus fuel velocity. The linear dependence with the free jet is not evident in the confined jets of various cylinder diameters (Cha and Chung, 1996).

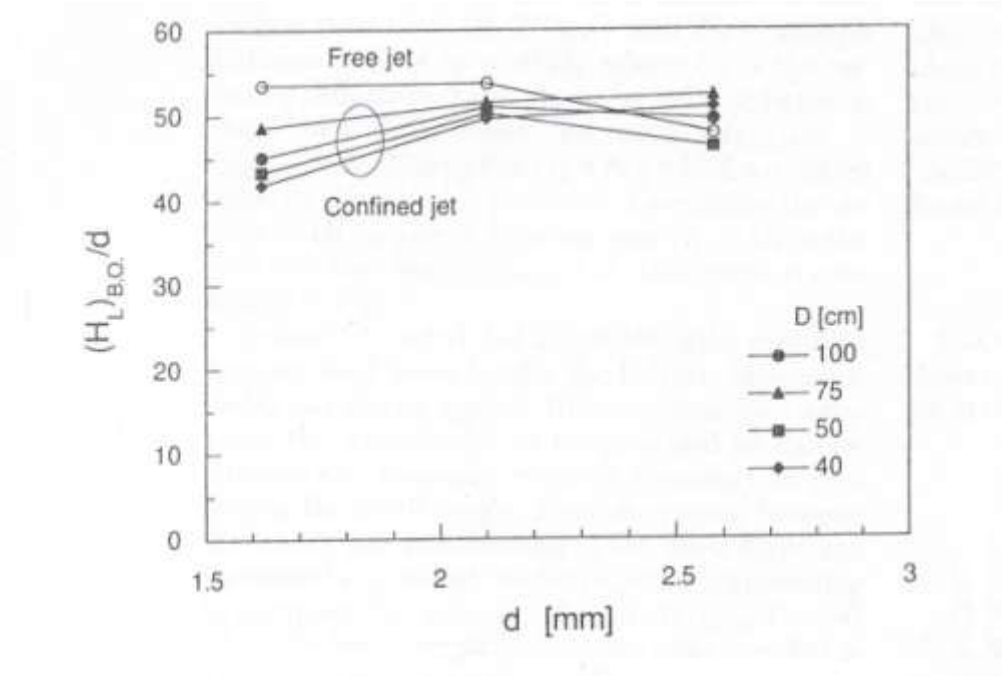

Figure 6.2 Lifted height at blowout, $(H_L)_{B.O.}$, nondimensionalized with the nozzle diameter, *d*, for free and confined jets (Cha and Chung, 1996).

Several numerical studies have also been performed to model the behavior of confined jets. Ellzey *et al.* (1991) simulated several confined diffusion flames and found that gravity has a significant effect on the flow field. Anderson *et al.* (1999) modeled a one-step reaction to determine the effects of confinement on flame broadening. They found that as the stoichiometric mixture fraction increased, the non-premixed flame zone broadened and the flame temperature decreased. Singh *et al.* (1999) studied entrainment and mixing in confined jets with a finite element model. The aspect ratio and density ratio, and not the Reynolds number, had the greatest effect entrainment and mixing. Their work used a modified Craya-Curtet number for variable density. The Craya-Curtet number is a function of the integrals of

mass and momentum fluxes across the inlet plane of the duct. The nondimensional Craya-Curtet number can describe and predict the flow of a confined jet (Singh *et al.*, 2003). The number is a well-known similarity parameter for co-axial confined jets (Woodfield *et al.*, 2000).

6.2.2 Future Research on Jet Confinement

Future research would provide insight into the flame structure, stability, and extinction of confined, lifted flames. Experiments will help identify the effect of different fuels and flow velocities on flame development and stabilization and the results can be compared to those of an unconfined flame at similar conditions to determine the optimal configuration for flame control.

Cylinders of various diameters (between 30 and 80 cm) placed over the burner apparatus would contain the flame. Cylinders made out of Pyrex have been used in previous studies (Brookes *et al.*, 1999). Because the flames will vary in length, the cylinders should have different lengths, initially 100 and 150 mm. The modifications necessary to study confined jets with a burner such as the one used for the present research (Section 1.4) are shown in Figure 6.3. The cylinder would be centered over the burner. The amount of air entrained into the flame is then a function of the cylinder diameter.

A similar experimental procedure as used in the present research would allow the overall propagation, recession, and extinction of the flame to be recorded and individual images at specific times analyzed. The effect of co-flow can be studied by varying the co-

flow velocity, including the case with no co-flow present. Previous research of free jets will be compared to the data to develop a paradigm to explain the difference between confined and free jets.

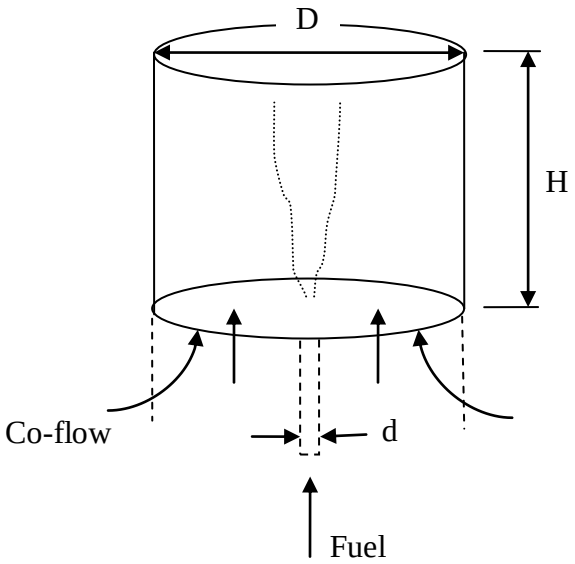

Figure 6.3 Schematic of Confining Cylinder. *d* is the fuel nozzle diameter, *D* is the cylinder diameter, and *H* is the cylinder height.

REFERENCES

Anderson, K.R., Mahalingham, S., and Hertzberg, J. A Two-Dimensional Planar Computational Investigation of Flame Broadening in Confined Non-premixed Jets. *Combustion and Flame*, 118: 233-47, 1999.

Boulanger, J., Vervisch, L., Reveillon, J., and Ghosal, S. Effects of Heat Release in Laminar Diffusion Flames Lifted on Round Jets. *Combustion and Flame*, 134: 355-68, 2003.

Broadwell, J.E., Dahm, W.J.A., and Mungal, M.G. Blowout of Turbulent Diffusion Flames. *Proceedings of the Combustion Institute*, The Combustion Institute, Pittsburgh, 20: 303-10, 1984.

Brookes, S.J. and Moss, J.B. Measurements of Soot Production and Thermal Radiation from Confined Turbulent Jet Diffusion Flames of Methane. *Combustion and Flame*, 116: 49-61, 1999.

Brown, C.D., Watson K.A., and Lyons, K.M. Studies on Lifted Jet Flames in Co-Flow: The Stabilization Mechanism in the Near- and Far-Fields. *Flow, Turbulence and Combustion*, 62: 249-73, 1999.

Burgess, C.P. and Lawn, C.J. The Premixture Model of Turbulent Burning to Describe Lifted Jet Flames. *Combustion and Flame*, 119: 95-108, 1999.

Carter, C.D., Donbar, J.M., and Driscoll, J.F. Simultaneous CH Planar Laser-Induced Fluorescence and Particle Imaging Velocimetry in Turbulent Nonpremixed Flames. *Applied Physics B*, 66: 129-32, 1998.

Cessou, A., Maurey, C., and Stepowski, D. Parametric and Statistical Investigation of the Behavior of a Lifted Flame Over a Turbulent Free-Jet Structure. *Combustion and Flame*, 137: 458-77, 2004.

Cha, M.S. and Chung, S.H. Characteristics of Lifted Flames in Nonpremixed Turbulent Confined Jets. *Proceedings of the Combustion Institute*, The Combustion Institute, Pittsburgh, 26: 121-28, 1996.

Chao, Y.-C., Chang, Y.-L., Wu, C.Y., and Cheng, T.S. An Experimental Investigation of the Blowout Process of a Jet Flame. *Proceedings of the Combustion Institute*, The Combustion Institute, Pittsburgh, 28: 335-42, 2000.

Chao, Y.-C., Wu, C. Y., Lee, K.-Y., Li, K.-Y., Li, Y. H., Chen, R.-H., and Cheng, T.-S. Effects of Dilution on Blowout Limits of Turbulent Jet Flames. *Combustion Science and Technology*, 176: 1735-53, 2004.

Chao, Y., Wu, C., Yuan, T., and Cheng, T. Stabilization Process of a Lifted Flame Tuned by Acoustic Excitation. *Combustion Science and Technology*, 174: 87-110, 2002.

Chen, C.J. and Rodi, W. Vertical Turbulent Buoyant Jets – A Review of Experimental Data, Pergamom, Oxford, 1980.

Chung, S.H. and Lee, B.J. On the Characteristics of Laminar Lifted Flames in a Nonpremixed Jet. *Combustion and Flame*, 86: 62-72, 1991.

Clemens, N.T. and Paul, P.H. Effects of Heat Release on the Near Field Flow Structure of Hydrogen Jet Diffusion Flames. *Combustion and Flame*, 102: 271-84, 1995.

Coats, C.M. Coherent Structures in Combustion. *Progress in Energy and Combustion Science*, 22: 427-509, 1996.

Dahm, W.J.A. and Dibble, R.W. Co-Flowing Turbulent Jet Diffusion Flame Blowout. *Proceedings of the Combustion Institute*, The Combustion Institute, Pittsburgh, 22: 801-08, 1988.

Dahm, W.J.A. and Mayman, A.G. Blowout Limits of Turbulent Jet Diffusion Flames for Arbitrary Source Conditions. *AIAA Journal*, 28 (7): 1157-62, 1990.

Daou, R., Daou, J., and Dold J. Effect of Volumetric Heat Loss on Triple Flame Propagation. *Proceedings of the Combustion Institute*, The Combustion Institute, Pittsburgh, 29: 1559-64, 2002.

Dowling, D.R. and Dimotakis, P.E. Similarity of the Concentration Field of Gas-Phase Turbulent Jets. *Journal of Fluid Mechanics*, 218: 109-141, 1990.

Echekki, T. and Chen, J. Structure and Propagation of Methanol-Air Triple Flames. *Combustion and Flame*, 114: 231-45, 1998.

Ellzey, J.L., Laskey, K.J., and Oran, E.S. A Study of Confined Diffusion Flames. *Combustion and Flame*, 84: 249-64, 1991.

Frank, J.H., Lyons, K.M., and Long, M.B. Simultaneous Scalar/Velocity Field Measurements in Turbulent Gas-Phase Flows. *Combustion and Flame*, 107: 1-12, 1996.

Hammer, J.A. Lifted Turbulent Jet Flames. Doctor of Philosophy. California Institute of Technology, Pasadena, CA, 1-140, 1993.

Hammer, J.A. and Roshko, A. Temporal Behavior of Lifted Turbulent Jet Flames. *Combustion Science and Technology*, 155: 75-103, 2000.

Han, D. and Mungal, M.G. Observations on the Transition from Flame Liftoff to Flame Blowout. *Proceedings of the Combustion Institute*, The Combustion Institute, Pittsburgh, 28: 537-43, 2000.

Han, D. and Mungal, M.G. Simultaneous Measurements of Velocity and CH Distributions. Part 1: Jet Flames in Co-Flow. *Combustion and Flame*, 132: 565-90, 2003.

Hottel, H.C. and Hawthorne, W.R. Diffusion in Laminar Flame Jets. *3rd Symposium on Combustion, Flame and Explosion Phenomena*, The Combustion Institute, Pittsburgh, 254-66, 1949.

Joedicke, A., Peters, N., and Mansour, M. The Stabilization Mechanism and Structure of Turbulent Hydrocarbon Lifted Flames. *Proceedings of the Combustion Institute*, The Combustion Institute, Pittsburgh, 30: 901-09, 2005.

Junus, R., Vierkant, J.E., Stubington, J.F., Sergeant, G.D., and Tas, I. The Effects of the Design of the Cap of a Natural Gas-Fired Cooktop Burner on Flame Stability. *International Journal of Energy Research*, 22: 175-84, 1998.

Kalghatgi, G.T. Blowout Stability of Gaseous Jet Diffusion Flames. Part 1: In Still Air. *Combustion Science and Technology*, 26: 233-39, 1981.

Kalghatgi, G.T. Blowout Stability of Gaseous Jet Diffusion Flames. Part III: Effect of Burner Orientation to Wind Direction. *Combustion Science and Technology*, 28: 241-45, 1982.

Kalghatgi, G.T. Lift-Off Heights and Visible Lengths of Vertical Turbulent Jet Diffusion Flames in Still Air. *Combustion Science and Technology*, 41: 17-29, 1984.

Karbasi, M. and Wierzba, I. Prediction and Validation of Blowout Limits of Co-Flowing Jet Diffusion Flames – Effect of Dilution. *ASME Journal of Energy Resources Technology*, 120: 167-71, 1998.

Kelman, J.B., Eltobaji, A.J., and Masri, A.R. Laser Imaging in the Stabilisation Region of Turbulent Lifted Flames. *Combustion Science and Technology*, 135: 117-34, 1998.

Kim, J., Kim, K.N., Won, S.H., Fujita, O., Takahashi, J., and Chung, S.H. Numerical Simulation and Flight Experiment on Oscillating Lifted Flames in Coflow Jets with Gravity Level Variation. *Combustion and Flame*, 145: 181-93, 2006.

Kumar, S., Paul, P.J., and Mukunda, H.S. Prediction of Flame Liftoff Height of Diffusion/Partially Premixed Jet Flames and Modeling of Mild Combustion Burners. *Combustion Science and Technology*, 179: 2219-53, 2007.

Law, C.K. Combustion Physics. Cambridge University Press, New York, 2006.

Lee, B.J., Cha, M.S., and Chung, S.H. Characteristics of Laminar Lifted Flames in a Partially Premixed Jet. *Combustion Science and Technology*, 127: 55-70, 1997.

Lee, B.J. and Chung, S.H. Stabilization of Lifted Tribrachial Flames in a Laminar Nonpremixed Jet. *Combustion and Flame*, 109: 163-72, 1997.

Lee, J., Won, S.H., Jin, S.H., and Chung, S.H. Lifted Flames in Laminar Jets of Propane in Coflow Air. *Combustion and Flame*, 135: 449-62, 2003.

Liñán, A. and Williams, F.A. Fundamental Aspects of Combustion. Oxford University Press, New York, 1993.

Lyons, K.M and Watson, K.A. Partially Premixed Combustion in Lifted Turbulent Jets. *Combustion Science and Technology*, 156: 97-105, 2000.

Lyons, K.M. and Watson, K.A. Visualizing Diffusion Flame Formation in the Wake of Partially Premixed Combustion. *Journal of Energy Resources Technology* 123: 221-27, 2001.

Miake-Lye, R.C. and Hammer, J.A. Lifted Turbulent Jet Flames: A Stability Criterion Based on the Jet Large-Scale Structure. *Proceedings of the Combustion Institute*, The Combustion Institute, Pittsburgh, 22: 817-24, 1988.

Montgomery, C.J., Kaplan, C.R. and Oran, E.S. The Effect of Co-Flow Velocity on a Lifted Methane-Air Jet Diffusion Flame. *Proceedings of the Combustion Institute*, The Combustion Institute, Pittsburgh, 27: 1175-82, 1998.

Moore, N., McCraw, J., and Lyons, K. Observations on Jet-Flame Blowout. *International Journal of Reacting Systems,* Article ID 461059, doi:10.1155/2008/461059, 2008.

Morcos, V.H. and Abdel-Rahim, Y.M. Parametric Study of Flame Length Characteristics in Straight and Swirl Light-Fuel Oil Burners. *Fuel*, 78: 979-85, 1999.

Müller, C.M., Breitbach, H., and Peters, N. Partially Premixed Turbulent Flame Propagation in Jet Flames. *Proceedings of the Combustion Institute*, The Combustion Institute, Pittsburgh, 25: 1099-106, 1994.

Mungal, M.G. Introduction to Turbulent Combustion: Experiments in Combustion, *von Karman Institute for Fluid Dynamics*, 1999.

Muñiz, L. and Mungal, M.G. Instantaneous Flame-Stabilization Velocities in Lifted-Jet Diffusion Flames. *Combustion and Flame*, 111: 16-31, 1997.

Peters, N. Laminar Diffusion Flamelet Models in Non-Premixed Turbulent Combustion. *Progress in Energy and Combustion Science*, 10: 319-39, 1984.

Peters, N. Turbulent Combustion. Cambridge, U.K.; New York: Cambridge University Press, 2000.

Phillips, H. Flame in a Buoyant Methane Layer. *Proceedings of the Combustion Institute*, The Combustion Institute, Pittsburgh, 10: 1277-83, 1965.

Pitts, W. M. Assessment of Theories for the Behavior and Blowout of Lifted Turbulent Jet Diffusion Flames. *Proceedings of the Combustion Institute*, The Combustion Institute, Pittsburgh, 22: 809-16, 1988.

Poinsot, T. and Veynante, D. Theoretical and Numerical Combustion. R.T. Edwards Inc., Philadelphia, PA, 2001.

Ruetsch, G., Vervisch, L., and Liñán, A. Effects of Heat Release on Triple Flames. *Physics of Fluids*, 6: 1447-54, 1995.

Savas, Ö. and Gollahalli, S. R. Stability of Lifted Laminar Round Gas-Jet Flame. *Journal of Fluid Mechanics*, 165: 297-318, 1986.

Savas, Ö. and Gollahalli, S.R. Flow Structure in Near-Nozzle Region of Gas Jet Flames. *AIAA Journal*, 24: 1137-40, 1986.

Schefer, R.W. and Goix, P.J. Mechanism of Flame Stabilization in Turbulent, Lifted-Jet Flames. *Combustion and Flame*, 112: 559-74, 1998.

Singh, G., Sundararajan, T., and Bhaskaran, K.A. Mixing and Entrainment Characteristics of Circular and Noncircular Confined Jets. *Journal of Fluids Engineering*, 125: 835-42, 2003.

Singh, G., Sundararajan, T., and Shet, U.S.P. Entrainment and Mixing Studies for a Variable Density Confined Jet. *Numerical Heat Transfer, Part A*, 35: 205-23, 1999.

Strehlow, Roger A. Combustion Fundamentals. McGraw-Hill, New York, 1984.

Su, L.K., Han, D., and Mungal, M.G. Experimental Results on the Stabilization of Lifted Jet Diffusion Flames. *Center for Turbulence Research Annual Research Briefs*, 2000.

Su, L.K., Han, D., and Mungal, M.G. Measurements of Velocity and Fuel Concentration in the Stabilization Region of Lifted Jet Diffusion Flames. *Proceedings of the Combustion Institute*, The Combustion Institute, Pittsburgh, 28: 327-34, 2000.

Su, L.K., Sun, O.S. and Mungal, M.G. Experimental Investigation of Stabilization Mechanisms in Turbulent, Lifted Jet Flames. *Combustion and Flame*, 144: 494-512, 2006.

Terry, S.D. and Lyons, K.M. Low Reynolds Number Turbulent Lifted Flames in High Co-Flow. *Combustion Science and Technology*, 177: 2091-112, 2005.

Terry, S.D. and Lyons, K.M. Turbulent Lifted Flames in the Hysteresis Regime and the Effects of Coflow. *ASME Journal of Energy Resources Technology*, 128: 319-24, 2006.

Terry, S.D. On flame stability in the hysteresis regime in co-flow. Doctor of Philosophy. North Carolina State University, Raleigh, NC, 1-114, 2005.

Tieszen, S.R., Stamps, D.W., and O'Hern, T.J. A Heuristic Model of Turbulent Mixing Applied to Blowout of Turbulent Jet Diffusion Flames, *Combustion and Flame*, 106: 442-66, 1996.

Turns, Stephen R. An Introduction to Combustion. McGraw-Hill, Inc, New York, 1996.

Upatnieks, A., Driscoll, J.F., Rasmussen, C.C., and Ceccio, S.L. Liftoff of turbulent jet flames — assessment of edge flame and other concepts using cinema-PIV. *Combustion and Flame*, 138: 259-72, 2004.

Vanquickenborne, L. and van Tiggelen, A. The Stabilization Mechanism of Lifted Diffusion Flames. *Proceedings of the Combustion Institute*, The Combustion Institute, Pittsburgh, 10: 59-69, 1966.

Watson, K.A. Experimental Studies on the Leading Edge and Local Extinction in Lifted-Jet Diffusion Flames. Doctor of Philosophy, North Carolina State University, Raleigh, NC, 2002.

Watson K.A., Lyons, K.M., Donbar, J.M. and Carter, C.D. Simultaneous Rayleigh Imaging and CH-PLIF Measurements in Lifted Jet Diffusion Flames. *Combustion and Flame*, 123: 252-65, 2000.

Watson, K.A., Lyons, K.M., Donbar, J.M. and Carter, C.D. Simultaneous Two-Shot CH-PLIF and Particle Image Velocimetry Measurements in Lifted CH_4-Air Diffusion Flames. *Proceedings of the Combustion Institute*, The Combustion Institute, Pittsburgh, 29: 1905-12, 2002.

Watson K.A., Lyons, K.M., Donbar, J.M., and Carter, C. D. On Scalar Dissipation and Partially Premixed Flame Propagation. *Combustion Science and Technology*, 175(4): 649-64, 2003.

Watson, K.A., Lyons, K.M., Carter, C.D., and Donbar, J.M. Scalar and Velocity Field Measurements in a Lifted CH_4-Air Diffusion Flame. *Combustion and Flame*, 117: 257-71, 1999.

Weiland, N.T. and Strakey, P.A. Stability Characteristics of Turbulent Hydrogen Dilute Diffusion Flames. *Combustion Science and Technology*, 181: 756-81, 2009.

Weinberg, F.J. Optics of Flames. Butterworth & Co. (Publishers) Ltd., London, 1963.

Williams, F.A. Mechanisms of Fire Spread. *Proceedings of the Combustion Institute*, The Combustion Institute, Pittsburgh, 16: 1281-94 (and Comment by I. Glassman p. 1292), 1977.

Woodfield, P.L., Nakabe, K., and Suzuki, K. Numerical Computation on Recirculation Flow Structures in Co-Axial Confined Laminar Jets. *Japan Society of CFD*, 2000.

Wu, C.-Y., Chao, Y.-C., Cheng, T.-S., Li, Y.-H., Lee, K.-Y., and Yuan, T. The Blowout Mechanism of Turbulent Jet Diffusion Flames. *Combustion and Flame*, 145: 481-94, 2006.

Wygnanski, I. and Fiedler, H. Some Measurements in the Self-Preserving Jet. *Journal of Fluid Mechanics*, 38: 577-612, 1969.

APPENDIX

Scalar and Velocity Field Data in Lifted Flames: Observations

A.1 Introduction

Numerous researchers have performed experiments to obtain reaction zone location and morphology and to determine the incoming reactant velocity and concentrations. Much of this research has been performed to yield insight into the mechanism of stabilization of lifted flames (partial mixing, local extinction, and large-scale structure effects). Additionally, efforts to predict these parameters using cold-jet solutions have appeared recently in the literature. While progress has been made, there is still much discrepancy, both among the experimental findings as well as between experiment and theory. Results from three published papers are compared to better understand the differences in flame analysis.

A.2 Experimental Data

The data from Su *et al.* (2000), Muñiz and Mungal (1997), and Watson *et al.* (2002) are used to compare experimental results of the flame location and velocity to estimates. All three experimented with lifted methane-air flames burning with co-flowing air. The

experiments of Su *et al.* (2000) maintained a constant co-flow velocity while varying the jet exit velocity for two cases, A and B. Particle image velocimetry (PIV) measurements were taken at three locations: on the flame interface, towards the centerline, and away from the centerline. Table A.1 shows the results of this study for both cases. At each location, the PIV velocity increases as the fuel velocity decreases. The velocity estimates, to be discussed in the next section, correspond to the location (given in millimeters and in terms of the jet diameter, d) and so do not change for the three PIV measurements.

Table A.1 Su *et al.* (2000) data.

	Case:	**A**	**B**
Flow conditions:	Jet exit velocity (m/s)	15.3	10.8
	Co-flow velocity (m/s)	0.36	0.36
Flame location:	Height, z (mm)	52.9 (11.5d)	39.56 (8.6d)
	Radial, r (mm)	10.58	8.74
PIV:	On the interface (m/s)	0.3698	0.4085
	Towards centerline (m/s)	0.8686	1.0793
	Away from centerline (m/s)	0.2193	0.2494
Estimates:	Without co-flow (m/s)	*0.1372*	*0.0567*
	With co-flow (m/s)	*0.4831*	*0.3996*

Muñiz and Mungal (1997) also took PIV measurements at three different locations, as shown in Table A.2. For each flow condition, PIV measurements were taken at the instantaneous location of the side of the jet, the average location of the side of the jet, and the instantaneous location on the centerline. The first three flames in the Muñiz and Mungal (1997) data (Cases 1-3) have the same fuel velocity but different co-flow velocities.

Comparison of the centerline locations for the first three flames show a clear trend of increasing velocity with decreasing co-flow velocity (since the fuel velocity is constant). The last two flames (Cases 3 and 4) have approximately the same co-flow velocities but different fuel velocities resulting in the fourth flame being at a greater axial and radial position, and having a greater PIV velocity.

Table A.2 Muñiz and Mungal (1997) data.

	Case:	**1**	**2**	**3**	**4**
Flow conditions:	Jet exit velocity (m/s)	14	14	14	38
	Co-flow velocity (m/s)	0.58	0.43	0.27	0.28
Flame location:	Height, z (mm)	21.6 (4.5d)	17.8 (3.7d)	14.0 (2.9d)	31.0 (6.5d)
	Radial, r (mm)	3.2	3.0	2.6	5.5
PIV:	Instant. location on side of jet (m/s)	0.9	0.9	0.8	0.8
	Avg. location on side of jet (m/s)	1.4	1.6	1.0	1.1
	Instant. location on centerline (m/s)	3.1	3.7	4.8	5.8
Estimates:	Without co-flow (m/s)	*1.7411*	*1.1536*	*0.8294*	*1.3482*
	With co-flow (m/s)	*2.3085*	*1.5716*	*1.0903*	*1.6196*

Watson *et al.* (2002) determined the flame location from two-shot CH-PLIF (planar laser-induced fluorescence) images. PIV measurements were made at the average location and the instantaneous location of the stabilization point on either side of the jet centerline (Table A.3). The velocity at the average location is the average velocity in a region centered about the average flame base location. The velocity at the instantaneous location is the average velocity in an equally-sized region that moves from one image to the next. The

height and radial locations are the mean values found in the experiments. The first two cases, α and β, have the same co-flow velocities. The PIV velocities increase at both imaging locations with the fuel velocity (as seen with the Su *et al.* (2000) data and the centerline data from Muñiz and Mungal (1997)). The velocities at the average locations are much greater than at the instantaneous locations in every case. Additional data supplied by the authors gave the radial locations of the rich and lean flammability limits for the flame at each height, which is also included in Table A.3.

Table A.3 Watson *et al.* (2002) data.

	Case:	**α**	**β**	**γ**
Flow conditions:	Jet exit velocity (m/s)	15.8	21.2	27.5
	Co-flow velocity (m/s)	0.13	0.13	0.19
Flame location:	Axial height, *z* (mm)	29.3 (5.9*d*)	48.5 (9.7*d*)	75.1 (15*d*)
	Radial, *r* (mm)	7.2	9.3	12.0
PIV:	Avg. location (m/s)	1.06	1.35	1.73
	Instant. location (m/s)	0.83	1.05	1.28
Estimates:	Without co-flow (m/s)	*0.0412*	*0.3050*	*0.7323*
	With co-flow (m/s)	*0.1635*	*0.4303*	*0.9176*
	Rich flammability limit, *r* (mm)	6.4	7.8	11.6
	Estimate with co-flow (m/s)	*0.2589*	*0.9741*	*1.0422*
	Lean flammability limit, *r* (mm)	7.9	9.7	20.3
	Estimate with co-flow (m/s)	*0.1339*	*0.3503*	*0.1851*

A.3 Velocity Estimates at the Reaction Zone

Tieszen *et al.* (1996) derived the following equation for the time-averaged velocity profile based on experimental data:

$$\bar{U}(r,z) = \left[11.8 \left(\frac{\rho_0}{\rho_\infty} \right)^{1/2} \left(\frac{r_0}{z} \right) \exp\left\{ -93.7 \left(\frac{r}{z} \right)^2 \right\} \right] U_0 . \qquad \text{A.1}$$

The equation is based on the exponential decay of the jet exit velocity, U_0, and the fuel-to-air density ratio, ρ_0/ρ_∞, which is assumed to remain constant despite changes in temperature. This equation is for pure, non-buoyant jets issuing into quiescent air with jet exit radius of r_0. It neglects the virtual origin, or the point at which the extrapolated mass flow rate is zero, and the constants were determined from various experimental data. For jets where the density ratio at the exit is not close to unity, the relation is still valid due to the decay of density differences downstream (Chen and Rodi, 1980). The similarity region begins at about twenty nozzle diameters downstream (Dowling and Dimotakis, 1990). Even though the flow is subsonic, the derivation assumes that combustion does not affect conditions upstream.

Several studies on different flame characteristics have noted the effect of co-flowing air on the flame's behavior (Lee *et al*., 2003; Lee and Chung, 1997). Thus, the co-flow velocity, U_{cf}, should not be considered negligible when predicting the velocity. One way to account for U_{cf} when estimating the velocity profile is to assume some amount of exponential decay in the co-flow velocity downstream. Thus, the velocity profile has been modified as shown in Equation A.2

$$\bar{U}(r,z) = \left[11.8 \left(\frac{\rho_0}{\rho_\infty} \right)^{1/2} \left(\frac{r_0}{z} \right) \exp\left\{ -93.7 \left(\frac{r}{z} \right)^2 \right\} \right] U_0 + U_{cf} \exp\left\{ -\left(\frac{r}{z} \right)^2 \right\}. \qquad \text{A.2}$$

For each set of published data shown in Tables A.1, A.2, and A.3, velocities estimates have been calculated from Equations A.1 and A.2.

The Su *et al.* (2000) data show that the velocity estimates with co-flow agree best with the PIV measurements made on the flame interface, particularly at the lower height. The measured velocities are plotted with the axial height normalized by the jet exit diameter in Figure A.1. For both cases the velocity is greater towards the centerline. Since the co-flow velocity remains unchanged for both cases, the accuracy of the Tieszen relation can be better determined. Figure A.1 also shows the Tieszen estimates with and without co-flow from Equations A.1 and A.2. The estimate without co-flow underestimates the data but agrees most closely with the PIV measurement furthest from the centerline. The other estimate shows better agreement for both cases and matches best with the data on the interface. Percent differences have been calculated and are shown in the figure. The velocity estimates increase with height while the PIV measurements decrease.

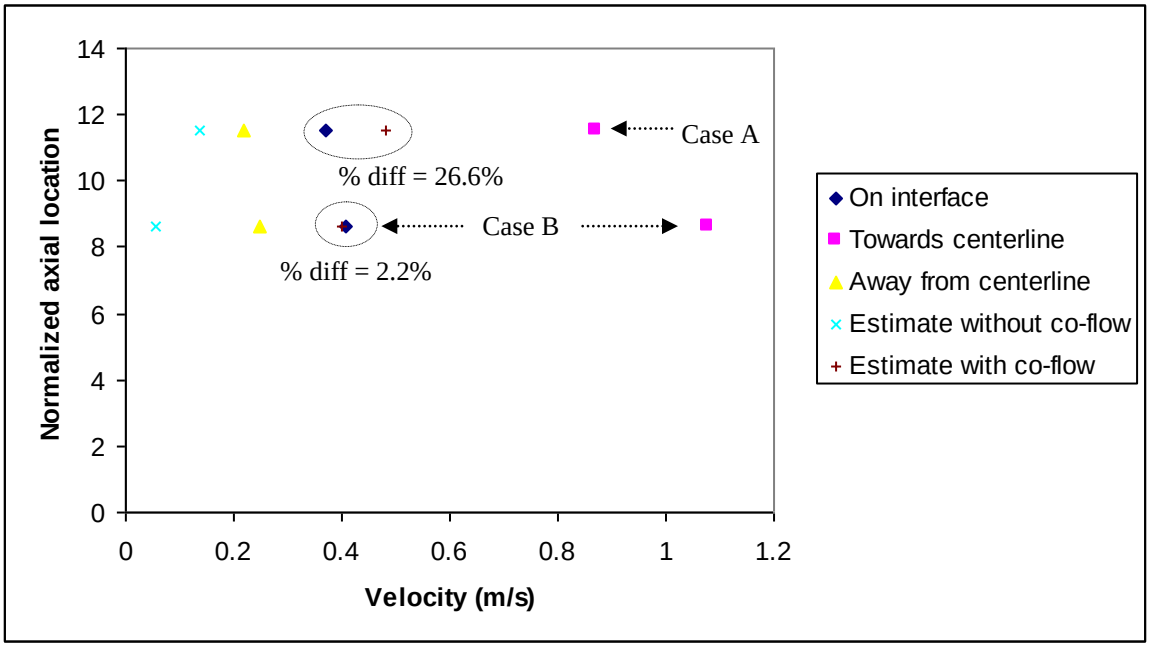

Figure A.1 Su *et al.* (2000) data.

Velocity estimates (shown in Table A.2) are plotted with the PIV data for the four cases of the Muñiz and Mungal data in Figure A.2. The PIV velocities for Cases 1, 2, and 3 on the side of the jet (both instantaneous and average) do not show the effect of decreasing co-flow velocity. The instantaneous location velocities stay nearly constant, and the average location velocities increase and then decrease. However, Cases 3 and 4 with similar co-flow velocities have the same PIV measurements for the instantaneous and average locations (within 0.1 m/s at the average location) which possibly indicates that the fuel velocity has a diminished role at these locations on the side of the jet.

Of the three PIV locations, the average location on the side of the jet has the best agreement with the Tieszen estimates overall. To be consistent with the analysis of the data from the other papers, the Tieszen estimate with co-flow is compared to the published data and the percent difference for each case is shown in Figure A.2. However, the estimates without co-flow are in closer agreement for some of the cases. Given the lack of dependence on co-flow for these PIV measurements, this is not surprising.

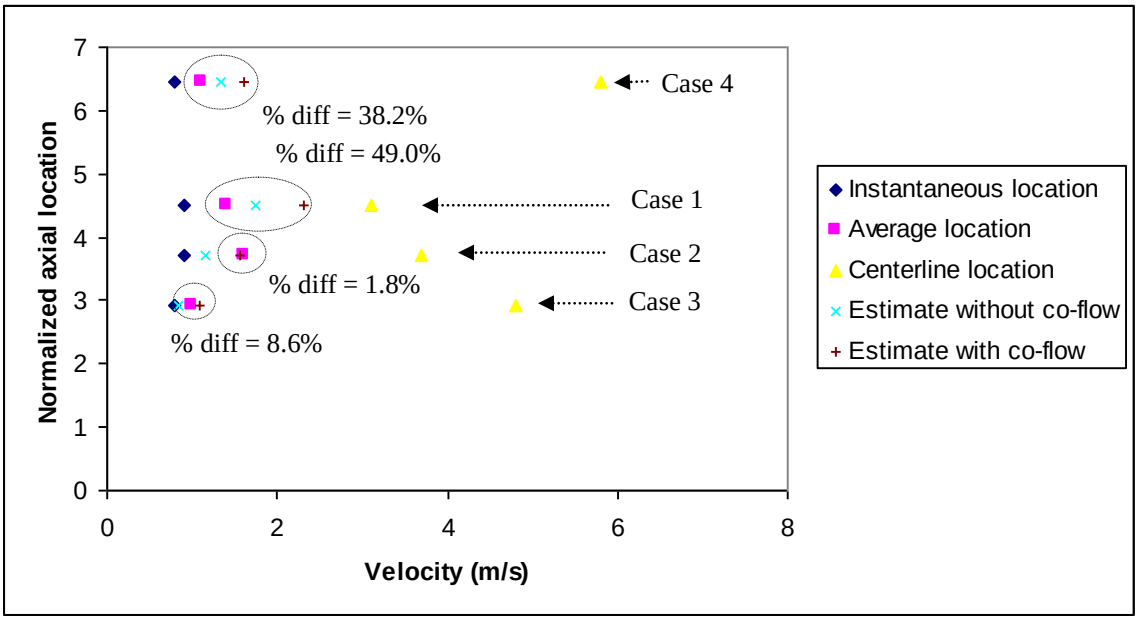

Figure A.2 Muñiz and Mungal (1997) data.

Figure A.3 shows the velocity at each location for the three flow conditions in Table A.3. Two estimates are shown for these locations. The estimate with the co-flow velocity is

closer to the data from the instantaneous imaging, since the measured velocity at the average location is greater for each case. The velocity estimates for the locations of the rich and lean flammability limits are also included. Due to the tendency of CH zones to lie towards the centerline, the PIV measurements were greater than one could expect from using the OH radical (Watson *et al.*, 1999). Thus, the estimates at the rich flammability limits are closer to the data than those at the CH-PLIF imaged location. The percent differences calculated in Figure A.3 are based on the Tieszen estimates at the rich limit. Case β has the smallest percent difference and Case α the largest.

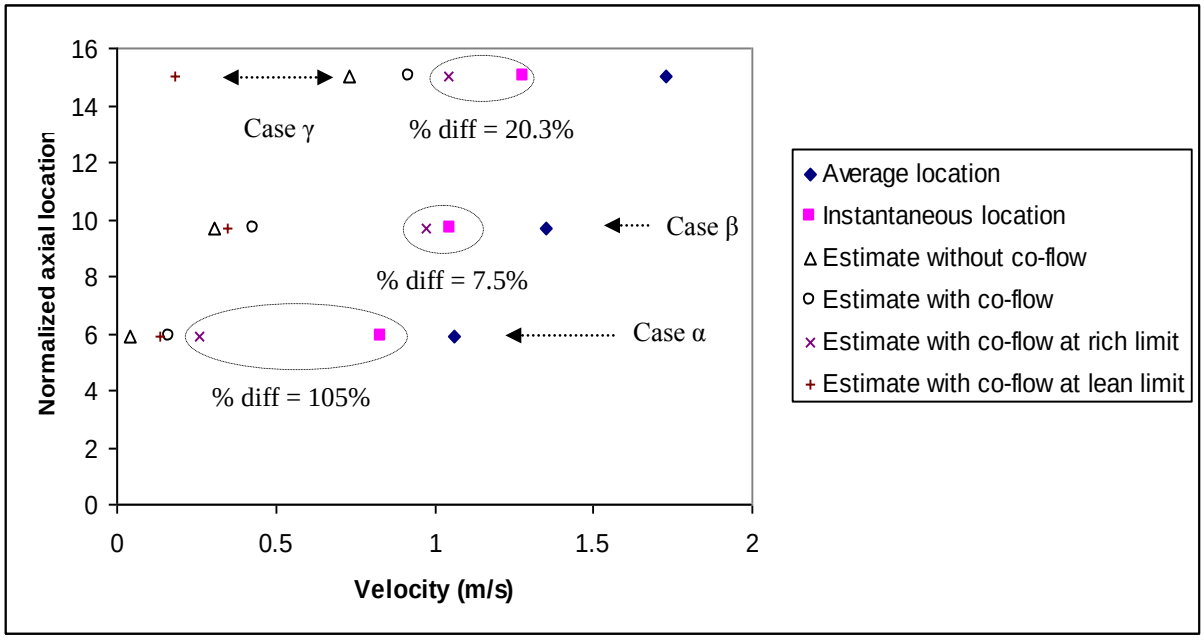

Figure A.3 Watson *et al.* (2002) data.

A.4 Comparison of Experimental Data

Plotting the data from the published studies together provides insight on the overall accuracy of the Tieszen relation. From each set of data, the PIV measurements that show best agreement with the velocity estimates are shown in Figure A.4 and Figure A.5. The figures arrange the data by the height normalized by the jet diameter and the horizontal position normalized by the jet radius, respectively, and the estimates are shown as outlined data points.

The experimental data itself shows a wide range PIV measurements are possible depending on the experimental procedure used. By limiting the discussion to comparison of data to the estimates, it is seen the Tieszen relation consistently under-predicts the Watson *et al.* (2002) data but mostly over-predicts data from the other two studies. Overall, the Tieszen relation is the most accurate with the Su *et al.* (2000) data. Note that the Watson *et al.* (2002) data shown in Figure A.4 and Figure A.5 are the published PIV measurements and the estimates found for the rich flammability limits, locations closer to the centerline due to the use of the CH radical.

A clear trend is not seen for an increase or decrease in accuracy due to a change in location. Thus, a change in the Tieszen relation is unlikely to improve the accuracy for all sets of data. The accuracy of the estimates highlights the differences in defining the flame location. The experiments vary in how they identify the flame's leading-edge which can significantly change the velocity measured.

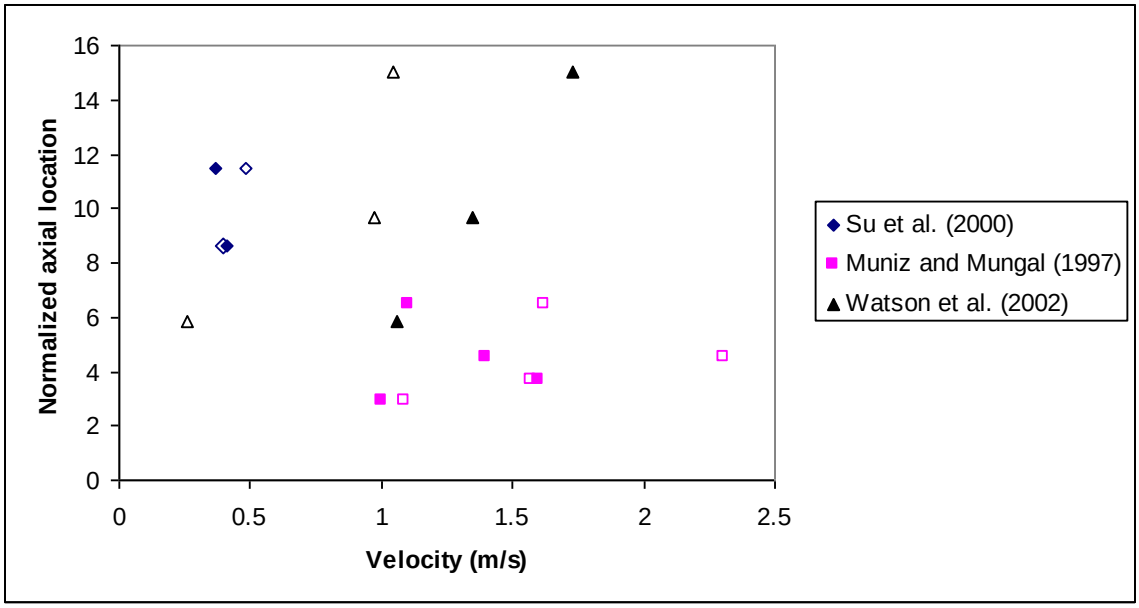

Figure A.4 PIV measurements at each flame height for the three studies.

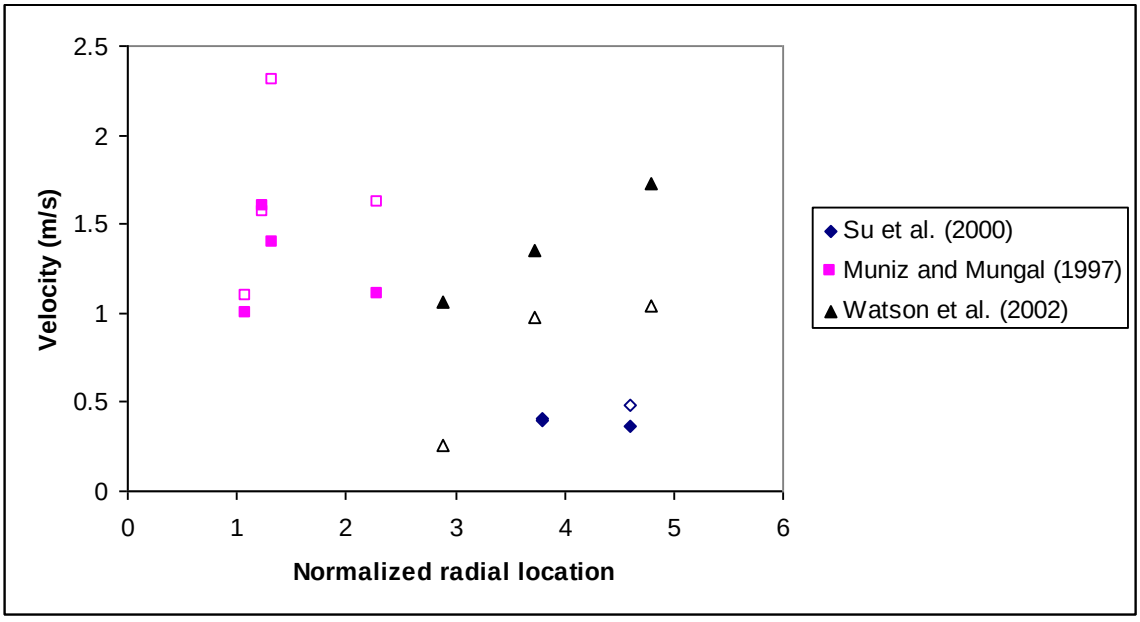

Figure A.5 PIV measurements at each flame radial location for the three studies.

The consolidation of the data in Figure A.6 shows inconsistencies in the velocities measured when compared by location. While the lowest velocities, predictably, are noted far from the centerline, a velocity of 1.28 m/s was recorded at the furthest radial and axial location. These differences indicate the significance of the procedure used to locate the flame on the results. The flame's location is not the sole consideration necessary since each of the studies compared in this paper used various co-flow velocities. The effect of co-flow on the velocity field has not been fully investigated.

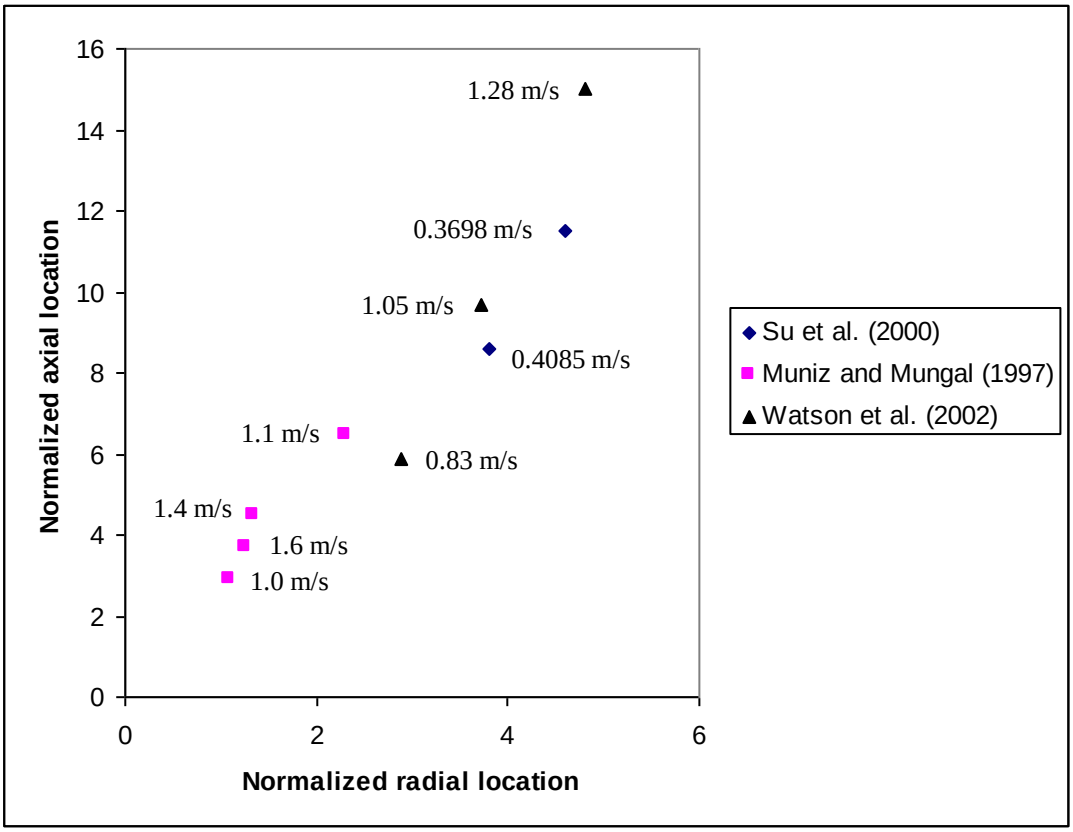

Figure A.6 PIV measured velocities are indicated at each location.

A.5 Conclusions

Several factors cause discrepancies between experimental findings and between these data and velocity estimates. Despite the lack of co-flow dependence in the Tieszen relation, the more noteworthy problem appears to be the difficulty in clearly defining the reaction zone location to make PIV data consistent. The analysis has yielded the following conclusions:

1. The PIV measurements from the three sets of data are not in agreement due to experimental differences (CH vs. OH) and possibly to the different flow conditions.
2. The Su *et al.* (2000) data on the flame interface showed the best agreement with the Tieszen estimates when co-flow was added.
3. The Muñiz and Mungal (1997) data from the average location on either side of the jet centerline was closest to the estimates. However, only two of the four points were more accurate when the co-flow was added to the estimate, an indication that additional changes to Equation A.2 are necessary for estimates with co-flow.
4. For the Watson *et al.* (2002) data, the rich flammability limit was used as the location of the estimate due to differences in imaging. The estimates with co-flow were closest to the instantaneous location. This was the only data set where the Tieszen relation consistently underestimated the velocity.
5. The estimates were closest to the Su *et al.* (2000) data of the three. However, when plotted according to location (Figure A.5 and Figure A.6), there is not a clear trend in the accuracy even within each set. As the flame location moves outward and downstream, the estimates are not seen to approach the measurements.